VALORISATION OF PULP AND PAPER MILL SLUDGE BY HYDROTHERMAL CARBONISATION

By

Englatina Ivandra Nogueira Craveiro de Assis

Submitted in partial fulfilment of the required for Degree of
Master of Applied Science (Water Utilisation)

In the

Department of Chemical Engineering
Faculty of Engineering, Built Environment and Information Technology

University of Pretoria

2021

ABSTRACT

Title: **Valorisation of pulp and paper mill sludge by hydrothermal carbonisation**

Supervisor: Prof. Evans M. N. Chirwa
Department: Chemical Engineering
University: University of Pretoria
Degree: Master of Applied Science (Water Utilisation)

Substantial amounts of waste residues in the form of sludge consisting of high moisture, organic and inorganic matter are continuously generated at the South African pulp and paper mills and disposed of through landfills, land applications and incineration. The methods are detrimental to the atmosphere, surface and groundwater resources, thereby threatening public health. The lignocellulosic composition in the paper sludge offers enormous potential for energy recovery. Common thermochemical technologies for energy recovery from lignocellulosic wastes such as pyrolysis, gasification and torrefaction, require feedstock pre-drying and elevated processing temperatures, thus making the overall process energy-intensive. Hydrothermal carbonisation (HTC) is an attractive technology to address problems associated with moisture-rich unconventional feedstock and convert it into high-value solid products for various applications.

This study evaluates the effect of HTC operating conditions on the physicochemical properties, fuel characteristics and combustion performance of the resulting hydrochar fuels from different recycling paper mill streams to select the best feedstock for the process optimisation and potential energy assessment. 10 g raw fibre rejects (RF), sludge generated at the primary clarifier (PS) and final waste sludge (FS) were individually mixed with 90 mL and hydrothermally carbonised in batch reactor autoclave at 205, 225 and 245 °C for 3 hours. The resulting hydrochars were analysed in terms of proximate, elemental composition, functional groups, mass yield and energy yield and combustion performance. Based on the evaluated results, the RF was considered the most suitable feedstock due to factors including relatively low ash, increased fixed carbon, energy content, and adequate

combustion performance in the hydrochar recovered compared to the hydrochars from the other substrates. Thus, consequently selected for process optimisation and further investigations.

Response surface methodology (RSM) was used to evaluate the interaction of the HTC process operating parameters, i.e. temperature, residence time and solid load, as well as to develop models for the process to predict the optimum condition to produce hydrochar from paper sludge with maximal mass yield and calorific value. The fuel properties and thermal behaviour of the resulting hydrochars were further assessed to determine their potential for energetic applications. Results showed that temperature and residence time were the most significant model variables and highly influenced the hydrochar yield and calorific values, while the solid load had no significant effect on both responses. The highest calorific value recorded was 22.9 MJ/ kg on a dry basis, approximately equivalent to the HHV of coal used for commercial utility in South Africa and corresponded to an increase of 50 % of the HHV of the original feedstock. Under the design space investigated, at the optimal condition of 232 °C and 2 h, a maximal hydrochar yield of 74.4 % and calorific value of 18.5 MJ/ kg are feasible.

The variation in HTC operating conditions resulted in hydrochars with improved physicochemical characteristics for the most part. Analysis of the influence of carbon on calorific values showed strong linear positive correlations. In contrast, the relationship between the oxygen and calorific values showed a negative correlation. Both correlations had p-values less than 0.0001, confirming that increased carbon and lower oxygen lead to increased calorific values. The coalification diagram showed that dehydration and decarboxylation were the dominant reactions during HTC. The H/C and O/C were reduced by 35.5 and 64 %, respectively. The energy assessment of hydrochar production from paper sludge showed that up to 58.3 % of the energy generated from hydrochar fuel combustion could be generated. Furthermore, considering the current waste of 0.5 million tonnes generated annually, over 2.4 million gigajoules could be generated from the pulp and paper wastes generated, which is equivalent to 20.9 % of the electricity currently generated at one of South Africa’s coal-fired power plants, thus contributing to the diversification of energy resources, thereby reducing environmental emissions.

Keywords: paper sludge, HTC, hydrochar, combustion, response surface methodology, optimisation, renewable energy.

DECLARATION

I, Englatina Ivandra Nogueira Craveiro de Assis, declare that the dissertation which I hereby submit the degree of Master of Applied Science (Water Utilisation) at the University of Pretoria, is original and has not previously or in parts been submitted by me for a degree at this or any other tertiary institution.

Signature: …….. Date: ……..

DEDICATION

To my parents

Eduardo Nelson Craveiro de Assis and **Rosa Joao Manuel Costa**

For the unconditional love, tremendous moral and emotional support

and

to my life partner

Tchisseke Loureiro Geraldo Vicente

For constantly boosting me with confidence, support and mentorship.

ACKNOWLEDGEMENTS

I would like to express my deepest gratitude to my supervisor, Professor Evans Chirwa, for awarding me with this project, for his support, supervision and complete guidance throughout my study. Conducting this research under his supervision allowed me to apply my knowledge in practice, work with unique equipment and acquire experience in the waste beneficiation sector. I also want to thank him for securing funding through Sedibeng Water Chair in Water Utilisation Engineering, thus enabling me to carry out my research work. Moreover, I am immensely grateful to Dr Shepherd Tichapondwa and Dr Ryan Merckel for their valuable inputs, guidance, and feedback throughout this study.

I would like to express my appreciation to Ministério dos Recursos Minerais e Petróleos (MIREMPET) Angola for the bursary programme to pursue my Master degree, as well as SETANGOL for caretaking and excellent administration of my studies in the Republic of South Africa throughout the years. I am thankful to the Water Utilisation Division staff at the University of Pretoria, especially Mrs Elmarie Otto and Mrs Alette Devega, for their outstanding assistance until the completion of this study. I wish to express my gratitude to the analytical team at the University of Pretoria and external laboratories.

I am thankful to my colleagues, especially Brian Gidudu and Job Tendenedzai, for their valuable help and encouragement throughout the years. Finally, my most profound and unlimited appreciation to my siblings and all family members whose unconditional love, support and encouragement contributed to my success.

Table of Contents

List of Tables

List of Figures

LIST OF ACRONYMS AND ABBREVIATIONS

A	Ash
ANOVA	Analysis of variance
C_{char}	Carbon retained in hydrochar
C_D	Carbon densification
db.	Dry basis
D_i	Ignition index
E_C	Electricity generated by coal-fired power plant
E_D	Energy densification
E_{HC}	Electricity generated from hydrochar
E_Y	Energy yield
FC	Fixed carbon
FS	Final sludge
GHG	Greenhouse gases
HHV	Higher heating value
HTC	Hydrothermal carbonisation
H_Y	Hydrochar yield
M	Moisture content
η	Average efficiency of coal-fired power plant
PMS	Paper mill sludge
PPMS	Pulp and paper mill sludge
PS	Primary sludge
P_Y	Unaxial pressure
Q_{in}	Input energy
Q_{net}	Net energy
Q_{out}	Output energy
RF	Raw fibre rejects
S	Comprehensive combustibility index
T_b	Burnout temperature
t_i	Ignition time
T_i	Ignition temperature
T_m	Maximum combustion rate temperature
t_{max}	Time at maximum combustion rate

TOC	Total organic carbon
σ_{max}	Unaxial stress
σ_r	Radial stress
σ_z	Axial stress
σ_θ	Circumferential stress
VM	Volatile matter

RESEARCH OUTPUTS

Journal articles

1. Assis, E. I. N. C. & Chirwa, E. M. N. Hydrothermal carbonisation of paper mill sludge: effect of process conditions on hydrochar fuel characteristics and energy recycling efficiency. *Journal of Cleaner Production PRES'21 Special Issue - Sustainable Cleaner Production Integration, Modelling and Optimisation* [Submitted].
2. Assis E. I. N. C. & Chirwa, E, M., N. Fuel properties and combustion performance of hydrochars prepared by hydrothermal carbonisation of different recycling paper mill wastes. *The Canadian Journal of Chemical Engineering CCEC 2021 Special Issue* [Submitted].
3. Assis, E. I. N. C., Chirwa E. M. N. & Tichapondwa, S., M. 2021. Hydrothermal Carbonization of Different Recycling Paper Mill Waste Streams. *Chemical Engineering Transactions, 88, 43-48*. https://doi.org/10.3303/CET2188007.
4. Assis, E. I. N. C. & Chirwa E. M. N. 2021. Physicochemical Characteristics of Different Pulp and Paper Mill Waste Streams for Hydrothermal Conversion. *Chemical Engineering Transactions, 86, 607-612.* https://doi.org/10.3303/CET2186102.

Conference presentations

1. Hydrothermal Carbonization of Different Recycling Paper Mill Waste Streams. 24th Conference on Process Integration for Energy Saving and Pollution Reduction. 31st October – 3rd November 2021, virtual. (Oral Presentation).
2. Evaluation of combustion properties of hydrochars produced via hydrothermal carbonization of different South African paper mill waste streams. The 71st Canadian Chemical Engineering Conference. 24th – 27th October 2021, Virtual. (Oral presentation).
3. Physicochemical Characteristics of Different Pulp and Paper Mill Waste Streams for Hydrothermal Conversion. The 15th International Conference on Chemical and Process Engineering. 23rd – 26th May 2021. (Poster).

CHAPTER 1: INTRODUCTION

1.1. Background

With the stringent environmental regulations, rising costs of solid management, and the continuous generation of waste resulting from pulp and paper production, the sustainable management of waste from these streams represents an economic and environmental problem. In South Africa, over 2 million tonnes of pulp are produced every year (Dillen et al., 2016, PAMSA, 2015, PAMSA, 2014, PAMSA 2013, PAMSA, 2012), which leads to the generation of 0.5 million tonnes of solid residues in the form of sludge consisting of moisture, organic and inorganic matter (Boshoff et al., 2016). These wastes are typically disposed of through incineration, landfills or land application (Kaur et al., 2020), thereby threatening the environment and public health (Majewski and Jääskeläinen, 2004, Bajpai, 2015, Likon and Trebe, 2012).

Currently, South Africa is planning to diversify its energy basket to reduce reliance on coal and mitigate the negative impact of coal on the environment, thereby reducing the carbon footprint (Department of Energy). This underlines the urgency to explore the potential of underutilised wastes as a renewable energy source. Pulp and paper mill sludge is mainly composed of lignocellulosic material (Kaur et al., 2020) which offers good potential for energy for fuel, heat and electricity production.

Some current ways of recovering energy from lignocellulosic wastes include thermochemical processes such as pyrolysis, gasification and torrefaction (Libra et al., 2011, Demirbas and Arin, 2002, Van der Stelt et al., 2011). However, due to high inherent moisture in the pulp and paper mill sludge, active pre-drying of the feedstock is required in addition to elevated processing temperatures, which turns the overall process energy-intensive and inefficient. Alternatively, hydrothermal technologies are investigated. These processes can produce high-quality fuels and materials with different characteristics than their dry initial substrates at lower temperatures, and more importantly, without the need for pre-drying (Kruse et al., 2013). The hydrothermal carbonisation (HTC) process is most commonly used to carbonise biomass. It is an emerging technology that upgrades unconventional wet substrates into carbon-rich products (Funke and Ziegler, 2010). The exothermic process occurs in the presence of liquid water at temperatures typically ranging from 180-260 °C, and autogenous pressure (Merzari et al., 2018). The resulting coal-like

material, commonly referred to as hydrochar, has a good dewatering property, improved hydrophobicity, and, when dried, has a higher calorific value compared to the initial feedstock (He et al., 2013b). The hydrochar obtained from the HTC treatment has a variety of benefits and applications in solid fuel, soil amelioration, low-cost adsorbent, catalyst, and contaminant removal (Fang et al., 2018b).

Several authors have reported the application of HTC on a variety of organic substrates, including raw sludge from municipal wastewater treatment plants (Chen et al., 2020), raw olive mill waste (Volpe et al., 2018), and wood biomass (Stirling et al., 2018) and pulp and paper mill sludge (Lin et al., 2015a, Areeprasert et al., 2015). However, the investigations on pulp and paper are mostly conducted on combined sludge, and studies on the HTC treatment at the subcritical water conditions on the different recycling paper mill streams have not been extensively reported. Moreover, there are no reports on statistically optimised conditions for producing the best-quality hydrochar from paper mill wastes for solid fuel applications.

1.2. Aim and Objectives

This study aims to process paper mill sludge using hydrothermal carbonisation (HTC) technology to produce a highly combustible solid, i.e. hydrochar for fuel applications, and develop models to predict the optimum process conditions for maximum hydrochar yield and energy content. The HTC process will transform a resource otherwise wastefully disposed into a highly combustible solid that is practicable in industrialised and emerging countries. The following sub-objectives are involved:

i. To design, build and test a batch HTC reactor autoclave for experimental purposes, according to technical requirements to ensure proper functionality and safe operation of the reactor and sample handling, to assess the suitability of the HTC technology to upgrade unconventional paper mill sludge into clean solid fuel.
ii. To evaluate the effect of the subcritical water HTC reaction temperatures on the physiochemical characteristics, i.e. visual aspects, elemental composition, proximate composition, mass yield, calorific value by means of higher heating value (HHV) and functional groups of the hydrochars obtained from different recycling paper mill streams.
iii. To further evaluate the combustion performance of the produced hydrochar fuels in terms of thermogravimetric analysis and derivative thermogravimetric

analysis profiles, ignition temperature, burnout temperature, combustibility index and residual ash, compared to their initial substrates. This is to facilitate the selection of the most suitable feedstock for optimisation studies.

iv. To optimise the operating conditions to produce high-value hydrochar fuel by studying the effect of reaction temperature, residence time, and solid load on the mass yield and calorific value, using response surface methodology (RSM).

v. To illustrate the effect of the three parameters (reaction temperature, residence time and solid load) on the structural, fuel, and combustion properties of the hydrochar fuels to further support their suitability for energetic applications.

vi. To perform an energy balance of hydrochar fuel production from paper sludge by HTC to further evaluate the energetic efficiency of the process and the potential of using the heat recovery from the hydrochar fuel.

vii. To estimate the electricity generation potential at the optimised HTC reaction conditions for one of South Africa's coal-fired power stations, demonstrate hydrochar fuel's potential as a coal substitute.

1.3. Benefits of the Study

The benefits of this study include:

- Recovery of a valuable resource that is wastefully disposed of and convert into a high-value product with the potential to play a role in the field of energy, water treatment, resource recovery such as phosphorous, catalysis, and soil amelioration.
- Solid waste minimisation while exploring reusing and recycling alternatives.
- The production of clean solid fuel through HTC will reduce the negative environmental and health impacts caused by unconventional pulp and paper mill wastes.
- The integration of HTC will help to minimise costs associated with solid waste management at wastewater treatment works and waste management facilities while recovering an income-generating recoverable resource.
- This study presents an opportunity to generate knowledge in bioremediation, clean technologies and renewable energy resources.

- The application of HTC solid fuel could contribute to the energy diversification in South Africa, thereby contributing to reducing pollutant emissions. Moreover, hydrochar fuels could be used in developing countries as an alternative energy source.

1.4. Project Limitations

The HTC process yields three different products, i.e. solid, liquid and gas. This study focuses on the effect of HTC on the main product, i.e. hydrochar. Moreover, hydrochar has a variety of applications, i.e. solid fuel, soil amelioration, low-cost adsorbent, catalyst, and contaminant removal; this study is limited to the solid fuel/ energetic application of the hydrochar.

1.5. Structure of the Dissertation

Thus dissertation consists of 9 chapters.

Chapter 1 is the introductory section and provides a background and problem statement highlighting the relevance of this work.

Chapter 2 provides a review of pulp and paper waste characteristics, management practices, environmental regulations. It also presents an overview of the different thermal conversion technologies and feasibility evaluation of the HTC technology for energy recovery underlining the science, i.e. reaction mechanisms, process conditions, products. Lastly, it presents potential applications of hydrochar, reported energy aspects of solid fuel produced from HTC and highlights the identified gaps covered by the present study.

Chapter 3 explains the different types of material analysis and characterisation by using different principles and equipment: Thermogravimetric Analyser (TGA), CHNS Elemental Analyser, Bomb Calorimeter, Scanning Electron Microscope (SEM), Energy Dispersed x-ray (EDS) and Fourier-transform Infrared Spectroscopy (FTIR), respectively. This includes the Total Organic Carbon (TOC) of the process wastewater by a TOC analyser.

Chapter 4 provides a description of the criteria followed for the design and construction of the reactor. This includes vessel specification, material, design dimensions, stress analysis, fabrication, the overall cost per unit and reactor test.

Chapter 5 presents the methodology for experiments and criteria followed model developments, statistical analysis, process optimisation and energy balance

for the hydrothermal carbonisation of paper mill sludge at subcritical water conditions.

Chapter 6 presents a study on the effect of subcritical water condition of HTC treatment on the physicochemical characteristics and combustion performance of hydrochars obtained from varying recycling paper mill streams.

Chapter 7 presents the influence of HTC operating conditions, i.e. reaction temperature, residence time and solid load, on the overall hydrochar properties by RSM. It investigates the interactive effect among the operating parameters and presents the developed models to predict the optimum condition for hydrochar with maximum yield and highest calorific values. It further evaluates the energetic aspects of HTC of paper sludge.

Chapter 8 presents the conclusions drawn from this study and highlights possible areas of research that could constitute future work for the scalability of the HTC process of HTC of paper mill wastes.

CHAPTER 2: LITERATURE REVIEW

2.1. The Generation of Pulp and Paper Mill Sludge (PPMS)

The South African paper and pulp manufacturing sector have grown substantially on an annual basis since 1970. Currently, South Africa is ranked the 15th largest producer of pulp in the world and 24th in paper production globally (FpmSeta, 2014). In 2018, forestry-to-paper value-add to South Africa's economy was approximately R62.2 billion, contributing to 0.53% of the country's gross domestic product (GDP) (PAMSA, 2018). Every year, over 2 million tonnes of pulp is produced from pulpwood and recycled fibre raw material as sources of cellulose for the manufacture of different paper grades, including printing and writing, packaging and tissue papers (Dillen et al., 2016, PAMSA, 2015, PAMSA, 2014, PAMSA 2013, PAMSA, 2012). However, the pulp production and paper manufacture lead to the generation of a substantial amount of wastes residues in the form of sludge from wastewater treatment operations such as primary clarifier (primary sludge), secondary clarifier or biological treatment (secondary sludge or bio-sludge), and after fibre deinking process (Bajpai, 2015). In South Africa, the pulp and paper industry is estimated to generate about 0.5 million tonnes of sludge every year (Boshoff et al., 2016) consisting of high moisture, organic and inorganic matter in different proportions, depending on the source of cellulose used, the process of production and the final products produced at the mills' operations (Cabrera, 2017, Lekha et al., 2017, Bahar et al., 2011, Pokhrel and Viraraghavan, 2004), as illustrated in Figure 2.1.

The characteristics of the pulp and paper sludge typically consist of cellulose, hemicellulose, lignin, wood resins, binders, paper additives, kaolinite (clay), calcium carbonate, heavy metals and ash (Gibril et al., 2018, Hubbe et al., 2016, Pokhrel and Viraraghavan, 2004).

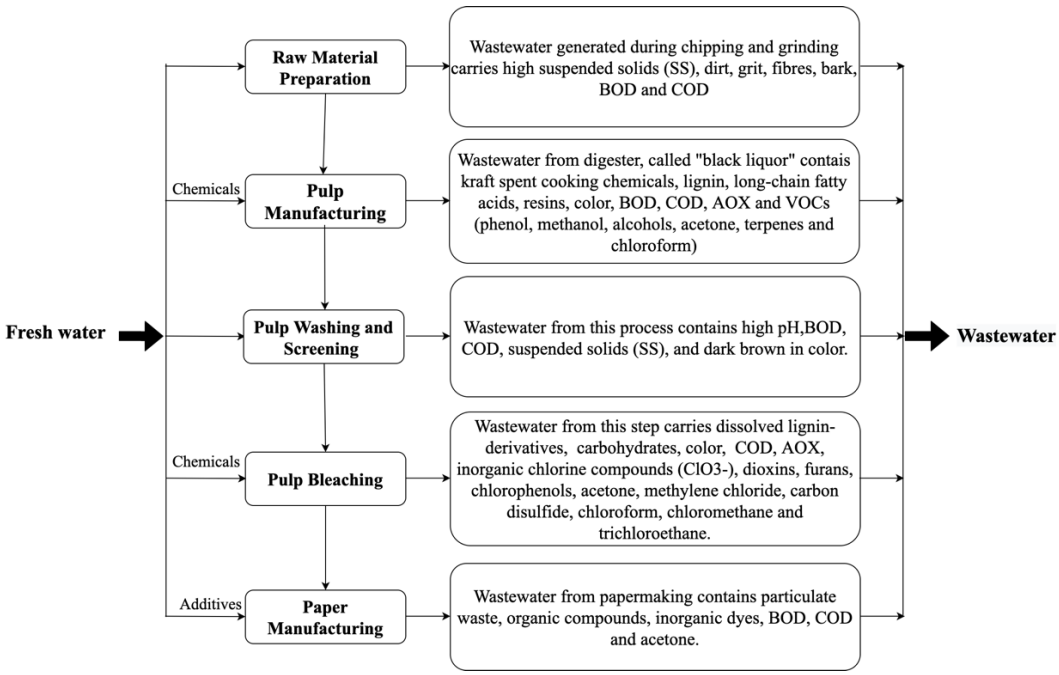

Figure 2.1: Schematic illustration of pollution source in pulp and paper manufacturing process.

Generally, mills that process recycled fibre as raw material generate higher waste residues than mills that use wood (Scott, 1995), as presented in Table 2.1. This is partially associated with fillers in the paper (clay or calcium carbonate) which makes the fibres inadequate for paper production (ibid.). The typical quantity of waste produced in recycling mills varies from 12-406 kg/ton, which must be disposed of in an economically and environmentally accepted manner.

Table 2.1: Typical waste load from different pulp and paper operational stages per tonne of virgin or recycled fibre raw material used (Scott, 1995).

Paper Grade	Wood	Recycled Paper	Both
	kg/ tonne		
Unbleached	43	43	43
Newsprint	57	164	69
Tissue	33	406	382
Printing & writing	62	18.7	165
Others	45	12	11

2.1. Current Sludge Disposal Methods

Due to high moisture content and poor dewatering properties, the management of pulp mill sludge requires major investment costs. In some cases, prior to final disposal, PPMS is subjected to a pre-treatment consisting of

stabilisation (Lenntech), thickening, conditioning, dewatering and drying (Bajpai, 2015). However, the overall process is energy-intensive, and the costs associated with solid waste management may reach up to 60 % of the total wastewater treatment plant (Canales et al., 1994). The most common sludge disposal methods are incineration, landfill or land application (Kaur et al., 2020).

2.1.1. Incineration

Incineration is the primary alternative disposal method. The process involves combusting sludge at high temperatures to generate power through steam turbines, reducing the waste volume up to 90% (Bajpai, 2015) and meeting steam demand. However, the presence of high moisture and low carbon content in the form of lignocellulosic matter makes the incineration process energetically unfavourable, as for each 1 % moisture present in the sludge, the combustion temperature must be 10 °C higher (Likon and Trebe, 2012). Moreover, sludge combustion deteriorates the air quality and threatens public health due to the emission of greenhouse gases (GHG) such as NO_x and SO_2, which are major precursors of acid rain (Majewski and Jääskeläinen, 2004). The emission of nitrogen oxides (NO_2) leads to the production of photochemical smog and nitrate particulates, destroying the stratospheric ozone (Sher, 1998). Furthermore, incineration of high-ash sludge produces elevated amounts of ash residuals containing toxic chemicals, thereby requiring further disposal, which is usually done through landfills (Majewski and Jääskeläinen, 2004).

2.1.2. Landfilling

Landfilling is another standard method of sludge management. The landfills are either industrial, constructed and operated by the mills or independently owned, requiring the mills to pay a fee for sludge disposal (Likon and Trebe, 2012, Scott, 1995). Similar to incineration, the method requires pre-processing, such as drying, prior to disposal. Since most landfills charge by weight or volume, it is uneconomical to pay for water disposal (Scott, 1995). PPMS is dewatered, spread or deposited onto the landfills (Likon and Trebe, 2012). However, PPMS with high organic content is subjected to anaerobic and aerobic decay, leading to GHG emissions and odour. According to Buswell and Mueller (1952), 1 tonne of low-ash paper mill sludge in landfills theoretically releases approximately 2.69 tonnes of CO_2 and 0.24 tonnes of methane (CH_4). Landfilling may also result in the leaching of toxic

substances in sludge (such as heavy metals) into the ground, leading to possible contamination of land and groundwater systems.

Furthermore, with the continuous increase in sludge generation, there is a shortage of landfill sites (IOL, 2018, Alive2green, 2019). Thus, obtaining a waste licence and constructing new landfill facilities may be time and cost-intensive (Alive2green, 2019). To avoid the adverse effects from landfilling activities, most developed countries are banning landfills in the near future (Bajpai, 2015). Hence, implementing alternatives to divert sludge from landfill sites will alleviate costs associated with sludge management and reduce GHG emissions.

2.1.3. Land application

Land application through land surface spreading and composting are also common methods for soil enhancement and preventing uncontrolled PPMS decay (Likon and Trebe, 2012). However, depending on the stream, PPMS may contain relatively high contaminants such as heavy metals, naphthalene, phthalates, chloroform, PCB, wood extractives or derivatives and chlorinated lignin derivatives with concentrations above 10 mg/ kg (ibid.). The maximum application rate for such sludge is 12 tons per 405 ha (ibid.)., thereby requiring a large land area and additional costs for storage. Moreover, these contaminants can remain in the soil for prolonged years and eventually enter the food chain. In addition, sludge containing unfavourable C:N ratios are inappropriate for plant growth (ibid.).

2.3. National Environmental Legislation of South Africa

2.3.1. Environmental Act

To preserve environmental protection, the environmental rights contained in the Constitution of the Republic of South Africa (Act 108 of 1996) states that everyone has the right to:

> *"a) An environment that is not harmful to their health or well-being.*
>
> *b) To have the environment protected, for the benefit of present and future generations through legislative and other measures that prevent pollution and ecological degradation; promote conservation, and secure ecologically sustainable development and use of natural resources while promoting justifiable economic and social development."*

This regulation falls under the Department of Environmental Affairs (DEA) responsibility. Moreover, the National Environmental Management Act (Act 107 of 1998), particularly the National Environmental Management: Waste Act (Act 59 of 2008) and the National Environmental Management: Air Quality Act (Act no. 39 of 2004) outline the requirements for the storage and handling of waste onsite for both hazardous and non-hazardous, licensing requirements, the establishment of waste management plans, the setting of limits for air emissions, and the setting of penalties for offences. This act emphasises the need to implement cleaner production and clean technologies to reduce pollution at the source.

2.3.2. Carbon Tax Act

The South Africa government has implemented a Carbon Tax Act (Act No. 15 of 2019) with effect from 1 June 2019 to reduce carbon dioxide (CO_2) equivalent of greenhouse gas emissions into the atmosphere resulting from combustion, industrial processes and fugitive emissions by 42 % by 2025 (GovernmentZA, 2019). This makes South Africa one of about 40 countries to implement a carbon-pricing program (WB, 2019). The tax is set at R120 per tonne of carbon dioxide equivalent emissions administered by The South African Revenue Service (SARS). This rate will increase annually by inflation plus 2% by 31 December 2022 and annually by inflation thereafter (GovernmentZA, 2019, SARS, 2019).

These Acts underline the urgency to adhere to clean processes for waste minimisation/ remediation, adopt new technologies for converting PPM waste into valuable products for beneficial use, and adhere to environmentally friendly waste disposal techniques.

2.4. Alternative Technologies

The utilisation of sludge as a renewable energy resource for energy recovery is the appropriate solution for effectively managing the continuously increasing waste sludge generation to meet stringent environmental quality standards (Tyagi and Lo, 2013). The PPMS is mainly composed of lignocellulosic material (Kaur et al., 2020) which offers potential for energy resource for fuel, heat and electrical power. Currently, there are several waste-to-energy systems options available. The most common are dry thermal conversion processes such as pyrolysis, gasification and torrefaction (Tyagi and Lo, 2013), discussed in the subsequent subsections.

2.4.1. Slow pyrolysis

Conventional or slow pyrolysis has been traditionally used for thousands of years for biochar conversion. In this process, the organic feedstock is heated in the absence of oxygen for long periods at temperatures around 400ºC to produce solid biochar as primary yield and tar-like substances typically known as bio-oil and gas (Demirbas and Arin, 2002). Reaction temperatures and residence times adjustments depend on the desired end product. Generally, lower temperatures and longer residence times result in higher amounts of solid products. Higher temperatures with shorter residence times result in higher gaseous and liquid products. Moderate heating rates with long residence times yield high amounts of gases and vapours (30–35%) and approximately 20–40% as char (Libra et al., 2011). Hence, the distinction between slow and intermediate pyrolysis is essential.

2.4.2. Fast pyrolysis

Fast pyrolysis processes are operated in special reactors allowing for high heating rates and good mixing conditions. During this process, the organic feedstock is rapidly heated to (500°C - 1000°C), and the organic fuels are devolatilised in the presence of little to no oxygen. The end products include small amounts of char and relatively high amounts of vapour containing tars and volatile gases, which are rapidly reduced into liquid through condensation. These liquids can then be further refined as valuable fuels. While the char itself may have several uses, the focus of fast pyrolysis is generally on the yield of liquid products (up to 75%) (Libra et al., 2011). At very high temperatures and very low residence times, one can distinguish fast pyrolysis from flash pyrolysis (Demirbas and Arin, 2002).

2.4.3. Gasification

Similar to pyrolysis, gasification involves heating and devolatilization of organic fuels. However, an oxidising atmosphere is applied by adding air, oxygen, steam or carbon dioxide or mixtures thereof so that only partial combustion may occur. During the operation, temperatures remain high (approximately 800°C) to encourage high yields (up to 85%) of gaseous products. Gaseous products consist of a mixture of mainly H_2, CO, CO_2 and CH_4, which can be used directly as a fuel or as a synthesis gas (syngas) in downstream catalytic conversion processes to

generate synthetic natural gas (SNG), methanol, Fischer-Tropsch fuels and many more products. As temperatures are generally higher than during pyrolysis and residence times are generally short (approximately 10-20 seconds), gasification yields very little char (10%) and even less liquid product (5%) (Libra et al., 2011).

2.4.4. Torrefaction

The Torrefaction process, also known as mild pyrolysis, occurs at relatively low temperatures (280-350°C) and moderate residence times (1-3 hours). The stages of this process include initial heating, pre-drying, post-drying and intermediate heating designed to facilitate evaporation of water and achieve a target torrefaction temperature. To achieve these stages, the consumption of external energy or auto-consumption of gaseous products to generate heat may be required. This process yields reasonably high levels of char (70%) and torrefaction gas (30%). Torrefaction gas contains large yields of products that can be condensed into liquids. Gaseous and liquid products are often used to provide heat for the torrefaction process or can be cleaned (as they will contain tars), collected and used elsewhere (Van der Stelt et al., 2011). The primary purpose of torrefaction solid products is to be used as renewable energy fuel for combustion, gasification and fast pyrolysis, often as a replacement for coal or in co-firing (ibid.). In general, torrefaction can yield char with an improved mass and energy balance over the original feedstock, improving the heating values. In addition, torrefaction char has improved grindability, resulting in less energy use for size reduction before firing. Lastly, torrefaction char has lower equilibrium moisture content and higher density. This results in lower transport and storage costs and higher received heating values. However, recent discussions suggest that critical properties and benefits are rarely achieved simultaneously and that economically profitable large-scale production should not be assumed (Agar and Wihersaari, 2012).

2.4.5. Process drawbacks

Dry thermochemical conversion processes mentioned above have been used for centuries, and recent developments have increased the quality of these processes to make them available for the urgently required shift from fossil to renewable resources. These processes are readily applicable to producing high-quality gaseous, liquid, and solid fuels. However, dry thermochemical conversion

processes have some limitations as they commonly require elevated temperatures and active pre-drying of the feedstock, consuming a significant amount of energy. When processing biomass with high moisture content, water is evaporated prior to reaching the desired reaction temperature. The evaporation process requires additional energy consumption, which leads to a negative effect on the energetic balance of the system, resulting in lower net energy efficiency, thereby affecting the process economy. These processes are more efficient for feedstocks with relatively low moisture; however, PPMS is available with a relatively high-water content of 37 to 99 % (Kaur et al., 2020). If water has to be evaporated, the process becomes energy-intensive and inefficient. Alternatively, hydrothermal processes are investigated. These processes can produce high-quality fuels and materials with different characteristics than their dry initial substrates at lower temperatures, and more importantly, without the need for pre-drying (Kruse et al., 2013). The hydrothermal carbonisation (HTC) process, in particular, is most commonly used to carbonise biomass. The process efficiently produces large amounts of char, has high carbon recovery rates, and can be applied to a broad range of feedstock (Fuertes et al., 2010, Titirici et al., 2007). The overview of the HTC process, including the chemistry, product yields, and hydrochar applications, will be discussed in the upcoming sub-sections.

2.5. Hydrothermal Carbonisation (HTC)

Hydrothermal carbonisation (HTC) is an emerging technology that upgrades unconventional substrates into carbon-rich products without the need for pre-drying (Funke and Ziegler, 2010). The exothermic process occurs in the presence of liquid water, at temperatures ranging from 180-350 °C, and self-generating pressure in a closed system from a few minutes to several hours (Berl and Schimdt, 1932, Funke and Ziegler, 2010, Merzari et al., 2018). The during HTC process, the predominant reactions, namely dehydration and decarboxylation, lower the oxygen and hydrogen content from the biomass or a source of starch while increasing the carbon fractions (Funke and Ziegler, 2010), leading to a conversion into a valuable carbon material in the form of a solid char. The resulting coal-like material, commonly referred to as hydrochar, has good dewatering properties, improved hydrophobicity, and, when dried, has a higher calorific value compared to the initial feedstock (He et al., 2013b). The hydrochar obtained from the HTC treatment has a variety of benefits and applications in solid fuel, soil amelioration, low-cost adsorbent, catalyst, and

contaminant removal (Fang et al., 2018b). Other products include non-condensable gases (mainly CO_2), aqueous phase products (residues, sugars and organic acids) and water (Hoekman et al., 2011).

HTC process, also referred to as hot compressed water treatment, subcritical water treatment, wet pyrolysis, wet torrefaction, and hydrothermal treatment, was first introduced by Friederich Bergius in 1913 to mimic the natural process of coal formation that converted cellulose into coal-like materials (Bergius, 1913, Funke and Ziegler, 2010). However, its application did not receive significant attention for upgrading various biomass and waste feedstocks until the recent ten years. Recently, hydrothermal treatment has been re-discovered as an essential method for the production of various carbonaceous solid products, means of CO_2 sequestration, soil quality upgrading and energy source (Wang et al., 2001, Titirici et al., 2007, Kleiner, 2009, Rillig et al., 2010, Ro et al., 2010, Libra et al., 2011). HTC seems feasible for upgrading wet, low-value fuels by increasing respective energy density, decreasing oxygen and volatile contents and enhancing hydrophobic properties (Libra et al., 2011, Funke and Ziegler, 2010), particularly sludge, a low-cost moisture-rich feedstock. The conversion of sludge to solid hydrochar increases potential use in energy production and provides significant ease in handling, storage, and transport (Mäkelä et al., 2015). The majority of published academic literature on HTC for hydrochar production use plant biomass, concentrating on carbonisation of model compounds such as cellulose (Lu et al., 2014, Gao et al., 2012) along with virgin wood materials (Reza et al., 2013b, Reza et al., 2014b), herbaceous (Hoekman et al., 2013, Oliveira et al., 2013) and mixed feedstocks (Oliveira et al., 2013, Lu and Berge, 2014, Prawisudha et al., 2012) for clarifying carbonisation mechanisms and hydrochar properties.

2.6. Advantages of HTC Conversion

A brief comparison of thermochemical processes for biomass conversion is presented in Table 2.2. Integrating the HTC process to beneficiate sludge as an alternative to waste disposal offers several environmental, economic and energetic advantages. HTC is widely considered more effective if compared to pyrolysis or biological treatments. Processing time is one of the various advantages HTC offers over biological treatments such as anaerobic digestion. For example, HTC takes several minutes to a few hours compared to days or months for biological processes. Unlike biological treatment, HTC is not affected by toxic compounds, as

high process temperatures eliminate pathogens and inactivate potential contaminants such as pharmaceuticals, yielding sterile and hygienic products (Libra et al., 2011).

Biomass feedstock such as agricultural residuals, food processing wastes, municipal, agricultural and industrial sludges generally contain high water content, representing a limitation for suitability for dry conversion processes, particularly pyrolysis, gasification torrefaction and combustion. These processes require feedstock drying prior to conversion and, depending on the feedstock moisture content, the process of drying alone may require a significant amount of energy.

Contrary to these thermal methods, heterogeneous wet organic residues and waste streams with moisture content higher than 70% can be processed through HTC without preliminary separating and drying. Furthermore, the phase change from water to steam is largely avoided; thus, the required energy to heat the water (in a closed system to saturation conditions) is smaller compared to the energy required to evaporate the same mass of water (Lu et al., 2012, Berge et al., 2011). HTC also requires lower process temperatures (180-350^{o}C) compared to pyrolysis and gasification (>400^{o}C and >800^{o}C, respectively).

The resulting suspension from the HTC process is easily dewatered, making an interesting application for the energetic use of organic waste with high moisture content, such as waste activated sludge from pulp and paper wastewater stream, which requires intensive energy for incineration.

HTC is an efficient process for carbon sequestration to mitigate environmental problems such as climate change. Organic wastes decompose in an oxygen-free environment, such as landfills, and release CH_4 and CO_2 into the atmosphere. HTC process transforms these organic wastes into carbon-rich solid, thereby reducing gas emissions from the natural decomposition of organic wastes, whilst producing a value-added product and unlocking most efficiently the energetic potential in organic wastes: waste-to-energy system. Gaseous products such as CO_2 and CO is limited as oxygen exposure is limited to its initial presence in the reactor headspace. Ramke et al. (2009) reported carbon content in solid, liquid and gaseous product yield is 75-80%, 15-20% and 5%, respectively. Thus, most of the original carbon present in the substrate stays bound to the final coal product. Moreover, HTC of biogenic materials produces high carbon-efficient hydrochar compared to other biomass treatment emerged as potential energy alternative strategy to produce renewable solid fuel source. Carbon efficiency higher than 90%

can be attained through HTC compared to other biomass treatment technology (Titirici et al., 2007).

The quality and quantity parameters such as structure, size and functionality of the hydrochar produced through HTC can be varied by changing residence time, feedstock type and concentration, and the addition of additives and stabilisers (Lu et al., 2012). The chemical structure of hydrochar more closely resembles natural coals than pyrolysis-derived chars (Libra et al., 2011), which is a critical characteristic to account for when considering future applications of hydrochar. Hydrochar has a variety of potential applications apart from solid fuel, some of which will be discussed in this review.

Table 2.2: Comparison of thermochemical conversion processes.

Treatment	Feed	Conditions	Products
Slow pyrolysis	Dry	~400°C, absence of air	Biochar (35 %), liquid (30%), gas (35%)
Fast pyrolysis	Dry	~500°C, absence of air	Biochar, mostly liquid, gas
Gasification	Dry	> 800°C, limited oxygen supply (O_2 or H_2O)	Solid (5-10%), syngas
Torrefaction	Dry	280-350°C, absence of air	Solid, torrefied biomass, gas
HTC	Wet	180-350°C, autogenous pressure	Hydrochar, process water, gas

2.7. HTC Process Conditions

The operational conditions of HTC differ in different works. Funke and Ziegler (2010) have outlined a range of operational conditions associated with HTC while cautioning that a strict, standard definition has yet to be established. General operation conditions have been established as follows:

- The operation should be limited to subcritical conditions of water to impede hydrothermal gasification that would result in carbon products such as CH_4 and H_2.

- Temperatures must be above 100°C so that reactions take place. However, it has been noticed that practical implementation of HTC is unlikely outside the range of 180-250°C.
- There needs to be a liquid water phase. Therefore, at least saturated pressure is necessary.
- Feedstock needs to be wholly submerged throughout the process to produce little to no gas (1-5%), whilst most organic remains or are converted to solid. In the absence of contact with water, biomacromolecules may undergo pyrolytic reactions that create such products as CO and tars. In real-life situations, this is likely to occur to a small degree and may help to explain the production of trace amounts of these substances during HTC. In addition, reactant material above the liquid surface may not carbonise.
- The pH value should be below 7. Alkaline conditions lead to a substantially different product. Due to by-products, the pH value drops automatically during hydrothermal carbonisation.
- The residence time cannot be limited to a meaningful range, as the reaction rates are largely unknown. Typically, residence times will vary between 1 and 72 hours. Residence times combine with the temperature regime to produce a ''reaction severity". Higher temperatures or longer residence times represent a high reaction severity. In such conditions, the solid product yields are lower, yet these products tend to have higher carbon content.

Higher temperatures up to 300°C, very high pressures (12-20 MPa), and the application of catalysts produces more liquid hydrocarbons and more gas. Hydrothermal treatment at this condition is called hydrothermal liquefaction (Behrendt et al., 2008, Yokoyama, 2008); however, most liquefaction processes are carried out using organic solvents instead of water (Behrendt et al., 2008) and in alkaline medium (Venderbosch and Sander, 2008). At further increase in temperature and pressure, usually above 350°C and 20 MPa, and with catalyst, the supercritical state for water is reached, forming mainly combustible gaseous products. This gasification process is termed "hydrothermal gasification" (Peterson et al., 2008, Yokoyama, 2008) or "hydrogasification" (Basu, 2010). The

hydrothermal routes which occur in hot-compressed water are illustrated in Figure 2.2.

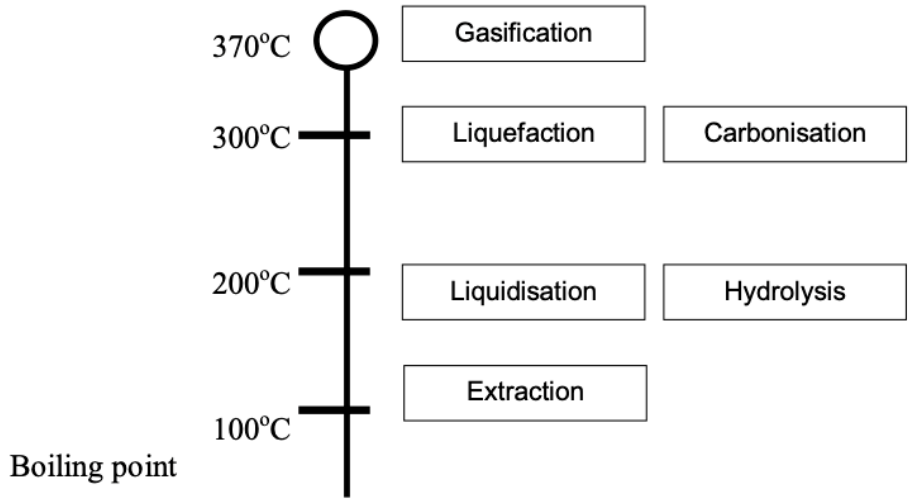

Figure 2.2: Hydrothermal routes occurring in hot-compressed water (Yokoyama, 2008).

2.8. HTC Reaction Mechanisms

As previously mentioned, wood is the primary source of cellulose for pulp and papermaking, and it consists of lignocellulose which makes up the main components of PPMS, thus considered biomass. This section presents the chemistry of hydrochar formation is discussed.

2.8.1. Biomass conversion

The primary variables of the HTC process are reaction temperature, reaction time, pressure and feedstock (Funke and Ziegler, 2010, Reza et al., 2014b). Under operational conditions, several reactions may occur during the HTC process, forming a complex chemical network. However, the complex reaction network is not known in detail yet; hence a chemical mechanism for HTC is difficult to define (Funke and Ziegler, 2010, Gómez et al., 2020). Thus far, a separate discussion and agreement of general reaction mechanisms have been identified to provide useful information about the possibilities of manipulating the reaction. These mechanisms include hydrolysis, dehydration, decarboxylation, condensation polymerisation, and aromatisation (Funke and Ziegler, 2010, Libra et al., 2011, Gómez et al., 2020). They do not represent consecutive reaction steps, instead form a parallel network of different reaction paths. The precise nature of these mechanisms and their

relative significance during the course of the reaction primarily depends on the type of feedstock (Funke and Ziegler, 2010).

The HTC process is mainly governed by hydrolysis, which leads to the cleavage of ester and ether bonds (mainly β-(1-4) glycosidic bonds) of hemicellulose temperatures higher than 180°C, and both cellulose and lignin (partially) at temperatures higher than 200°C by the addition of water (Funke and Ziegler, 2010). Hydrolysis of hemicellulose produces acetic acid, D-xylose, D-mannose, D-galactose and D-glucose. These last three are typically converted into 5-hydroxy-methyl-furfural (5-HMF) followed by formic or levulinic acid (Wang et al., 2018). The cellulose follows an analogous pathway, hydrolysing into D-glucose, producing 5-HMF and subsequently into formic or levulinic acid. The degradation of lignin typically releases/forms phenol and phenolic derivatives (Figure 2.3).

It has been reported that dehydration and decarboxylation govern the process; therefore, it is an exothermic process. Dehydration and decarboxylation mechanisms mainly lower H/C and O/C ratios during HTC (Wang et al., 2018). Hydroxyl groups are generally eliminated by dehydration, while carbonyl and carboxyl groups are removed during decarboxylation (ibid.). Hydrolysis fragments formed during HTC are reactive; hence they undergo condensation and polymerisation to form hydrochar. At subcritical and near-critical temperatures (Figure 2.4), ionic reactions are the main mechanism of formation, while at supercritical temperatures, free-radical reactions are predominant. High reaction conditions lead to the formation of aromatic structures (aromatisation) (Basso et al., 2013). Experiments on the enhancement of the formation of aromatic compounds with the enhancement of temperature and pressure during an HTC process have been reported (ibid.). The formation of aromatic bonds during the hydrothermal process could decrease the total carbon content of the hydrochars.

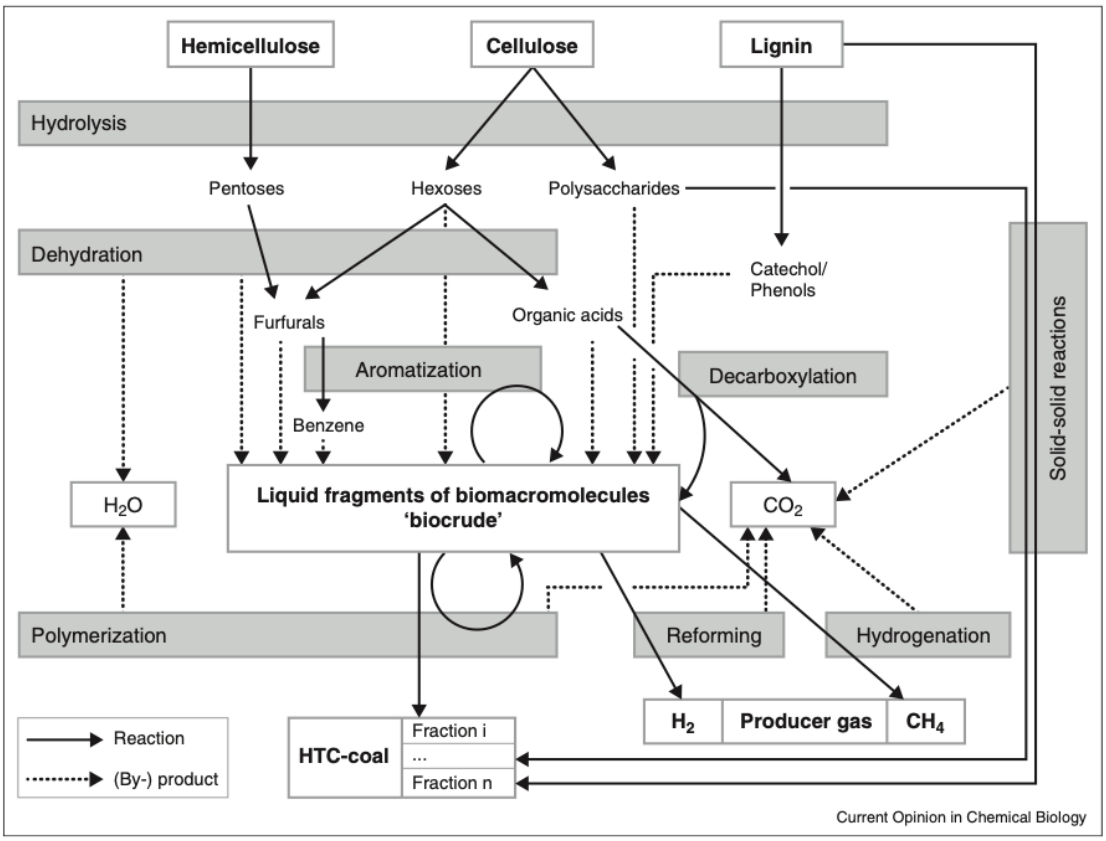

Figure 2.3. Reaction routes of hydrochar formation in subcritical water temperature (Kruse et al., 2013).

Other mechanisms involved in HTC include demethylation, transformation reaction, pyrolytic reactions and Fisher-Tropisch-type reactions (Basso et al., 2013). Demethylation is the chemical process through which a phenol becomes part of a catechol-like structure of the coal (ibid.) and consists of the removal of a methyl group (CH_3) from the molecule. Transformation reactions in lignin may occur when the hydrolysis and the subsequent condensation cannot occur, mainly for stable compounds with a crystalline structure and oligomer fragments (ibid.). Pyrolytic reactions may occur at temperatures higher than 200°C and contribute to forming carbonaceous products from the fragments of feedstock that could not come into contact with water because they are trapped by precipitation of condensed fragments (ibid.).

2.8.2. Energetic Aspects of HTC

HTC is considered an exothermic process. During the process, part of the chemical energy present in the feedstock is released in the form of heat, reflected

by the negative sign of enthalpy of reaction. As an example, Bergius (1913) described the occurrence of degradation of cellulose during HTC as follows:

$$(C_6H_{12}O_5)_4 \rightarrow C_{21}H_{16}12H_2O \qquad (2.1)$$
$$\Delta H_R = -297.9\ \mathrm{Kj/mol}$$

The simplified dehydration mechanism of glucose formulated by Titirici et al. (2007) takes place as follows:

$$C_6H_{12}O_6 \rightarrow C_6H_4O_2 + 4H_2O \qquad (2.2)$$
$$\Delta H_R = -1040\ \mathrm{Kj/mol}$$

Also commonly found, according to Ramke et al. (2009), Röthlein (2006) and Buttmann (2011):

$$C_6H_{12}O_6 \rightarrow C_6H_2O + 5H_2O \qquad (2.3)$$
$$\Delta H_R = -950\ \mathrm{Kj/mol}$$

For the energy to be released and utilised, the activation energy has to be overcome. Once activated, HTC is a spontaneous process liberating up to a third of the combustion energy stored in the carbohydrates through dehydration (equations 4 and 5). A comparison of the input energy content versus the output energy content has been reported by Ramke et al. (2009) using the higher heating value (gross calorific value). 60-90% of the gross calorific value of the feed was found in the solid yield, whilst the remainder was released as heat during the HTC process (exotherm) or chemically bonded in carbon dissolved in the liquid products. The quantity of the heat released depends on the type of feedstock and process conditions. However, Buttmann (2011) indicated that the heat released by the exothermal process does not compensate for the heat losses during the process. Hence, external heat is required to sustain the reaction.

2.9. Effect of Process Operating Parameters

HTC process is mainly governed by temperature, pressure, residence time, pH, feedstock composition and water to biomass ratios (w/b) (Basso et al., 2013, Funke and Ziegler, 2010).

2.9.1. Role of water

Water is evaluated to be the best HTC medium due to its behaviour in hot-compressed conditions. Under these conditions, water behaves as a catalyst and reactant for organic compounds and as a solvent for polar macromolecules (Basso

et al., 2013). Water also has good heat transfer properties, allowing a homogeneous temperature distribution throughout the reactor volume (ibid.). Figure 2.4 shows the general HTC condition on the phase diagram of water. Water density is strongly influenced by pressure. An increase in pressure allows operating conditions with medium-high densities, resulting in higher solvent power than water vapour.

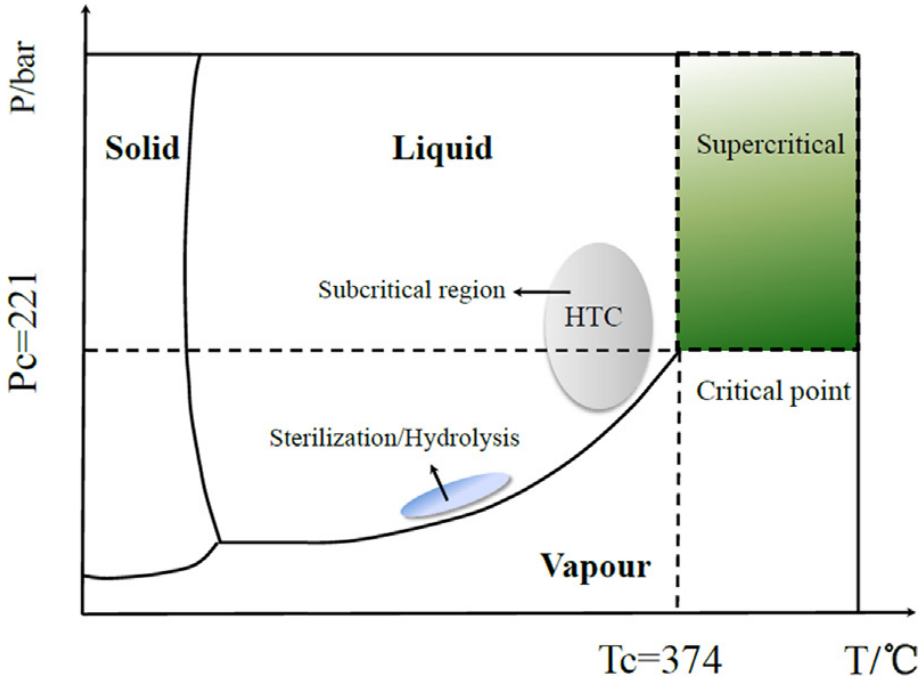

Figure 2.4: Water property changes under different temperatures and the application field of hydrothermal processes (Wang et al., 2018).

Furthermore, the dielectric constant (ε) parameter is directly connected with the possibility for a solvent to dissolve polar rather than nonpolar compounds. A high value of ε is typical for polar solvents, such as water at standard conditions. The dielectric constant of water decreases with an increase in temperature, as shown in Figure 2.5. At hydrothermal conditions, ε value of liquid water is considerably lower than that at standard conditions. At 200°C, the value of ε of water is very close to that of methanol at standard conditions. As a result, the solubility of many organic compounds is highly improved, thus providing a more homogeneous reaction environment, useful to achieve higher conversions (Basso et al., 2013).

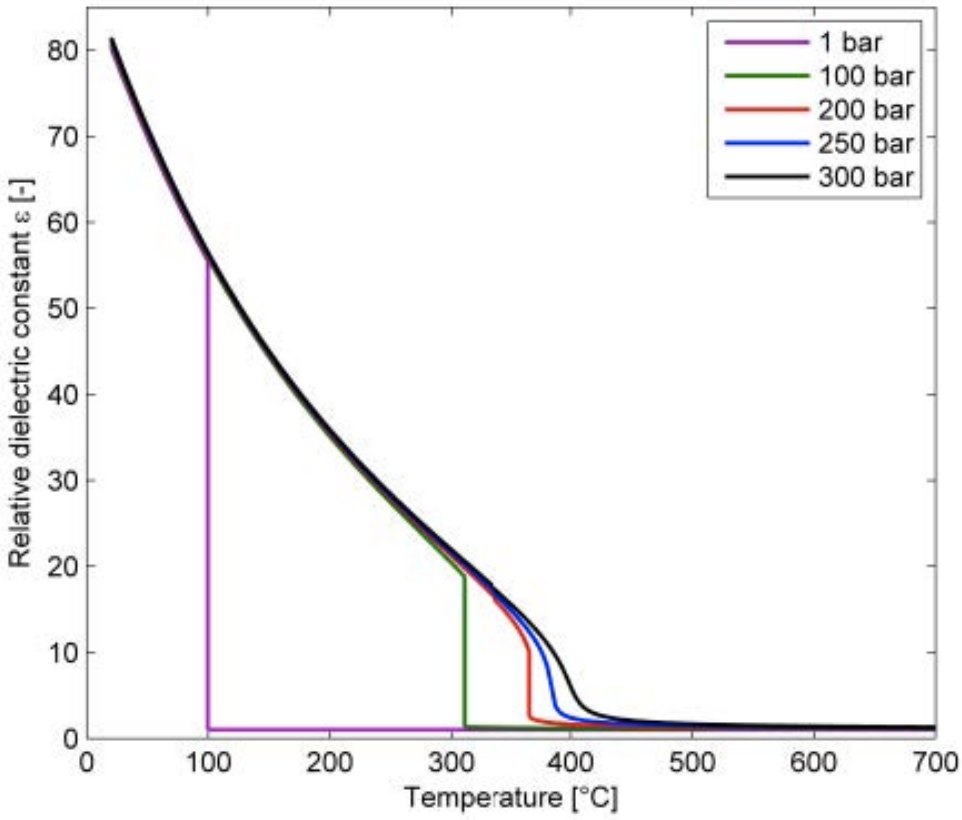

Figure 2.5. Relative dielectric constant of water as a function of temperature and pressure (Basso et al., 2013).

In the HTC process, the amount of water should be enough to ensure the complete dispersion of biomass in the reaction medium, which results in more efficient hydrothermal reactions. Water consumption and required energy for heating increase with an increase in water to biomass ratios (Heidari et al., 2019).

2.9.2. Temperature

The HTC process is mainly influenced by temperature (Funke and Ziegler, 2010). It determines the water properties that cause ionic reactions in the supercritical region (Wang et al., 2018). An increase in temperature leads to an increase in the carbon content of the solid product and a general decrease in hydrochar yield (ibid.). HTC experiments on loblolly pine at 200 and 230°C showed that hydrochar mass yield at 230°C was about 10% lower than that of 200°C for the same retention time (Yan et al., 2014). A similar effect is observed from HTC on law grass at 200 and 240°C and retention time of 180 min (Guo et al., 2015). This is because, at higher temperatures, a more significant portion of lignin and cellulose will participate in the reaction, while at lower temperatures, mostly hemicellulose

undergoes degradation (Heidari et al., 2019). Higher temperatures favour the dehydration and decarboxylation reactions, which correspond to a decrease of the feedstock's oxygen and hydrogen contents, consequently decreasing the O/C ratio enhancing the carbon content of the solid product.

On the other hand, Higher temperatures drive the reactions to generate more liquid and gaseous products, decreasing the solid phase. The partial degradation of hydrochar produced at higher temperatures contributes to lower hydrochar mass yield (Basso et al., 2013). Carbonisation occurs with difficulty at temperatures lower than 180°C because cellulose and hemicellulose typically decompose at temperatures higher than 180-200°C (ibid.). Temperatures below 180°C have negligible influence on the chemical composition of hydrochar, as most of the polysaccharides do not degrade in lower temperatures (ibid.), resulting in hydrochar more similar to the original feedstock. The higher the temperature, the more homogeneous, dense and uniform solid product of the HTC reaction (ibid.). Lignin content decreases with an increase in temperature. This is mainly due to enhancing its degree of oxidation with temperature. The Decrease in O/C ratio corresponds to the removal of oxygen from the feedstock and results in hydrochar with enhanced higher heating value (HHV) with an increase in temperature (Heidari et al., 2019, Basso et al., 2013). In terms of energy, dehydration and decarboxylation have a negative heat of reaction. Therefore the amount of energy released is expected to increase, making the HTC process exothermal at higher temperatures (Basso et al., 2013).

2.9.3. Pressure

Pressure is self-generating and increases autogenously during the HTC process. It is mainly considered an indirect parameter since the HTC process is highly dependent on temperature. Maintaining water in the liquid phase is compulsory to develop an HTC system. In a closed system, the increase in pressure results from increased temperature. If the temperature rises above 100°C, then the resulting vapour pressure in the system is the saturated pressure of water, which means that further evaporation of water will lead to condensation of the same amount of water vapour (equilibrium). For example, in a pressure vessel with temperatures ranging from 180-220°C, the resulting water vapour pressure (saturated vapour pressure) ranges between 9-22 bars (Ramke et al., 2009).

Temperatures above 100°C result in higher pressure than the saturated water pressure due to the formation of gases.

Pressure variations are considered to move the equilibrium of an HTC process according to Le Chatelier's principle (Basso et al., 2013). Dehydration and decarboxylation reactions are reported to be weakened by higher pressures. However, pressure increase results in easier dissolution in the water-extractable present in biomass (ibid.).

2.9.4. Residence time

Residence time plays an important role, especially regarding process design, as it strongly affects thermal and energy consumptions. Residence time for an HTC process typically ranges from a few minutes to several hours. An increase in residence time generally results in higher carbon content hydrochar (Basso et al., 2013), translating to higher calorific values in the solid product. Residence time reduces the total solid yield, favouring the formation of higher quantities of water-soluble compounds (Basso et al., 2013, Funke and Ziegler, 2010, Wang et al., 2018). Longer residence times allow improvement of dehydration and decarboxylation reactions (Basso et al., 2013) and lead to the polymerisation of fragments solved in the liquid phase involving the formation of secondary hydrochar with a polyaromatic structure (Wang et al., 2018). Longer residence times result in secondary hydrochar formation, especially for lignocellulose feedstock, as the dissolved monomers require extensive polymerisation (ibid.). However, the behaviour of non-dissolved monomers is affected by temperature; hence residence times allows the control of the degree of polymerisation of the soluble monomers during the HTC process (ibid.). Moreover, cellulose can carbonise at lower temperatures (200°C) if longer residence times are employed (ibid.).

2.9.5. pH

During HTC reactions, acidic compounds, including acetic, formic, levulinic and lactic acids, are formed, which usually cause the pH to drop (Basso et al., 2013, Wang et al., 2018, Funke and Ziegler, 2010). The acidic conditions commonly catalyse the carbonisation of biomass by facilitating the hydrolysis of cellulose (Basso et al., 2013); thus, HTC is considered an autocatalytic process. The effect of pH influence on decarboxylation and condensation polymerisation is still

unknown. Higher pH values in HTC leads to the formation of products with higher H/C ratios, corresponding to hydrochars with more bituminous characteristics (ibid.). Adding acids to the process does not result in different amounts of heat release during HTC (ibid.).

There are different conclusions on the influence of pH on the HTC process. Mumme et al. (2011) observed interference in the carbonisation process at low pH conditions, while the carbon content in hydrochar does not seem to be affected by this parameter. Titirici et al. (2007) suggested a catalytic effect of acidic conditions on the HTC process. Heilmann et al. (2011) did not find such an effect on the HTC process in the presence of citric acid. Funke and Ziegler (2010) observed that neutral to weakly acidic conditions improve the overall rate of the HTC reaction and is necessary to achieve a simulation of natural coalification.

2.9.6. Water: biomass ratio

The water to biomass ratio is defined in equation 6. Its inverse is called solid load.

$$\frac{w}{b} = \frac{mass_{biomass\ moisture} + mass_{added\ water}}{mass_{dry\ biomass}} \quad (2.4)$$

Higher w/b ratios favour hydrolysis reactions, resulting in higher carbonation rates (Heidari et al., 2019). An increase in water positively affects the surface and volume of solid yield (ibid.). However, a lower w/b ratio leads to lower residence times (due to earlier polymerisation) and higher hydrochar yield (ibid.). During HTC, the amount of water should be enough to ensure HTC reaction throughout the feedstock sample and ensure sufficient heat and mass transfer, as these factors highly affect the density, structure and hydrophobicity of feedstock (ibid.). They also affect the reactor design. Higher biomass density requires a high amount of water to ensure enough heat and mass transfer throughout. Biomass with porous structure can easily allow water penetration to the porous, hence requiring less water. More hydrophobic feedstock requires a higher amount of water to ensure HTC reaction.

2.9.7. Other parameters

Feedstock composition, i.e. low in carbon and high in ash, results in hydrochar with poor quality. Heat and mass transfer limitations decrease with an increase in heating rate and consequently reduce the time for secondary reaction of the intermediate products (Wang et al., 2018). Hydrolytic agents or catalysts

improve hydrolysis rate. Acidic catalysts are more effective for hydrolysis, whilst basic catalysts inhibit the formation of solid products and promote the formation of liquid oil. Moreover, the use of catalysts may reduce NO_x converting into N and H_2O (Nizamuddin et al., 2017).

2.10. Products of HTC

The products resulting from HTC treatment are a solid phased mainly composed of carbon content, generally known as hydrochar, a liquid phase composed of phenolic compounds and furan derivatives (Xiao et al., 2012) dissolved and a small quantity of a gas which is mostly carbon dioxide (Basso et al., 2013). Typical product yield in comparison to other thermal treatments is shown in Table 2.2. The carbon fraction distribution depends on the feedstock type and reaction conditions such as temperature, residence time, and total solid content. Table 2.3 shows the carbon distribution in the three different phases for different substrates after HTC.

Table 2.3: Carbon fraction distribution in the HTC product (Ramke et al., 2009).

Substrate	C in solid (%)	C in liquid (%)	C in gas (%)
Organic waste	74.9	19	6.1
Green cuttings	75.3	19.7	5.0
Biogas slurry	72.2	22.1	5.7
Straw	75.4	19.7	4.9
Chipped wood	82.9	14.1	3.0

Upon completion of the HTC process, about 14-20% of the organic carbon initially present in the feedstock remains in the liquid phase in the form of total organic carbon (TOC) such as organic acids, furfurals and phenols, among others, and only 3-6.1% of the carbon is converted to gas products. The remaining 72-82.9% of the carbon fraction from the feedstock is thus bound in the solid product.

2.10.1. Gas yield

The gas formed during the HTC process mainly consists of CO_2 with traces of CO, CH_4 and H_2 (Funke and Ziegler, 2010). Traces of ethane, ethylene and propene, propane and butane have also been detected (Lu et al., 2012). The amount of carbon present in the gaseous product is mainly due to decarboxylation. Gaseous products increase with the increase in reaction temperature whilst the fraction of CO decreases while CH_4 and H_2 increase (Funke and Ziegler, 2010). Compared to combustion or pyrolysis, the lower yield of gaseous oxidation compounds during the HTC process could be attributed to the limited oxygen available given the reaction conditions. HTC conditions, mainly temperature and retention time, and the biomass feedstock determine the yield of products.

2.10.2. Liquid yield

The process water remaining after the filtration of hydrochar usually contains high loads of inorganic and organics (Funke and Ziegler, 2010). The organic compounds include acetic acid, aldehydes and alkenes, and aromatics such as furanic and phenolic compounds (Berge et al., 2011, Lu et al., 2012). The liquid product may also contain non-agglomerated colloidal carbonised material (Heilmann et al., 2011) and the formation of tar fraction consisting of polar compounds of high molecular mass (Müller and Vogel, 2012). A GC-MS analysis performed by (Xiao et al., 2012) detected the presence of sugar compounds such as furfural, 2-ethyl-5-methyl-furan and 2-hydroxy-3-methyl-2-cyclopenten-1-one, and lignin-derived compounds including phenols, particularly phenol monomers such as 2,6-dimethoxyl, butyl-2-methylpropy-lester-1,2-benzenedicarboxylic acid and butyl 4-ethoxy-2,5-dimethoxy-benzaldehyde. BOD, COD and TOC concentrations of process water are similar to those typically found in landfill leachate. BOD/COD ratios of the liquid products are commonly higher than 0.3 (Berge et al., 2011). TOC in HTC wastewater represents the dissolved carbon that could not stay bound to the hydrochar. Process water from HTC can be treated with aerobic or anaerobic treatment to lower TOC concentration significantly (Funke and Ziegler, 2010). The pH of the liquid product is usually acidic due to the presence of organic acids formed during the reaction.

2.10.3. Solid yield

The solid product, called hydrochar, is the main product resulting from HTC and is usually separated from the liquid product by filtration. Depending on the operating conditions, the structure of hydrochar resembles lignite or sub-bituminous coal (Funke and Ziegler, 2010). Hydrochar is higher in C content and lower in H/C and O/C ratios than the initial feedstock due to dehydration and decarboxylation mechanisms. The increase in reaction severity leads to a decrease in solid yields; however, both H/C and O/C ratios also decrease, leading to higher densification and higher energy values (Berge et al., 2011, Hoekman et al., 2011, Sevilla and Fuertes, 2009). Typical values of coal resulting from different reaction severity are shown in the Van Krevelen diagram (Figure 2.6). The molar H/C ratio is plotted against the molar O/C ratio in the diagram. The dehydration pathway follows a straight line which decreases both H/C and O/C ratios, moving from top right to bottom left; decarboxylation moves from bottom right to top left, thus enhancing the H/C ratio and lowering the O/C ratio. The degree of carbonisation can be visualised by the length of the vector that binds the two dots representing the input and the output material for different feedstocks. During the HTC process, the dehydration mechanism is generally more critical than decarboxylation; this explains why the products of HTC are always located at the bottom left of the diagram. Berge et al. (2011) reported higher H/C and O/C ratios associated with hydrochar from food waste substrate and anaerobically digested sewage sludge.

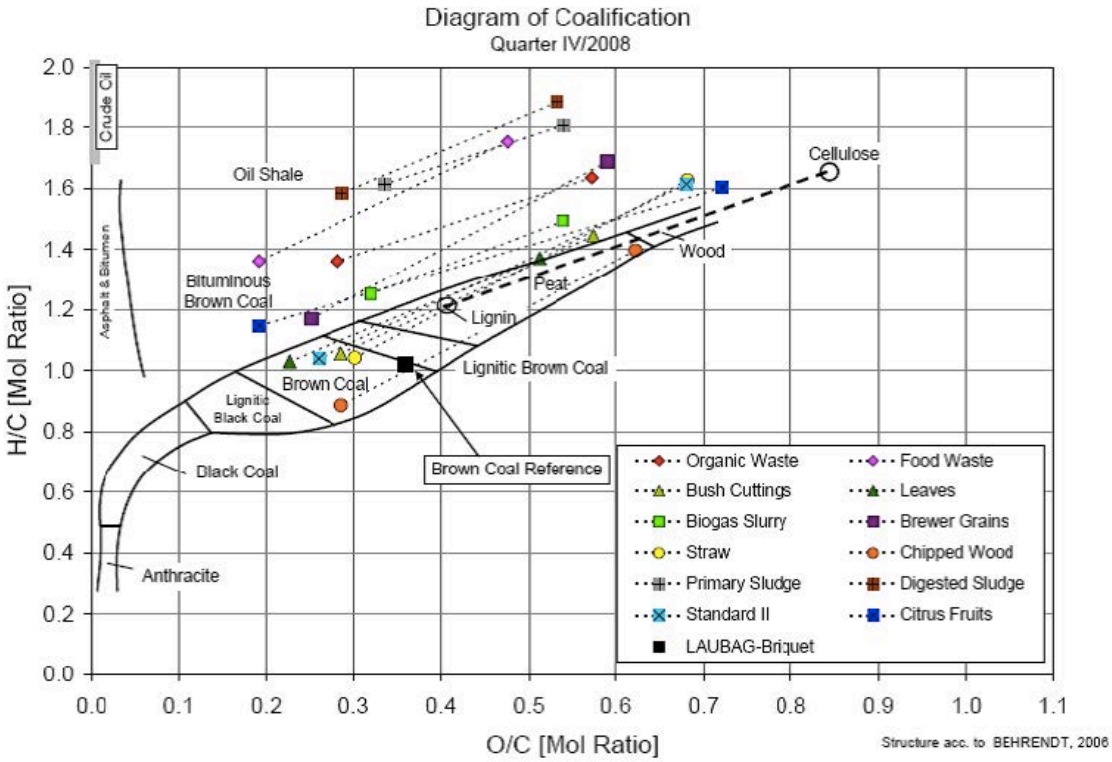

Figure 2.6: Typical coalification diagram (Ramke et al., 2009)

In terms of structure, hydrochar resulting from non-structural carbohydrates are generally agglomerations of micrometre-sized carbon spheres that result in a sponge-like network of particles; however, the nature of the particle morphology depends on the feedstock and process conditions (Titirici et al., 2007). Moreover, the chemical properties in the particle core differ from the shell. Oxygen bonds are fairly stable in the core, and fewer oxygen bonds are found on the shell (ibid.). Therefore, particle cores tend to have hydrophobic properties composed of fused aromatic rings, and the shell tends to have hydrophilic properties; this is because longer carbonisation times lower amounts in carboxyl and hydroxyl groups which increases the hydrophobic properties of hydrochar particles (Funke and Ziegler, 2010). The hydrophobicity of the hydrochar makes the dewatering process of the solid product easier than the original feedstock and improves its stability for the use of hydrochar as an amendment (Berge et al., 2011). The surface area of hydrochar varies from 25-30 m^2/g, and the adsorption isotherms fit type II isotherm, according to IUPAC classification (Prawisudha et al., 2012) which is an essential characteristic for adsorption applications and carbon precursor (Kumar et al., 2011, Bernardo et al., 2012, Unur, 2013).

2.11. Potential Applications of Hydrochar

Recently, various value-added applications of hydrochar have received significant attention in energy storage and environmental protection. The applications of hydrochar for solid fuel, energy storage, soil amendment, adsorbent and catalyst are discussed hereunder.

2.11.1. Solid fuel

Combustion is one of the primary uses of hydrochar produced from HTC. The CO_2 emitted during combustion is balanced by the CO_2 captured by the biomass growth, thus being considered a carbon-neutral energy source. Options in which hydrochar can be used as combustible include combustion plants, combined heat and power plants, cement and steel factories, mono-combustion plants and gasification (Kläusli, 2012). Hydrochar can be used in developing countries as cooking fuels replacing firewood or charcoal derived from wood, consequently positively impacting deforestation. Escala et al. (2013) investigated the application of HTC for the treatment of sewage sludge from the wastewater treatment plant. The study involved comparing two scenarios; one where sewage sludge was dried and incinerated in a combustion plant, and the other where the sewage sludge was hydrothermally carbonised, mechanically dewatered and then incinerated. It was concluded that approximately 10% of energy and up to 75% of the cost for waste management could be saved per year with the application of HTC. Moreover, this process could improve the CO_2-balance by 95%.

AVA-CO2 Schweiz AG introduced the world's first industrial-scale HTC plant in 2010 to convert biomass waste into an energy resource. The plant produces CO_2-neutral hydrochar (bio-coal) with a calorific value of 25 MJ/kg from various waste streams. It produces roughly 8 000 tons annually from approximately 40 000 tons of biomass and 10 000 m^3 of water. Both feedstock and process water are recirculated and easily treated upon use. The feedstock includes agricultural residues, oil-bearing plant plantation residues, fruit industry waste, spent grains, malting waste, and waste coffee grounds and tea leaves, which are relatively high in sugars, starches, and cellulose hemicellulose. Due to process efficiency and related environmental issues, feedstock containing relatively high protein or lignin is avoided. The HTC operating conditions at the AVA-CO2 plant occurs at 220^{o}C and about 20 bars of pressure. According to AVACO2, the advantages over biomass

waste includes higher suitability for long term storage, reduced storage, transport and drying costs, easier and more stable fuel combustion, higher carbon efficiency, lower fuel sulphur and nitrogen levels, hydrophobicity, ease of grinding and lower ash melting point (AVA-CO2 Schweiz AG, 2012). Such results and advantages are consistent with those found in the literature for laboratory-scale fuels (He et al., 2013a, Reza et al., 2012, Liu et al., 2014).

Similarly, TerraNova (2017) introduced a commercial-scale HTC plant to convert 40,000 tons per year of sewage sludge from 50,000 habitants into regenerative fuel. The plant, located in Jining, China, operates at 200ºC and 20-35 bar with the addition of catalyst. The lignite-like fuel produced from this process generates energy in lignite-fired power plants or reduces energy requirements in cement plants or waste incineration plants.

2.11.2. Energy storage

Carbonaceous materials produced from hydrochar have promising properties such as energy density, surface area, portability, and stability for application as supercapacitors and as anode and cathode materials for Na^+ and Li^+ batteries and fuel cells (Reza et al., 2014a). Graphite and activated carbon are mainly used for Li-ion batteries and supercapacitors. Hydrochar presents potential application as anode for both Li-ion and Na-ion batteries (ibid.). Activated hydrochar is reported to have higher capacitance than graphite or activated carbon (ibid.). However, the activation of the hydrochar is required by a strong base and temperatures above 600 C is required to increase the Brunauer-Emmett-Teller (BET) surface area with the removal of volatiles from the pores. During the process, the pores generate active sites upon activation, leading to hydrochar with active pores and BET surface area similar to that of activated carbon (ibid.). Authors have reported satisfactory performance of capacitors made from hydrochar produced from substrates such as cellulose, starch, sawdust and nitrogen-containing hydrochar (Wei et al., 2011, Zhao L et al., 2010). Nitrogen-doped graphene materials produced by HTC have the potential to reduce metal usage in anodes and cathodes (Reza et al., 2014a).

2.11.3. Soil amendment

The use of hydrochar for soil amendment has been outlined by (Fang et al., 2018b). Hydrochar can be used for carbon sequestration if they present a similar

recalcitrant form as biochar produced from pyrolysis. However, studies reported that HTC chars are less effective for climate mitigation. There were found to increase NH_3, CO_2 and NH_4 emissions from soil, although they decreased NO_2 emissions compared to unamended soil (ibid.); this is due to less stability of C in the hydrochar, as well as the fact that it stimulates more microbial activity, compared to biochar, as a result of its higher degradability (ibid.). Hydrochars, especially those derived from plant biomass, have low nutrient content; hence they cannot be used as fertilisers. However, they can be added to the soil to improve its fertility by reducing the amount of fertiliser lost through surface run-off (ibid.). Hydrochar consists of a porous structure which results in high surface area (Glaser et al., 2001). The nutrients are sorbed into the pores on the surface of the hydrochar, which consequently slowly releases them into the soil over time for plant uptake (Fang et al., 2018b). The effect of hydrochar on soil improvement has been reported by researchers. Bargmann et al. (2014) found that when hydrochar was added to soil, it improved yield for *phaseolus beans*; however, it decreased yield for leek to a small degree. Gajić and Koch (2012) reported reduced sugar beet growth by adding hydrochar to the soil. Furthermore, hydrochar can increase the amount of water that can be retained by the soil (Fang et al., 2018b). When added to soils such as sand soil known to have low available water capacity, hydrochar decreases the bulk density of soil and increases the total pore volume, allowing more water retention by the soil (ibid.).

2.11.4. Adsorbent

Adsorption is one of the main essential applications for hydrochar, particularly water remediation. Hydrochar can be activated to increase its pore size and surface area. The increased adsorption capacity allows activated carbons to adsorb various contaminants from the water or soil. Activated carbon is typically physical or chemical (Fang et al., 2018b). The physical activation process occurs with activating agents such as CO_2 or steam above 800^oC. Chemical activation occurs by mixing the hydrochar with a chemical activating agent such as KOH or H_3PO_4 and heating the mixture at different temperatures in an inert environment (*ibid.*). Due to its mean pore diameters (mesopores), hydrochars can adsorb large-sized molecules such as sugar and heavy metals, as well as small-sized molecules such as micropollutants (Fakkaew et al., 2018). Thus, hydrochars are potential adsorbents for removing heavy metals and micropollutants from wastewater.

2.11.5. Catalyst

Hydrochars can be used as heterogeneous catalysts or catalyst supports (Baccile et al., 2013). When HTC is processed in the presence of noble metal salts, it yields hydrochar loaded with metal nanoparticles (Baccile et al., 2013, Xu et al., 2007). These substances have been proven to catalyse the hydrogenation of phenol to cyclohexanone in a single step; this presents a significant improvement over the two-step or one-step process that traditionally occurs under harsh conditions and using commercially available catalysts. Moreover, carbonaceous nanofibers obtained through HTC have successfully been loaded with noble metal nanoparticles to create a hybrid catalyst for the conversion of CO to CO_2 under a low-temperature environment (Titirici and Antonietti, 2010); this presents a possibility for further improvement of fuel cells (Baccile et al., 2013). Liang and Yang (2009) synthesised a strong acid catalyst through HTC at low temperature; this can replace catalysts typically obtained through high heat and a two-step process. Furthermore, the nitrogen-doped char from HTC can act as catalysts or catalysts supports and offer a variety of possibilities of reaction selectivity and higher conversion efficiency in several processes (Libra et al., 2011). Hydrochar doped with TiO_2 through HTC has enhanced photocatalytic activity and is currently being investigated as a material that can boost solar photo-conversion (Baccile et al., 2013).

2.12. Gaps in literature

The mechanisms of hydrochar formation through HTC are mostly elucidated using pure organic substrates such as cellulose (Sevilla and Fuertes, 2009, Saha et al., 2019a), hemicellulose (Kang et al., 2012) and lignin model compounds, including guiacol (Wahyudiono et al., 2007), catechol (Wahyudiono et al., 2009), eugenol (Besse et al., 2015) and phenolic model compounds such as vanillin (Barbier et al., 2012) and diphenylether (Penninger et al., 1999). Complex feedstocks such as lignocellulosic biomass (Güleç et al., 2021, Kruse et al., 2013, Stirling et al., 2018, Xiao et al., 2012), sewage wastes (He et al., 2013a, Danso-Boateng et al., 2015, Spitzer et al., 2018), municipal wastewater sludge (Chen et al., 2020), olive wastes (Yay et al., 2021, Volpe et al., 2018) have also been explored to understand the reaction pathways involved. The physicochemical characteristics of the solid product, such as high energetic densities, increased carbon content and improved dewaterability allow hydrochar to be used directly as fuel to generate

power (Fang et al., 2018a). In addition, various studies have reported hydrochar with decreased levels of inorganic minerals, including Si, K, Na, Cl, P, Ca, Mg and Fe, which are known to cause toxic emissions, fouling, slagging and corrosion in combustion chambers (Yang et al., 2016, Lin et al., 2015b, Smith et al., 2016).

The majority of the research on the energy potential of hydrochar has been focused on the direct application of solid fuel (Antero et al., 2020). There are limited publications on the energetic aspects of hydrochar recovered from pulp and paper solid wastes. Lin et al. (2015b) examined the effect of HTC temperature (180-300 °C) on the conversion of paper sludge into clean solid fuel at a fixed holding time (30 min), solid load and stirring rate (300 rpm) and observed hydrochar with the highest improvement in calorific value at 210 °C (> 8 %), lower H/C and O/C ratios, reduced nitrogen and sulphur, in addition to lower ash as a result of the reduction in the concentration of chlorine, sodium and potassium species. Oumabady et al. (2020) optimised the HTC process parameters for producing hydrochar from board mill effluent treatment plants with maximum surface area and pore volume and lowest H/C and O/C ratios and further reported lower ash-residue as a result of co-combustion of the hydrochar fuels and commercial coal. Saha et al. (2019b) investigated the fuel characteristics of hydrochar generated from primary sludge, de-inked paper sludge, combined sludge and pre-thickened sludge at varying temperatures (180-260 °C) for 30 min and reported hydrochar calorific values ranging from 11.4±0.7 to 31.5±3.7 at maximum temperature, depending on the initial substrate. Unlike temperature, the difference in feedstock quality had a substantial impact on the combustion performance of the derived hydrochar. Mäkelä et al. (2016) examined the effect of additives (HCl and NaOH) on the HTC treatment of mixed sludge and found that acidic conditions had a statistically significant effect on the hydrochar energy yield with theoretical energy efficiencies ranging from 97-147 %. Moreover, higher reaction temperatures enhanced the biological decomposition of the organic matter in the liquid phase, making it sufficiently treatable by conventional biological treatment.

The effect of HTC at subcritical water conditions on the physicochemical characteristics of hydrochars produced from different recycling paper mill streams has not been extensively addressed. Parameters such as the influence of solid load on PPMS hydrochar properties has not been reported, and, despite the potential of the HTC technology, no research has been conducted on optimising the process parameters for producing the best-quality hydrochar from paper mill wastes for solid

fuel applications. Thus, it is crucial to study the physicochemical property and the combustion behaviour of hydrochar from different recycling mill sources to investigate their potential as fuels, as well as to investigate the operation conditions, i.e. reaction temperature, residence time, solid load and interactions during HTC conversion of PPMS in order to develop appropriate models to predict the optimum process conditions to produce hydrochar with maximal solid yield and calorific value while minimising the energy consumption.

CHAPTER 3: MATERIAL CHARACTERISATION AND ANALYTICAL METHODS

This chapter describes the methods used for characterisation and analysis of the raw samples and hydrochars to evaluate the physicochemical properties of the products as a result of hydrothermal carbonisation (HTC) compared to that of the raw feedstocks. Proximate analysis, elemental analysis, calorific values, scanning surface morphology, functional groups, total organic carbon analyses of the raw substrates and hydrochars were performed Thermogravimetric Analyser (TGA), CHNS Elemental Analyser, Bomb Calorimeter, Scanning Electron Microscope (SEM), Energy Dispersed x-ray (EDS) and Fourier-transform Infrared Spectroscopy (FTIR), respectively. The Total Organic Carbon (TOC) of the process wastewater was measured using a TOC analyser. For all products, analyses were conducted under different HTC operating conditions.

3.1. Raw Materials

Raw fibre rejects (RF) and sludge generated at the primary clarifier (PS), with a total moisture content of 25.10 % and 17.50 %, respectively, were collected from Mpact (Springs, Gauteng). Additionally, final waste sludge (FS), consisting of 36.46 % total moisture, was collected from Neopak (Pretoria, Gauteng). The recycling fibre mills produce approximately 6,000-20,000 tonnes of sludge per year on a dry basis. The samples were collected in a closed polyethylene terephthalate (PET) container and stored in a cold room for analysis.

3.2. Proximate Analysis of Raw Substrates and Hydrochar

For preliminary experiments, the raw samples and the produced hydrochar were dried in an oven at 80 °C 24 h to minimise the effect of inherent moisture. For modelling and optimisation studies, the raw samples and the produced hydrochar were dried in an oven at 105 °C for a period of 12 h. Further descriptions of the methods are available in Chapter 5.

The residual moisture, volatile matter (VM), fixed carbon (FC) and ash content were analysed using a thermogravimetric analyser (Hitachi STA300 TGA-DTA) according to ASTM method D7582-15 (ASTM, 2015). For residual moisture determination, about 10 mg of solid samples in crucibles without covers were heated at a heating rate of 20 °C/min from room temperature to 107 ° ± 3 °C, followed by a

107 °C isothermal hold for 1 h under nitrogen atmosphere at a flowrate of 80 mL/ min. The residual moisture content was calculated according to equation 3.1.

$$\mathrm{M} = \left[\frac{(\mathrm{W} - \mathrm{B})}{\mathrm{W}}\right] \times 100 \tag{3.1}$$

Where *M* is the residual moisture (%), *W* is the mass of the sample used (mg), and *B* is the mass of the sample after drying at 107 °C (mg).

For volatile matter, the heating ramp of 40 °C/min was programmed until a temperature of 950 ± 20 °C was achieved, followed by a 950 °C isothermal hold of 7 min. The volatile matter was calculated using equation 3.2.

$$\mathrm{VM} = \left[\frac{(\mathrm{B} - \mathrm{C})}{\mathrm{W}}\right] \times 100 \tag{3.2}$$

Where VM represents the volatile matter (%), and C is the mass of the sample after heating at 950 °C (mg).

The TGA was cooled from 950 °C to 600 °C at a cooling rate of -40 °C/min for ash determination. Once the desired temperature was achieved, the flowing gas was changed to air, and a heating ramp of 2.5 °C/min was programmed to reach a final temperature of 750 ± 15 °C at the end of 1 h, followed by a 750 °C isothermal hold for 2 h. The ash composition was then estimate according to equation 3.3.

$$\mathrm{A} = \left(\frac{\mathrm{D}}{\mathrm{W}}\right) \times 100 \tag{3.3}$$

Where A is the ash content present in the sample (%), and *D* is the mass of residue remaining after the ash test (mg).

The fixed carbon content was determined according to equation 3.4.

$$\mathrm{FC} = 100 - \mathrm{M} - \mathrm{VM} - \mathrm{A} \tag{3.4}$$

Lastly, the VM, FC, and A values were converted to dry basis (db) according to equation 3.5.

$$\mathrm{VM, FC, A\ (db)} = \mathrm{VM, FC\ or\ A} \times \left(\frac{100}{100 - \mathrm{M}}\right) \tag{3.5}$$

3.3. Elemental Analysis of Raw Substrates and Hydrochar

The elemental carbon (C), hydrogen (H), nitrogen (N) and sulphur (S) composition was assessed using a Flash 2000 Elemental Analyser (Thermo Fisher Scientific) at the University of Johannesburg (South Africa), according to Kirmse

(2012). The analysis was conducted through the combustion of approximately 2 mg of sample in a controlled atmosphere, and the gas products in the form of CO_2, H_2O, N_2 and SO_2, and NO_x (which was subsequently reduced to N_2) were subsequently analysed to determine the CHNS composition. The oxygen weight percentage was calculated according to equation 3.6.

$$O = 100 - C - H - N - S - A \tag{3.6}$$

Where O represents the oxygen content present in the sample (%).

3.3.1. Carbon properties

The carbon retained in the hydrochar, C_{char}, was determined according to equation 3.7.

$$C_{char}(\%) = \frac{\%C_{hydrochar} \times \text{mass of hydrochar}}{\%C_{feedstock} \times \text{mass of feedstock}} \tag{3.7}$$

The carbon densification (C_D) was calculated according to equation 3.8.

$$C_D = \frac{\%C_{hydrochar}}{\%C_{feedstock}} \tag{3.8}$$

The percentage carbon increase was determined according to equation 3.9.

$$\%C_{increase} = \frac{\%C_{hydrochar} - \%C_{feedstock}}{\%C_{feedstock}} \times 100 \tag{3.9}$$

3.4. Calorific Values of Raw Substrates and Hydrochar

The calorific value, based on the higher heating value (HHV) of the dried samples, were analysed using a bomb calorimeter (Parr 6200 Oxygen Bomb Calorimeter). About 800-1000 mg of the sample with particle size less than 250 µm was placed in a crucible and transferred to the vessel. The vessel was pressurised with oxygen to 3000 kPa for optimum combustion and placed in the chamber. The sample was combusted in the vessel, and the energy released by the combustion (observed by water temperature increase) was measured.

3.4.1. Energy properties

The energy densification, Ed, was calculated according to equation 3.10.

$$E_D = \frac{HHV_{hydrochar}}{HHV_{feedstock}} \tag{3.10}$$

The percentage calorific value improvement, % $HHV_{improvement}$, was determined according to equation 3.11.

$$\%\ \mathrm{HHV_{improvement}} = \frac{\mathrm{HHV_{hydrochar}} - \mathrm{HHV_{feedstock}}}{\mathrm{HHV_{feedstock}}} \times 100 \qquad (3.11)$$

Lastly, the energy yield, E_Y, was calculated according to equation 3.12.

$$\mathrm{E_Y} = \mathrm{E_D} \times \mathrm{Hydrochar\ yield} \qquad (3.12)$$

3.5. Scanning Electron Microscope Analysis of Raw Substrates and Hydrochar

The dried and sieved samples were mounted on an aluminium plate using a double-sided carbon adhesive tape and coated with films of carbon using Quorum Q150T ES at a chamber pressure of 1×10^3 mBar. Scanning electron microscopy (SEM) using FEG SEM (Zeiss Gemini 2 Crossbeam 540, Oxford Instruments) to analyse the surface morphology of the samples. The working distance (WD) was between 3.6-3.8 mm, with fixed magnifications of 1 000 and 18 000 times, at a voltage (EHT) of 5 kV.

3.5.1. Energy dispersed X-raw spectroscopy (EDS)

Elements on the surface of the raw substrates were analysed following Scanning Electron Microscopy by Energy dispersed X-ray spectroscopy (Zeiss Gemini 2 Crossbeam 540 FEG-SEM with EDS & BS detector, Oxford Instruments) using a microanalysis software (Aztec 3.0 SP1). The working distance was 8.3-8.8 mm, and the target voltage (EHT) of 20 kV.

3.6. Fourier-transform Infrared Spectroscopy (FTIR)

FTIR investigation was conducted to understand better the functional groups on the surface of the raw substrates and the produced hydrochars. The analyses were performed in a PerkinElmer 100 Spectrometer. The transmission spectra were recorded in the range of 4000 to 550 cm^{-1}, resolution of 4 cm^{-1} by averaging 32 scans.

3.7. Total Organic Carbon

Prior to analysis, the process wastewater was filtered through a hydrophilic 0.45 µm nylon syringe filter (Membrane Solutions) and diluted to a ratio of 1:2.5, making up a volume of 35 mL. The mobile phase included an oxidiser solution and phosphoric acid solution. In order to ensure no contamination in the TOC injector and tubes, a blank ultra-pure water (35 mL) was programmed to run prior to the process wastewater analysis. An ASI-V autosampler measured the total organic carbon (TOC) of the process wastewater with a TOC-V analyser (Shimadzu Scientific Instruments). The measurements were conducted in triplicate, and the average was calculated.

3.7.1. Carbon in liquid phase

The carbon recovered in the liquid phase, C_{liquid}, was determined using equation 3.13

$$\%\ C_{liquid} = \frac{TOC\ \times\ volume\ of\ filtrate}{mass\ of\ feedstock\ \times\ \frac{\%C_{feedstock}}{100}} \times 100 \qquad (3.13)$$

3.8. Gas Phase

To further illustrate the carbon mass distribution between the hydrochar, process wastewater and the gas phase, the carbon content in gas was estimated according to equation 3.14.

$$\%\ C_{gas} = 100 - \%\ C_{char} - \%\ C_{liquid} \qquad (3.14)$$

CHAPTER 4: DESIGN AND FABRICATION OF A BATCH AUTOCLAVE HYDROTHERMAL CARBONISATION REACTOR

This chapter describes the criteria followed for the design and construction of the reactor. The reactor was designed to produce enough hydrochar for analysis for experimental purposes. The vessel specification, material, design dimensions, stress analysis, fabrication and overall cost per unit are given.

4.1. Reactor Specification

The laboratory-scale reactor autoclave consists of a seamless vessel with a flat end. The top part is equipped with a seamless flange and a lid that can be bolted into the flange, thus facilitating access to the internal part of the reactor. This configuration enables the reactor to be easily opened, filled, and tightly closed. A heat resistant gasket was considered to ensure a proper sealing system. A removable polytetrafluoroethylene (PTFE) vessel lining was also implemented due to its highly non-reactive and nontoxic property to reduce corrosion, sample contamination and facilitate sample handling. The schematic drawing of the reactor is illustrated in Figure 5.1.

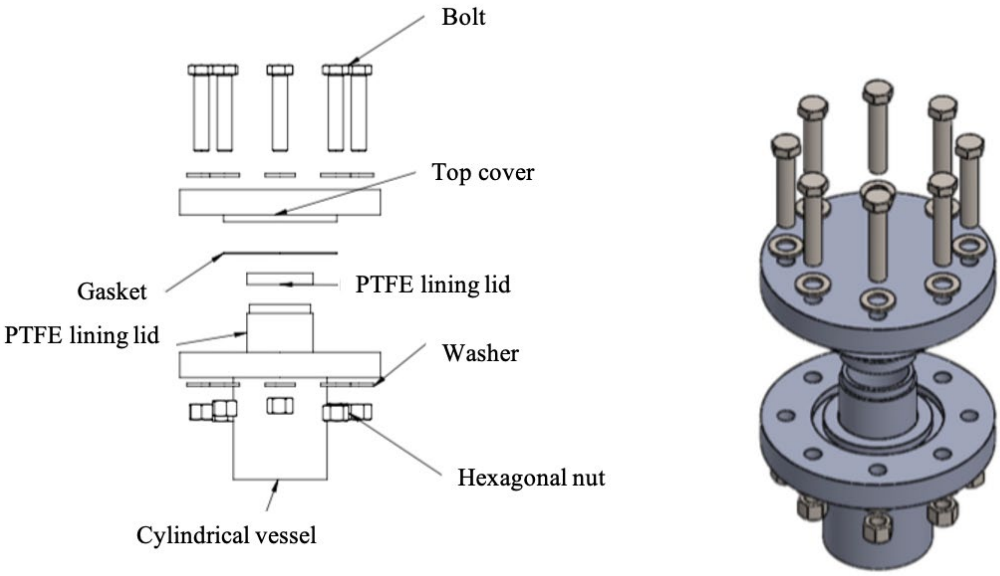

Figure 4.1: Schema of the prototype reactor.

4.1.1. Reactor size

The vessel was designed according to mechanical design for a cylindrical vessel under internal pressure (Sinnott, 1993). The batch reactor has an inner diameter of 55 mm and an internal height of 95 mm, which makes a capacity of

approximately 226 mL. The PTFE lining has an inner diameter of 43 mm and an internal height of 86 mm, resulting in a capacity of about 125 mL, thus set as maximum reactor volume capacity.

4.1.2. Maximum reactor conditions

At subcritical water temperature, the self-generating pressure during hydrothermal carbonisation reactions varies between 1-3 MPa (Wang et al., 2018). Thus, the reactor autoclave was designed to operate at pressures to accommodate such pressures. In terms of maximal design temperature, not only the temperature of the substrate was considered, but also the highest temperature possible of the material with the lowest thermal stability. In this case, the maximum allowable temperature was set to 260 °C, which is the temperature limit for the PTFE material (McKeen, 2012).

4.2. Vessel Material

DIN EN19 Alloy structural steel was selected to fabricate the cylindrical vessel due to its extreme strength, machinability, cost-effectiveness and availability. The material, also designated as 42CrMo4, was purchased from NJR Steel (Pretoria, Gauteng) and contains about 0.37-0.44 % carbon (C), 0.15-0.35 % silicon (Si), 0.65-1.10 % manganese (Mn), up to 0.04 % phosphorous (P) and sulphur (S), 0.75-1.20 % chromium (Cr) and 0.15-0.25 % molybdenum (Mo). These properties improve yield strength and hardenability, prevents brittleness and inhibit grain growth of the material, which results in overall excellent quality high tensile steel grade (Black and Kohser, 2017, Elliott, 1988). The material has a wide range of applications in military vehicles, construction equipment, machine tools, automotive gears, ships, pipelines, pressure vessels, oil drilling platforms and structural components.

4.3. Reactor Design and Dimensions

The technical drawing of the reactor was done in SolidWorks software. The 2D, 3D views and dimensions are illustrated in Figure 4.2. The list of the different parts is presented in Table 4.1.

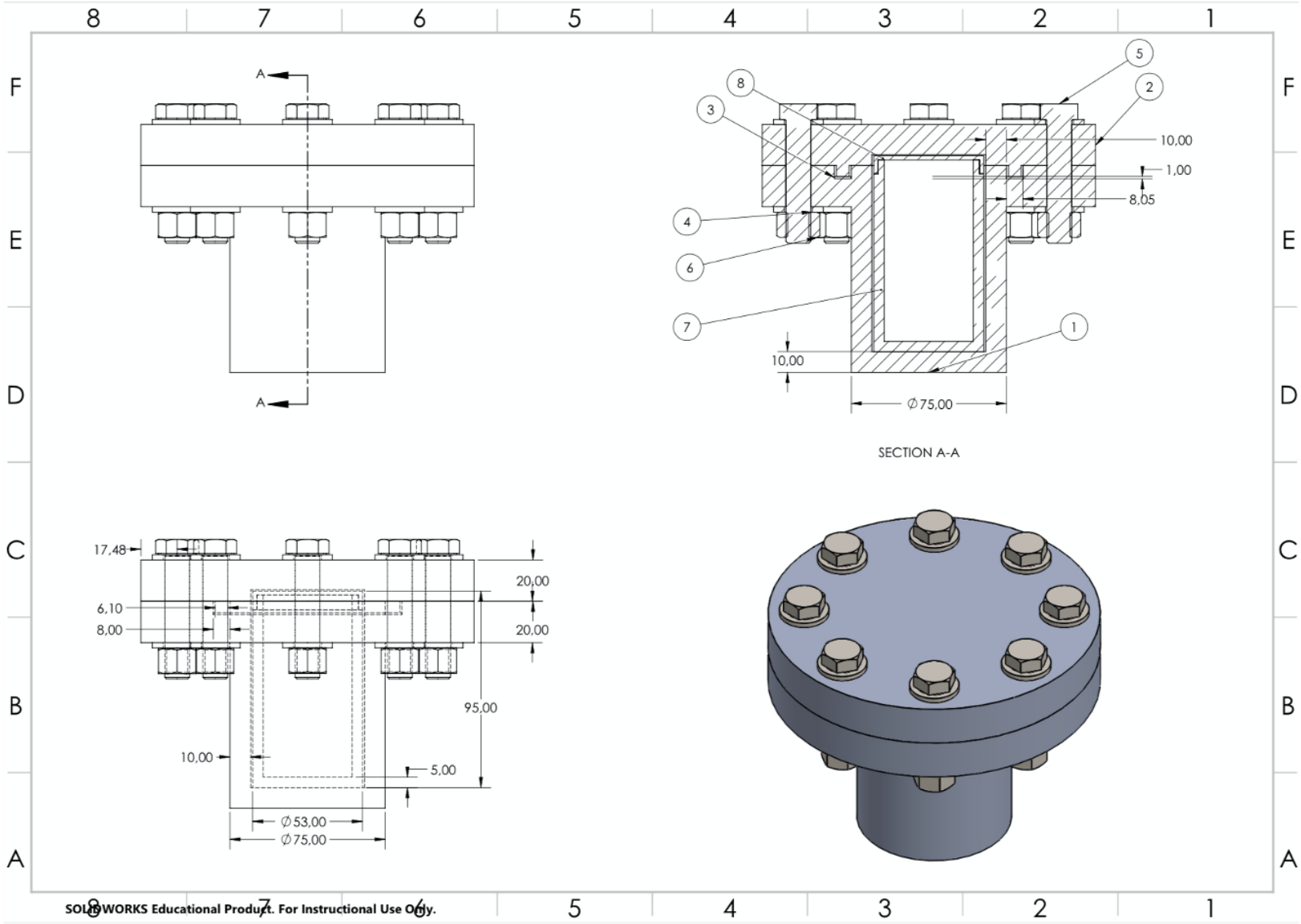

Figure 4.2: Technical drawing of the reactor

Table 4.1: Different parts of the reactor.

Item	Designation	Quantity
1	Cylindrical vessel	1
2	Vessel Lid	1
3	Gasket	1
4	Washer	16
5	Hexagonal screw	8
6	Hexagonal nuts	8
7	PTFE lining	1
8	PTFE lining lid	1

4.4. Stress Analysis

Before reactor fabrication, stress analysis was conducted to ensure the reactor sustains the design HTC pressure of 1-3 MPa. The designed cylindrical vessel is considered thick-walled because the ratio of the radius and the wall thickness is smaller than 10 (Fryer and Harvey, 1998). During HTC, the pressurised vessel experiences stress across the thickness of the wall. Yielding initially occurs at the internal pressurised space and spreads through the wall thickness from the inside to the non-pressurised outer wall as pressure rises. Thus, when the entire wall thickness reaches yield, failure occurs. A thick-walled cylindrical pressure vessel experiences longitudinal or axial stress, circumferential or hoop stress, and radial stress (Mott, 2008); the three forces combined is designated uniaxial force. The stress distribution across the steel vessel is illustrated in Figure 4.3.

For the reactor vessel, parameters such as yield pressure and internal stress limit were calculated considering the vessel internal radius of 27.5 mm, the external radius of 37.5 mm, EN19 steel material yield strength of 415 MPa, and allowing a design stress factor of 1.5.

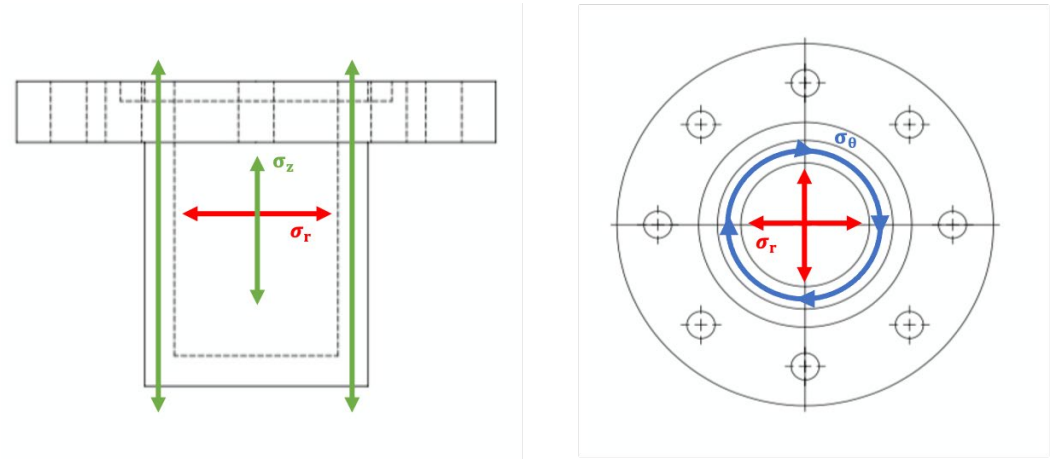

Figure 4.3: Stress across the cylindrical vessel.

Since pressure is internal, the first yield occurs at the internal part of the vessel in the radial direction; the following assumptions were made for radial stress (σ_{ri}) determination:

- σ_{ri} at internal diameter $(27.5) = -P$
- σ_{r0} at external diameter $(37.5) = 0P$, as the vessel is subjected to internal pressure (P) only.

Considering that the stress across the sectional area of a material is given by equation 4.1.

$$\sigma = \frac{F}{A_x} \tag{4.1}$$

Equation 4.1 can be written as:

$$\sigma = \frac{P \times \frac{\pi {r_i}^2}{2}}{\frac{\pi {r_o}^2}{2} - \frac{\pi {r_i}^2}{2}} \tag{4.2}$$

Which, after simplification, becomes:

$$\sigma = \frac{{r_i}^2}{{r_o}^2 - {r_i}^2} P \tag{4.3}$$

Thus, radial stress at internal diameter (σ_r) for the first yield was determined according to equation 4.4.

$$\sigma_r = \left(A - \frac{B}{r^2}\right) P \tag{4.4}$$

Variable A was determined according to equation 4.5.

$$A = \frac{{r_i}^2}{{r_O}^2 - {r_i}^2} \quad (4.5)$$

Variable B was determined according to equation 4.6.

$$B = \frac{{r_i}^2 \times {r_O}^2}{{r_O}^2 - {r_i}^2} \quad (4.6)$$

The circumferential stress at the internal radius (σ_θ) for the first yield was calculated using equation 4.7.

$$\sigma_\theta = \left(A + \frac{B}{r^2}\right) P \quad (4.7)$$

The axial stress (σ_z) at internal diameter for the first yield was calculated according to equation 4.8.

$$\sigma_z = 0.5(\sigma_r + \sigma_\theta) \quad (4.8)$$

The uniaxial stress at internal diameter for the first yield is given by equation 4.9.

$$P_y = \frac{\sigma_y}{\sigma_{max}} \quad (4.9)$$

Where P_y represents the uniaxial or internal pressure for first yield, σ_y represents the stress yield, and σ_{max} is the uniaxial stress calculated according to Tresca or Von Mises method (Fryer and Harvey, 1998).

The pressure at the limit was calculated according to equation 4.10.

$$\sigma = \sigma_y \ln r + C \quad (4.10)$$

Where C is a constant and it was calculated for σ_r, σ_θ and σ_z based on the outer radius and the assumption that the external pressure (OP) equals 0.

4.4.1. Tresca method

For the Tresca method, the uniaxial stress at first yield is given by equation 4.11.

$$\sigma_{max} = \sigma_\theta - \sigma_r \quad (4.11)$$

Limit occurs when all values of radius reach yield; thus, assuming uniform stress across the wall of the vessel, stress limit was given by equation 4.12.

$$\sigma_\theta - \sigma_r = \sigma_y \quad (4.12)$$

4.4.2. Von Mises method

For the Von Mises method, the uniaxial stress at first yield is given by equation 4.13.

$$2\sigma_{max}{}^2 = (\sigma_r - \sigma_\theta)^2 + (\sigma_\theta - \sigma_z)^2 + (\sigma_z - \sigma_r)^2 \quad (4.13)$$

Limit occurs when all values of radius reach yield, thus assuming uniform stress across the wall of the vessel; stress limit was given by equation 4.14.

$$\sigma_\theta - \sigma_r = \frac{2}{\sqrt{3}}\sigma_{max} \quad (4.14)$$

Where σ_{max} equals yield stress (σ_y).

The stress analysis parameters for the PTFE lining were determined following the steps described above, but considering the lining internal radius of 21.5 mm, external radius of 26.5 mm, typical PTFE tensile yield strength of 28.68 MPa, and allowing a design stress factor of 1.5.

Table 4.2: Stress analysis parameters

Parameter	EN19 Vessel		PTFE Lining	
	Tresca	Von Mises	Tresca	Von Mises
P_y (MPa)	64.04	73.97	3.26	3.76
C_r	908.42	1048.85	69.42	80.16
C_θ	1185.07	1368.42	88.54	102.24
C_z	1046.75	1208.69	78.98	91.2
σ_{ri} (MPa)	- 85.81	- 99.09	- 4	- 4.62
σ_θ (MPa)	276.67	319.45	19.12	22.08
σ_z (MPa)	138.33	159.74	9.56	11.03

The stress analysis, constants and pressure limits for the vessel and the lining are presented in Table 4.2. For the vessel, the uniaxial pressure required for the first yield at the internal diameter is 64.04 and 73.97 MPa for the Tresca and Von Mises method, respectively, based on radial stress. The internal stress limit for

the design is 85.81 and 99.09 MPa for the Tresca and Von Mises method, respectively.

For the lining, the uniaxial pressure required for the first yield at the internal diameter is 3.26 and 3.76 MPa for the Tresca and Von Mises method, respectively, based on radial stress. The internal stress limit for the design is 4 and 4.62 MPa for the Tresca and Von Mises method, respectively. These values are higher than the maximal operating HTC pressure of 1-3 MPa, which suggest that the designed reactor is safe to sustain typical HTC reaction pressures at subcritical water condition. Thus, since PTFE lining has the lowest stress limit, which was 3.26 MPa according to Tresca theory, the pressure of 3 MPa will be set as the maximal pressure for the reactor unit, to give a margin of approximately 7%.

Table 4.3: Summary of the reactor design.

Reactor Specification	
Material	EN19 and PTFE
Type	Batch
Capacity	125 mL
Maximum operating temperature	260 °C
Maximum operating pressure	3 MPa

Based on the design specification and material stress analyses, the summary of the assembled reactor is presented in Table 4.3. The reactor material consists of EN19 steel and PTFE lining, and it is designed for batch mode operation with a maximum volume of 125 mL. The maximum operating temperature and pressure is 260 °C and 3 MPa, respectively.

4.5. Reactor Construction and Costs

The reactor was constructed at Specialist Mechanical Engineers Pty Ltd (Pretoria, South Africa), and the PTFE was manufactured by Rui Jorge Pty Ltd (Johannesburg, South Africa), according to the design specifications. The assembled reactor is shown in Figure 4.4, and the overall costs to fabric one reactor unit are summarised in Table 4.4.

Table 4.4: Costs of the reactor fabrication.

Item	Cost (ZAR)
EN19 round steel bar (250 mm OD x 250 mm L)	3, 200
PTFE lining and lid fabrication	1,229
Cylindrical vessel fabrication	5, 965
Others (includes bolts, nuts and washers)	500
Total	**10894**

Figure 4.4: Visualisation of a) alloy steel vessel; b) vessel with the PTFE lining; c) top view of the assembled reactor; d) view of the reactor after running the first HTC test.

Prior to HTC experiments, an aluminium foil adhesive type was placed on the surface of the vessel flange and on the lid to reinforce proper sealing. Since the vessel material has a very low concentration of chromium (Cr) and lacks elements such as copper (Cu), Nickel (Ni) and Vanadium (V) which are corrosion, oxidation and wear-resistant (Black and Kohser, 2017), the vessel corroded as a result of the exposure to moisture and heat for a prolonged period of time.

CHAPTER 5: EXPERIMENTAL AND MODELLING METHODOLOGY

This chapter presents the experimental procedures and modelling methods used in the present study. The first section describes the preliminary experimental method used to investigate the effect of HTC on the physicochemical characteristics of hydrochar produced from different feedstocks. The next section describes the method used to investigate the fuel combustion performance of the hydrochar fuels, as well as the determination of combustion parameters (i.e. ignition index, comprehensive combustibility index, ignition and burnout temperature). The third section describes the methods followed for process modelling of hydrochar production from raw fibre sludge using Response Surface Methodology and the investigation of the optimal process conditions for hydrochar production of maximal solid yield and calorific value at the lowest possible temperature and residence time. Lastly, the fourth section presents the methods for determining the input and output energy for the hydrochar production at all modelling temperatures and solid loads.

5.1. Hydrothermal Carbonisation

HTC experiments were conducted on three different substrates; namely, raw rejects raw fibre rejects (RF) collected from the repulping process, sludge generated at the primary clarifier (PS) during physicochemical treatment of the raw wastewater from the paper mill, and final waste sludge (FS) generated from the raw wastewater, consisting of 25.10 %, 17.50 % and 36.46 %, respectively. The samples were dewatered at the mills and collected on an air-dried basis. For each experiment, 10 g wet sample was mixed with 90 mL of deionised water, stirred manually for 3 min, and transferred to the mL Teflon-lined alloy steel reactor autoclave. Once sealed and bolted, the reactor was placed into a conventional oven where it was heated to the desired temperature of 205, 225 and 245 °C, followed by an isothermal hold of 3 h. Once the carbonisation time elapsed, the reactor was removed from the oven, placed in a cold room at 4°C, and allowed to cool down to room temperature in 2 h. The produced hydrochar was filtered through a cellulose phosphate-free filter paper with 4-12 µm average retention capacity (grade MN 615, USA) and dried in an oven at 80 °C for 24 h. Once dried, the samples were ground with a mortar and pestle and sieved through a particle size less than 250 µm prior to further analysis. The hydrochar yield was calculated according to equation 5.1:

$$H_y\ (\%) = \frac{Wt_{H(d.b.)}}{Wt_f(d.b.)} \times 100 \quad (5.1)$$

Where H_y is the hydrochar yield, Wt_H and Wt_f represent the mass of dried hydrochar and mass of dried raw sludge, respectively.

5.2. Combustion Performance

5.2.1. Thermogravimetric analysis

Combustion tests were conducted in a TG analyser (Hitachi STA300 TGA-DTA). About 10 mg of each hydrochar sample was placed in a crucible and heated to 950 °C at a flow rate of 80 mL/min under air atmosphere, followed by an isothermal hold for 10 min. The weight loss and the corresponding weight loss rate (DTG) of the samples were measured continuously under the non-isothermal condition at a constant heating rate of 20 °C/min. The ignition temperature (T_i), maximum combustion rate temperature (T_m), and the burnout temperature (T_b), as well as the corresponding times, were recorded from the TG-DTG curves using the Intersection Method (IM) as described by Lu and Chen (2015).

5.2.2. Calculation of combustion parameters

For further evaluation of the combustion ability and performance of the samples, the ignition index (D_i) and the comprehensive combustibility index (S) were estimated using equations 5.2 and 5.3:

$$D_i = \frac{\left(\frac{dm}{dt}\right)_{max}}{t_{max} \times t_i} \quad (5.2)$$

Where t_{max} is the time corresponding to the maximum combustion rate (min), and t_i is the ignition time (Li et al., 2006).

$$S = \frac{\left(\frac{dm}{dt}\right)_{max}\left(\frac{dm}{dt}\right)_{me}}{T_i^2 \times T_b} \quad (5.3)$$

Where $\left(\frac{dm}{dt}\right)_{max}$ is the maximum combustion rate (%/min), $\left(\frac{dm}{dt}\right)_{me}$ is the mean combustion rate, T_i and T_b is the ignition and burnout temperature (°C) (Lin et al., 2015a).

5.3. Modelling and Optimisation of Hydrochar Production

5.3.1. *HTC experiments*

Raw fibre rejects (RF) sludge was selected for modelling and optimisation studies. For each HTC experimental run, approximately 100 g of sample consisting of feedstock and deionised water at varying solid loads (8 %, 10 % and 12 % on a dry basis) was stirred manually for 3 min and transferred into the vessel. The reactor was placed in an oven pre-heated to $\mathrm{T_{set}} - 50°\mathrm{C}$, and allowed to reach the desired carbonisation temperature at a heating rate of 2.5 °C/min. Following carbonisation, the sealed vessel was placed under running water and cooled down within 10-15 minutes. The carbonised material was removed, filtered through a cellulose phosphate-free filter paper with 4-12 µm average retention capacity (grade MN 615, USA) and dried in the oven for 105 °C for 12 hours. For rapid homogenisation and small particle size, an electric grinder (Breville Coffee & Spice Grinder) was employed to process the dry samples for 1 min and sieved through a particle size less than 250 µm prior to further analysis.

5.3.2. *Experimental design*

Response Surface Methodology (RSM) was used to study the influence of the three variables (reaction temperature, residence time, solid load and their interaction on hydrochar yield and calorific value by means of higher heating value (HHV). Due to technical limitations, face-centred Central Composite Design (CCD) was employed. Design Expert ® 11.1.0.1 software (Stat Ease Inc, Minneapolis, MN, USA) was used for the CCD and statistical analysis of variance (ANOVA). The factors were coded at α=± 1, which requires three levels: -1, 0, 1.

5.3.3. RSM model design for hydrochar yield and calorific value

The CCD was experiments consisted of 20 runs: 8 factorial points, 6 axial points and 6 central points to provide quality prediction and improve model reliability. The three independent variables were coded according to equation 5.4:

$$\mathrm{X_i} = \frac{\mathrm{x_i} - \mathrm{x_0}}{\Delta \mathrm{x_i}} \qquad (5.4)$$

Where $i = 1, 2\ and\ 3$. X_i and x_i are the dimensionless and the actual values of the independent variable i, x_0 the actual value of the independent variable i at

the central point, and Δx_i the step change of x_i corresponding to a unit variation of value. The coded and uncoded (actual) levels of the independent variables are given in Table 5.1. Prior to designing of experiments, RF samples were carbonised at temperatures of 220 °C, 240 °C and 260 °C for 1 h, 3 h and 5 h. The results are presented in Table C 1. No major difference was observed in hydrochar yield and, especially, calorific values obtained at the maximum reaction conditions (260 °C for t > 3 h) compared to shorter reaction residence times. Thus, taking this into account and the reactor temperature limitations, the experimental design limit was set to a maximum of temperature and time of 250 °C and 3 h, respectively, and minimum reaction temperature and residence time of 210 °C and of 0.5 h, respectively.

Table 5.1: Independent variables and their corresponding levels used in the RSM design.

Independent variable	Symbol	Coded levels		
		-1	0	1
Temperature (°C)	X_1	210	230	250
Residence time (h)	X_2	0.50	1.75	3.00
Solid load	X_3	0.08	0.10	0.12

The residence time did not include the time required to reach the desired reaction temperature. All experiments were performed in random order and in triplicate.

Once the experiments were conducted, the average results were fitted to a second-order polynomial equation to correlate the response variables and the independent variables as follows:

$$Y = \beta_0 + \beta_1 X_1 + \beta_2 X_2 + \beta_3 X_3 + \beta_{12} X_1 X_2 + \beta_{13} X_1 X_3 + \beta_{23} X_2 X_3 + + \beta_{11} X_1^2 + \beta_{22} X_2^2 + \beta_{33} X_3^2 \varepsilon \quad (5.5)$$

Where Y represents the response variables, i.e. hydrochar yield (H_Y, %) and higher heating value (HHV, MJ/kg), β_0 is a constant, β_i represents the linear terms, β_{ii} stands for the quadratic terms for one variable, β_{ij} represents the interaction terms (i=1, 2 and 3; j =1, 2 and 3; j=1,2 and 3), and ε is the random error.

5.3.4. Statistical analysis

The experimental data were analysed by multiple linear regression using the ANOVA approach in order to fit the second-order polynomial equation, as well as to evaluate the validity and significance of the fitted model. The regression coefficient

determination R^2, adjusted R^2, predicted R^2, lack of fit, adequate precision, F- value and p-value were used to further assess the quality and accuracy of the developed models. The p-values equal to or less than 0.05 were considered to be statistically significant.

5.3.5. Optimum HTC process conditions

After the determination of the fit model, the optimal conditions for hydrochar production were determined by solving the equation derived from the final quadratic model and by evaluating the RSM plots with restrictions on responses of minimum values for temperature and residence time, solid load in the range of 0.08-0.12 (8-12 % dry solids) and maximum hydrochar yield, HHV and desirability.

5.4. Energy Balance

The net energy (Q_{net}) was calculated from the energy required for hydrochar production and the energy produced from the combustion of the hydrochar fuel. For the input energy (Q_{in}), the energy required to heat the reactor and to maintain it at constant temperature was not considered, as, in a process development perspective, it varies with reactor design and operating procedures (Mau et al., 2016, Afolabi et al., 2020). Assuming the wet substrate as a non-reactive mixture of water and dry solids, Q_{in} was calculated as the sum of the energy required to heat both the dry feedstock and the water content during HTC, according to equation 5.6.

$$\mathrm{Q_{in}} = \mathrm{m_w}(\mathrm{H_{w,HTC}} - \mathrm{H_{w,25}}) + \mathrm{m_s}\mathrm{C}_{p,s}(\mathrm{T_{HTC}} - 25) \quad (5.6)$$

Where $\mathrm{m_w}$ and $\mathrm{m_s}$ are the water and solids content, respectively; $\mathrm{H_{w,HTC}}$ and $\mathrm{H_{w,25}}$ are the enthalpy of water at the final HTC temperature and at 25 °C, respectively; $\mathrm{C}_{p,s}$ is the approximate specific capacity of sludge, i.e. 1.05 J/kg K, assuming dry basis (Stoica et al., 2009); and $\mathrm{T_{HTC}}$ is the HTC reaction temperature. Lastly, the energy output (Q_{out}) was estimated from the combustion of the hydrochar fuel, according to equation 5.7.

$$\mathrm{Q_{out}} = \mathrm{m_{HC}} \times \mathrm{HHV_{HC}} \quad (5.7)$$

Where m_{HC} and HHV_{HC} represent the dried mass (kg) and HHV (MJ/kg) of the hydrochar.

The electricity production per year from the optimised hydrochar was estimated according to the equation below:

$$E_{HC}(GWh) = \frac{\eta \times M_{PMS} \times HHV_{HC}}{3.6 \times 10^3} \quad (5.8)$$

Where E_{HC} is the electricity from hydrochar production, η represents the average efficiency of coal-fired power plants in South Africa of 0.352 (Eskom, 2021), M_{PMS} is the mass of hydrochar produced in tonnes, and HHV is the calorific value of the solid fuel in GJ/tonnes.

Lastly, the electricity generated from hydrochar (E_{HC}) was compared to the electricity generated at one of the coal-fired power plants in South Africa (E_C), according to equation 5.9.

$$\frac{E_{HC}}{E_C} \times 100\ \% \quad (5.9)$$

CHAPTER 6: HYDROTHERMAL CARBONISATION OF DIFFERENT RECYCLED PAPER WASTE STREAMS

In this section, the data obtained using the methodology and characterisation from the previous chapters are presented. The elements on the surface of the raw samples and the effect of HTC reaction temperatures on the physicochemical characteristics of the hydrochar obtained from different recycling paper sludges are discussed. In addition, the evaluation of the combustion performance, ignition and burnout temperature, combustion parameters and the residual ash post-combustion of the hydrochar fuels are discussed.

6.1. Elements on the Surface of the Raw samples

Identifying the elements bound to the raw samples is indispensable, as this has implications for their application as solid fuel and consequent environmental impact. The major elements detected on the surface of the dried raw samples by energy dispersed X-ray spectroscopy (EDS) analyses are shown in Figure 6.1-Figure 6.3**.** The EDS spectrum indicates that all samples consist mainly of oxygen and calcium, with relatively small percentages of sulphur, aluminium, silicon and traces of chlorine. Other minor elements, such as sodium and magnesium, were also detected on Raw fibre sludge (RS) and final sludge (FS) samples, whilst traces of iron were detected on FS and primary sludge (PS) samples. These elements contribute to the impurity of the raw feedstock and further affect the ash composition of the corresponding hydrochar.

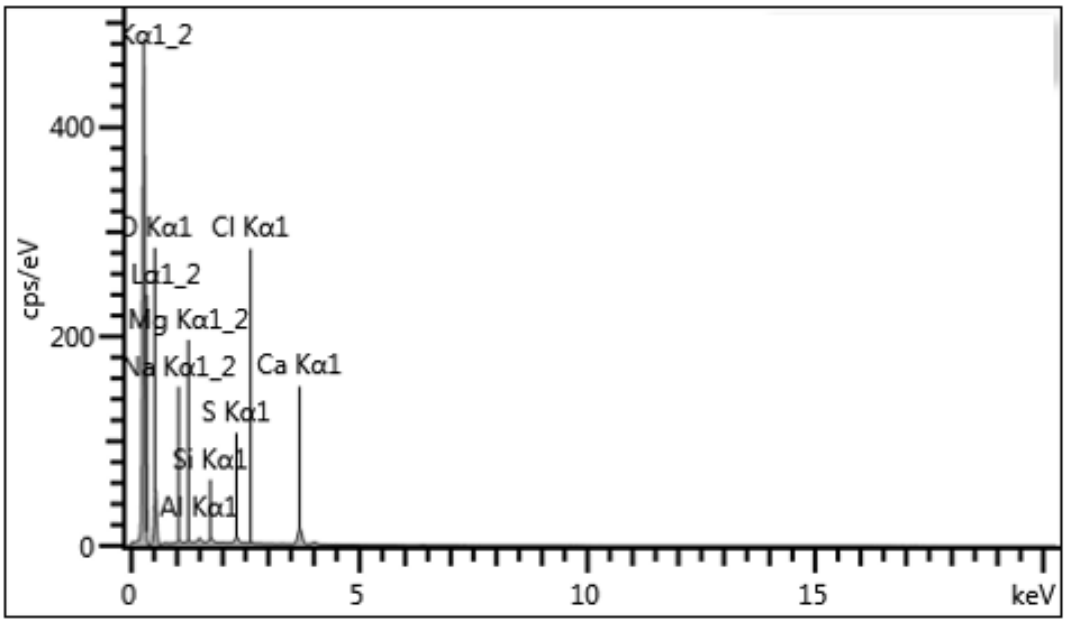

Figure 6.1: Elemental composition of dried raw fibre rejects (RF) from EDS.

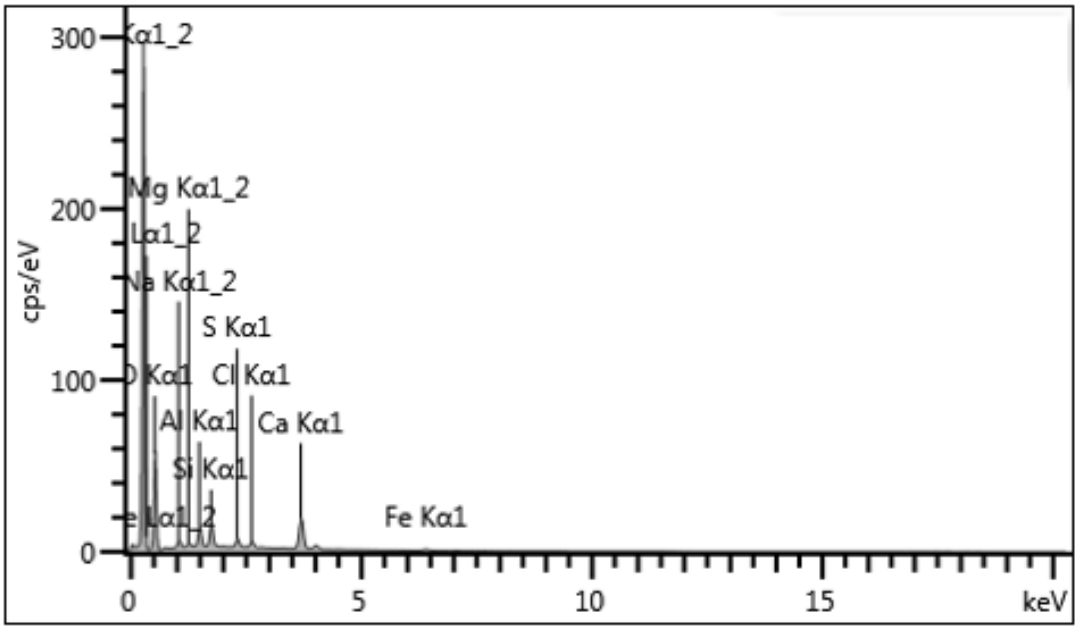

Figure 6.2: Elemental composition of dried final waste sludge (FS) from EDS.

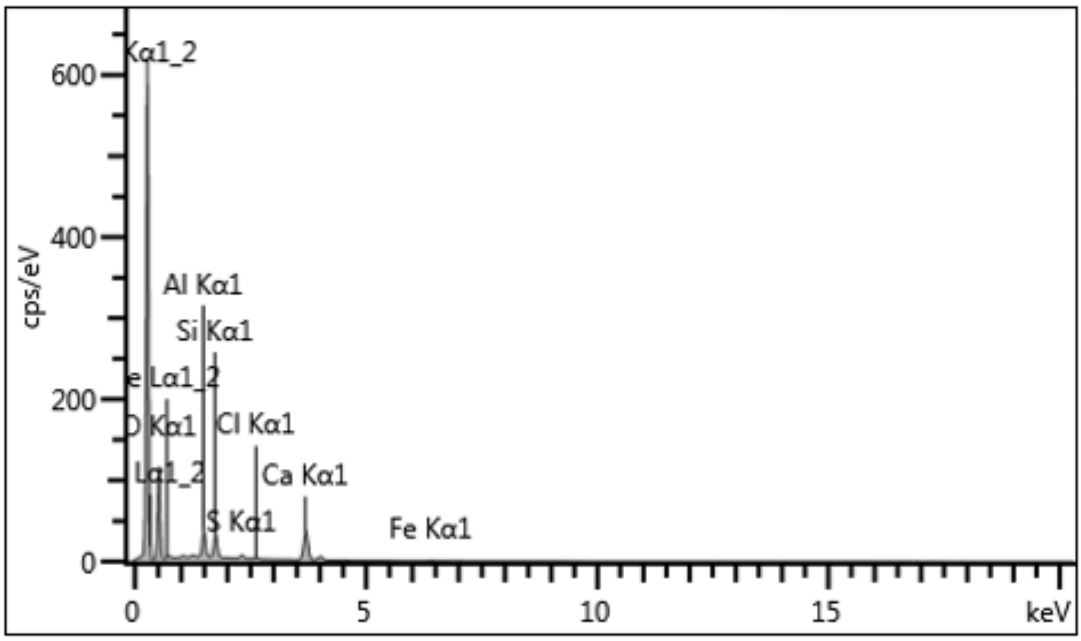

Figure 6.3: Elemental composition of dried primary clarifier sludge (PS) from EDS.

6.2. Visual Assessment of the Feedstocks and Hydrochars

The physical appearance of dried feedstock and dried hydrochars obtained at different carbonisation temperatures are illustrated in Figure 6.4. It is evident that HTC resulted in hydrochar with physical characteristics distinctive from the initial samples. Compared to the raw samples, hydrochars could easily be ground into smaller particles by mortar and pestle. In addition, the increase in carbonisation temperatures resulted in hydrochar with more hydrophobic properties. This was observed through the increased rate of filtration and decreased water-holding capacity at higher temperatures, as the amount of process water collected during filtration which was minimum at 205 °C. When the temperature was ≥ 225 °C for RF and FS, the produced hydrochars were darker in colour with more uniform and compacted particles; however, these characteristics were not significantly distinctive for PS at ≥ 225 °C. In general, the change in characteristics is due to reaction mechanisms occurring during HTC conversion, which are further discussed in the subsequent subsections.

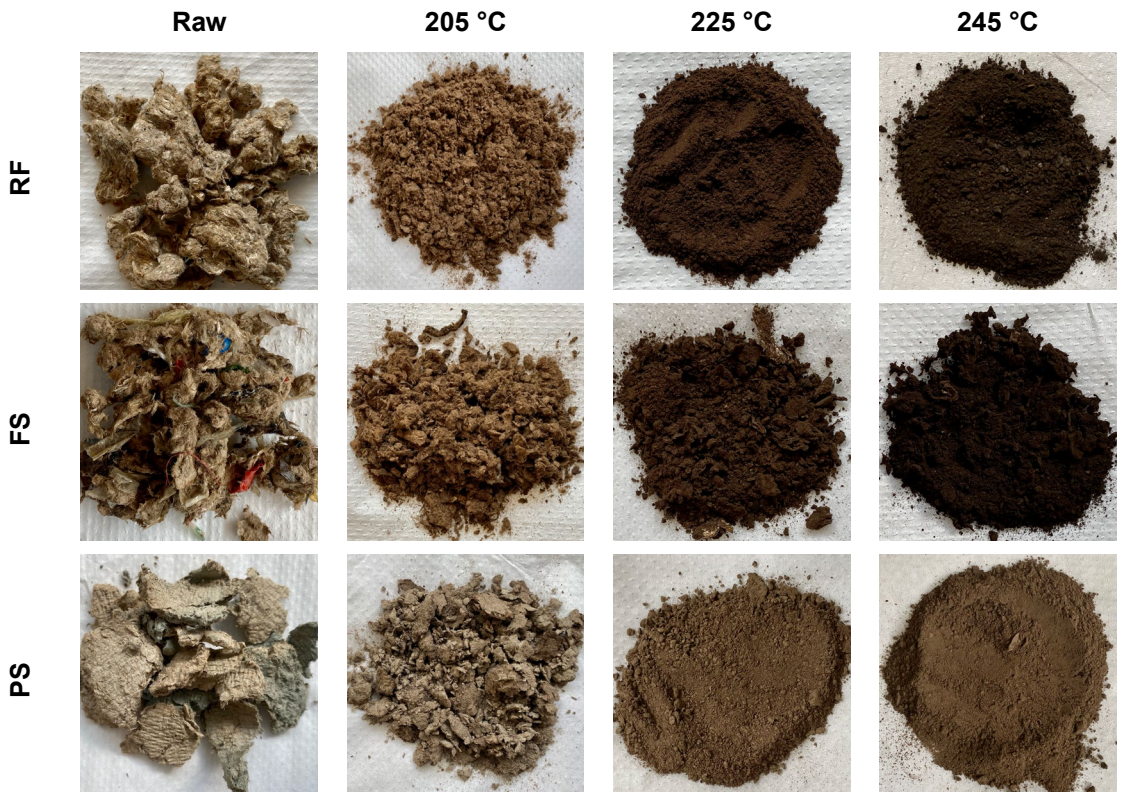

Figure 6.4: Samples of dried substrates and dried ground hydrochars obtained at 205, 225 and 245 °C.

6.3. Ultimate Analysis

HTC treatment resulted in hydrochars with different physicochemical properties compared to the untreated samples. Results on the elemental analysis are illustrated in Figure 6.5. In comparison to the raw samples, the carbon content of the hydrochars increased with an increase in reaction temperature, whilst the oxygen content simultaneously decreased. This change is mainly attributed to dehydration and decarboxylation reactions which hydroxyl and carboxyl groups are removed from the solid phase and released in the form of H_2O and CO_2 (Wang et al., 2018); as a result, a more aromatic carbon is formed in the hydrochar (He et al., 2013a). The increase in carbon and decrease in oxygen content contribute to the increase in higher heating value (HHV). The carbon content for RF, FS and PS hydrochar ranged from 45.18-60.30%, 47.18-83.75% and 40.94-48.63%, respectively. When comparing the hydrochars obtained from the three different substrates, HTC of FS produced hydrochars with the highest carbon proportion at 245 °C (83.75 %), corresponding to an increase of 87.12 %. This was followed by RF at 245 °C, which presented a carbon increase of 31.21%. HTC of PS, however, produced hydrochars with the lowest carbon content and lowest carbon increase (up to 18.78 % increase).

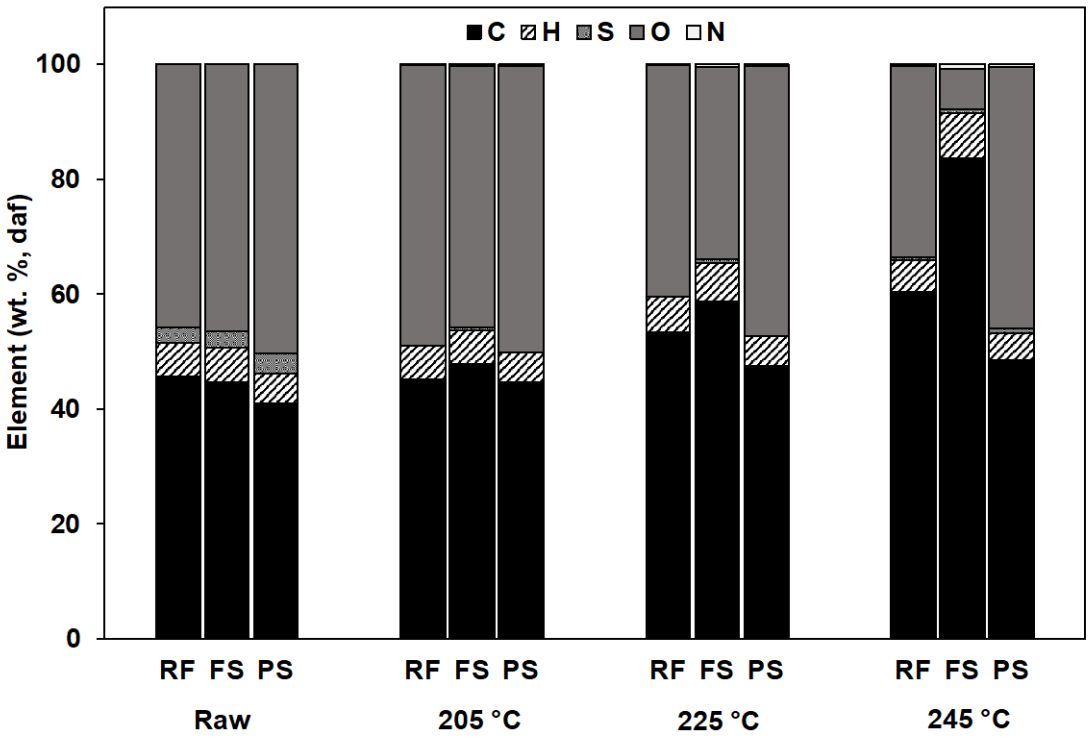

Figure 6.5: C, H, O, N, S content of raw RF, FS and PS and hydrochar at different reaction temperatures on dry ash-free basis (daf).

The oxygen content decreased by 27.22%, 85.03% and 9.54% for RF, FS and PS, respectively. Higher carbon and lower oxygen percentage have a positive influence on the calorific value of the solid fuel. The hydrogen content was not significantly affected by the reaction temperature, but overall the H/C ratio decreased.

Regarding the sulphur content, at 205°C < T ≤ 225 °C, the sulphur content reduced to the lowest values corresponding to < 0.001 %, 0.51 % and 0.001 % for RF, FS and PS, respectively. This is due to the formation of sulphur oxides during HTC, which are then dissolved in the process water (Lin et al., 2015b). At 245 °C the sulphur content slightly increased to 0.50 %, 0.73 % and 0.83 % for RF, FS and PS, respectively. This is attributed to the formation of sulphur species precipitate on the surface of the hydrochar (Wang et al., 2020b). Just as sulphur, the nitrogen content for all samples remained less than 1 %. For solid fuel application of hydrochar, low to no S and N content is desired, as these characteristics mitigate the emission of acid rain persecutors such as NO_x SO_2 and SO_3 during the combustion process.

6.4. Proximate Analysis

The proximate analysis is illustrated in Figure 6.6. The residual moisture (RM) decreased with an increase in reaction temperature, reaching the lowest values of 0.65 % at 245 % for PS. This trend confirms the improvement in hydrophobicity properties of the hydrochars. As a result of the increase in carbonisation temperature, the volatile matter (VM) content decreased significantly with a simultaneous increase in fixed carbon (FC). These changes are due to the degradation of the lignocellulosic component, mainly hemicellulose and cellulose, which start dissolving at 180-220 °C (Wang et al., 2018); this is more predominant at 245 °C where the maximum loss of 54.55 %, 64.36 % and 63.60 % of the initial volatile content for RF, FS and PS, respectively, is observed. In contrast, the fixed carbon showed a significant increase. The maximum proportion of fixed carbon for hydrochars was observed at 245 °C, which corresponds to 59.04 %, 52.37 % and 36.18 % for RF, FS and PS, respectively. These analyses are in agreement with reported works (Saha et al., 2019a, Volpe et al., 2018, Kim et al., 2015).

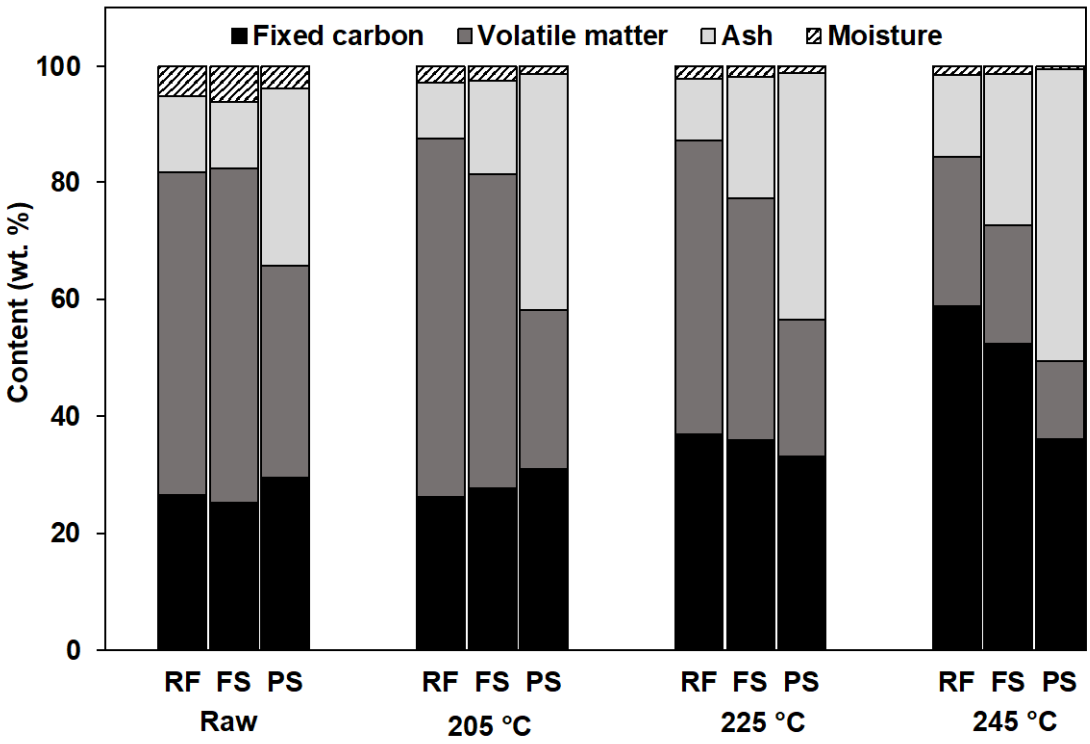

Figure 6.6: Proximate Analysis of the raw samples and obtained hydrochars.

The ash content was predominantly inert during HTC treatment. Although it slightly decreased for RF at 205 °C and 225 °C, it generally increased as the

reaction progressed, reaching 49.90 % at 245 °C for PS. This is because, during the degradation of organic substances, the inorganic content is retained in the hydrochars (McGaughy and Reza, 2018). The trend in ash content reported in this study is in agreement with previous work (Saha et al., 2019b). Apart from contributing to the poor calorific properties of the fuel material, a high level of ash affects the technical design of a processing plant as it often leads to metal corrosion, operating problems during combustion due to the risk of fouling, scaling, slagging and corrosion in the chambers (Wang et al., 2020a). Depending on the melting point, high ash may lead to clogging of burners during incineration, as well as flame suffocation due to deposition of ash in the vicinity of the burner. Furthermore, high ash content requires further disposal of residues. Thus, RF and FS are preferable for thermochemical conversion due to the relatively lower ash content. This will also help minimise accumulation sintering and agglomerations in boilers, which often leads to failure of the plant.

6.5. Hydrochar Yield and Energy Content

The reaction mechanisms of hydrochar formation through the HTC process are mainly affected by temperature (Sharma et al., 2020). Temperature increment favours devolatilization and dehydration, which consequently decreases the hydrochar yield. As a result, a solid product with distinctive energy properties from its initial sample is obtained. The energy properties of the hydrochar yield, energy yield and calorific value (CV) on a dry ash-free basis (daf) at different reaction temperatures are illustrated in Figure 6.7-Figure 6.9. The mass and energy yield decreased with an increase in carbonisation temperature for all samples, while the CV and the energy densification increased. This is a result of hydrothermal degradation of the main organic components contained in the raw sludges, such as cellulose, hemicellulose and lignin (Lin et al., 2015b). The reactivity of the samples is more predominant at higher temperatures; consequently, hydrochar with increased CV is obtained. The CV for RF and FS hydrochar ranged from 18.62-26.24 MJ/kg, 19.08-26.47 MJ/kg, respectively, corresponding to an increase of 6-49.35 % and 10-58.51 %. In contrast, HTC did not have a significant effect on the CV for PS. The values ranged from 13.27-14.33 MJ/ kg. For energy applications, fuels with relatively higher HHV are preferred.

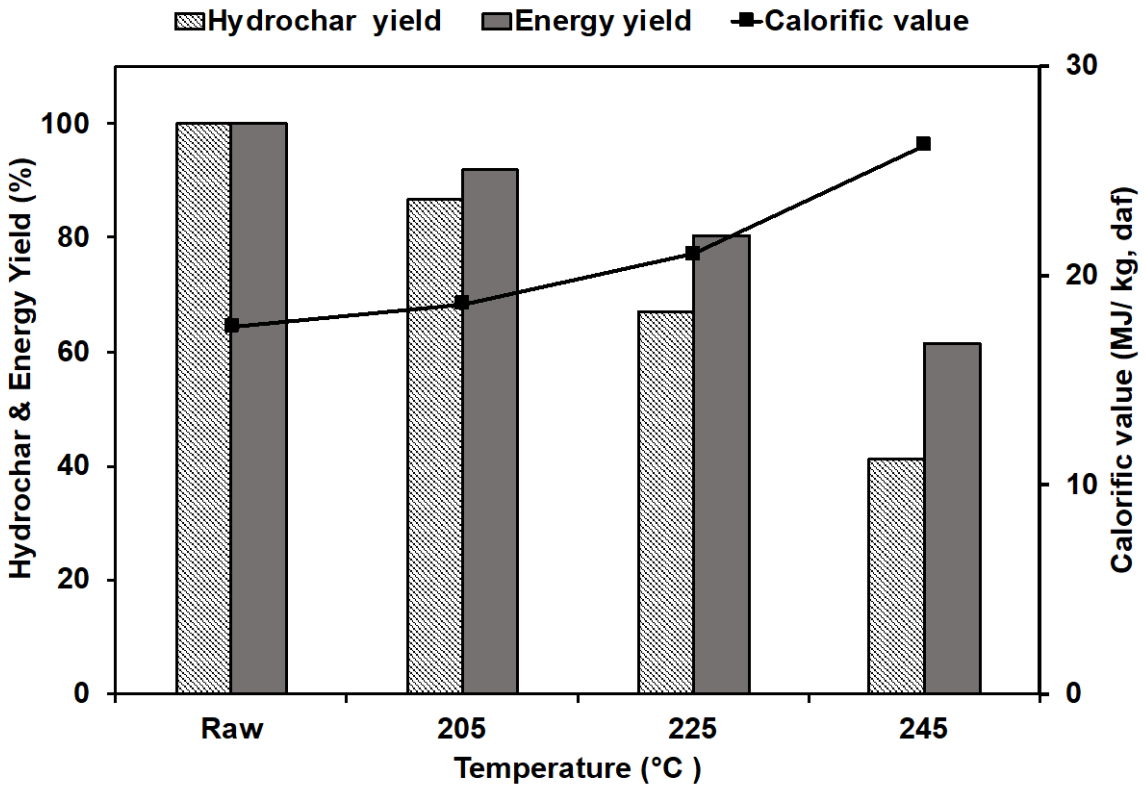

Figure 6.7: Effect of HTC temperature on hydrochar yield, energy yield and calorific value of RF hydrochars.

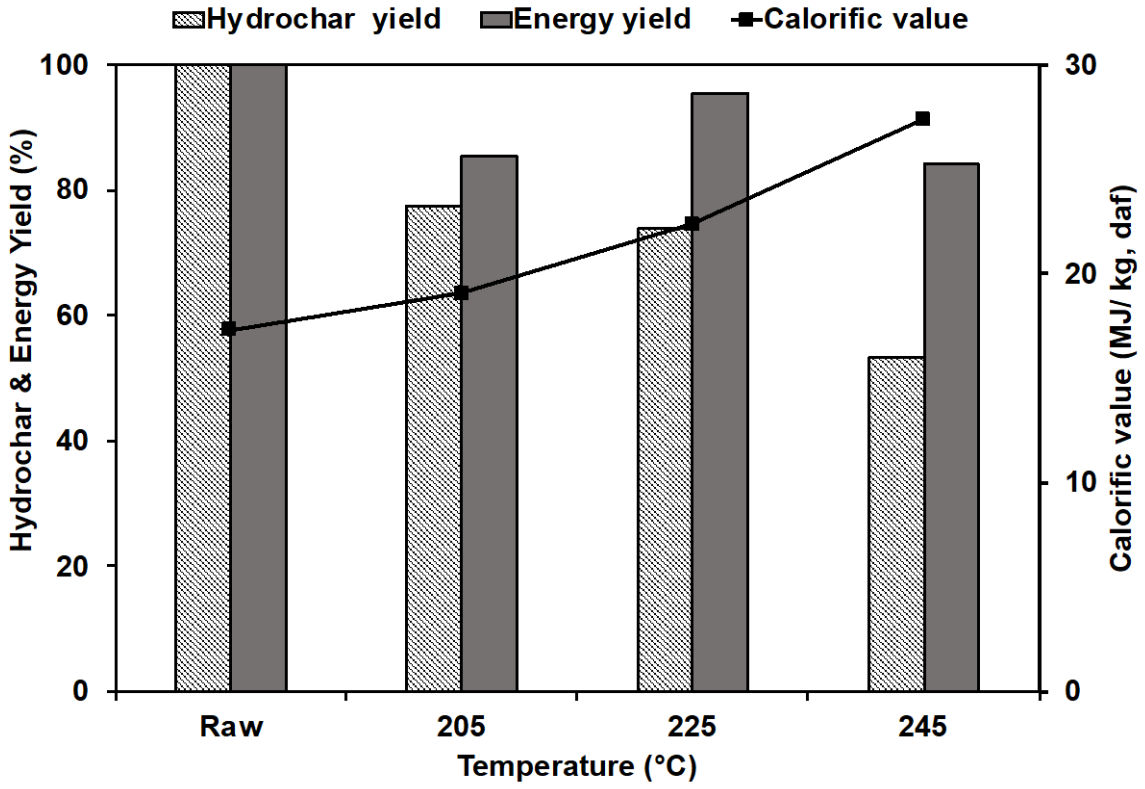

Figure 6.8: Effect of HTC temperature on hydrochar yield, energy yield and calorific value of FS hydrochars.

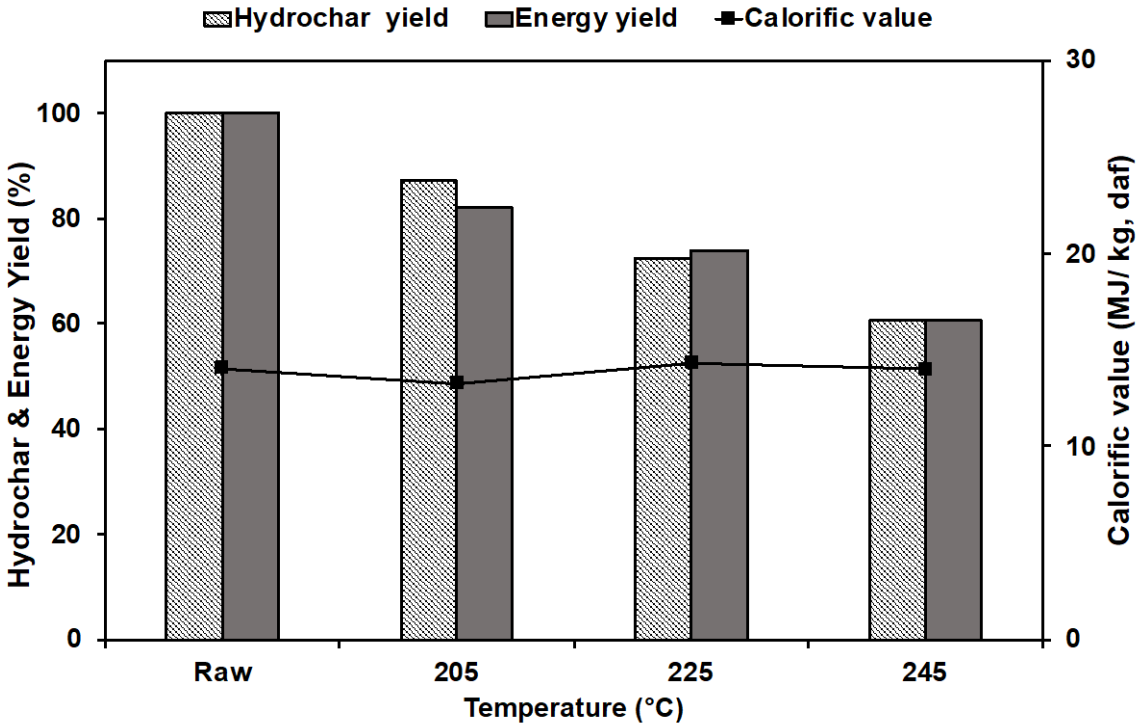

Figure 6.9: Effect of HTC temperature on hydrochar yield, energy yield and calorific value of PS hydrochars.

6.6. Fourier-transform Infrared Spectroscopy (FTIR) characteristics

The FTIR spectra shown in Figure 6.10-Figure 6.12 were used to analyse the structure of the raw feedstocks and hydrochars obtained at different HTC reaction temperatures and to identify the reaction mechanisms further. The bands at 3693 and 3621 cm^{-1} in the PS samples could be associated with the presence of kaolinite (Méndez et al., 2009), which, according to the observations, remained inert during HTC treatment.

The adsorption peak at 3328, 3321, and 3327 cm^{-1} (between 3200-3650 cm^{-1}) mainly reflect the O-H stretching vibration from carboxyl or hydroxyl groups of phenolic structures, alcohols and carboxylic acids (Santos et al., 2021); the bands were less pronounced at HTC- 245 °C, which confirms the occurrence of dehydration reaction during the HTC process.

The absorption peak at 2899 and 2901 cm^{-1} (between 2500-3200 cm^{-1}) for RF and PS samples are mainly caused by aliphatic C-H bonds from alkyl groups (Saha et al., 2019a). The peaks at 2921 and 2850 cm^{-1} for FS samples are associated with C-H symmetric and asymmetric stretching in CH_2 and CH_3 groups (Santos et al., 2021); these peaks become less evident at higher temperatures, which suggests demethylation reaction occurred and was more pronounced at 245 °C.

Regarding the 1500-2000 cm^{-1} range, the peaks at 1504-1506, 1592-1594 cm^{-1} for RF and FS correspond to C=C in-plane aromatic vibration (Li et al., 2018, Coates, 2006). The bands became more evident with an increase in HTC reaction temperatures and are more pronounced for RF-225°C and RF-245 °C. This trend suggests the occurrence of aromatisation reaction during the HTC process. The absorbance peaks at 1695 and 1696 cm^{-1} attributed to C=O stretching in ester groups (Li et al., 2018), and it is due to further dehydration and decarboxylation products formed and retained in the hydrochar (Saha et al., 2019a); this observation is more prominent at HTC-245 °C for RF and FS hydrochars. This indicates that, under this condition, the chemical components of RF underwent simultaneous degradation and polymerisation reaction (Guo et al., 2015).

As for the range of 1300-1500 cm^{-1}, the peaks at 1314, 1418-1422 and 14577 cm^{-1} for RF and FS could be due to CH_2 rocking, CH_2 scissoring and O-H in-plane deformation, respectively (Abidi et al., 2014). The peaks at 1422 and 874 observed in PS samples are associated with elevated calcium carbonate content in the sample (Méndez et al., 2009, Thriveni et al., 2017), which remained unreactive during HTC. Lastly, organic matter at bands in the region of 1000-550 cm^{-1} could be attributed to single bonds single bond-stretching vibration frequencies (Li et al., 2018), including anti-symmetrical bridge C-O-C, C-O stretching and β-linkage of cellulose and hemicellulose, C-H angular deformation in C≡CH groups and O-H angular deformation in R-OH groups (Abidi et al., 2014, Coates, 2006).

From these results, it is evident that HTC had little effect on the surface properties of PS hydrochar but a significant effect on RF and FS hydrochars. Dehydration and decarboxylation reactions governed the hydrochar formation, especially for RF and FS samples at 245 °C. Moreover, polymerisation and aromatisation reactions took place to some extent.

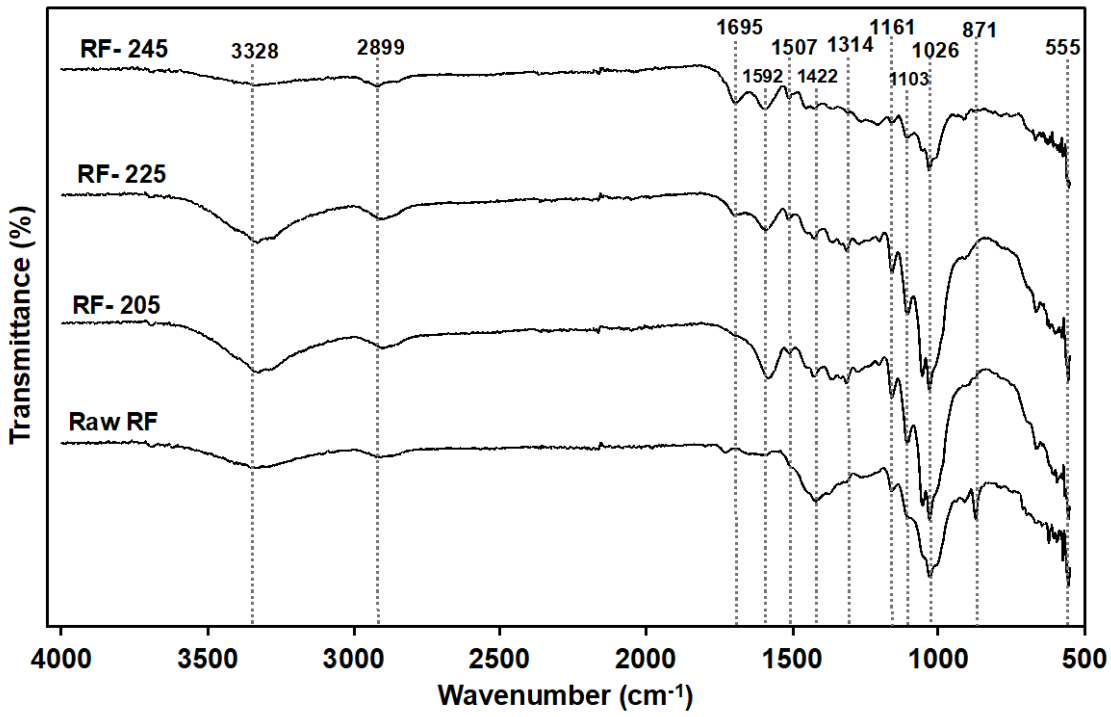

Figure 6.10: FTIR spectra of raw RF and hydrochars.

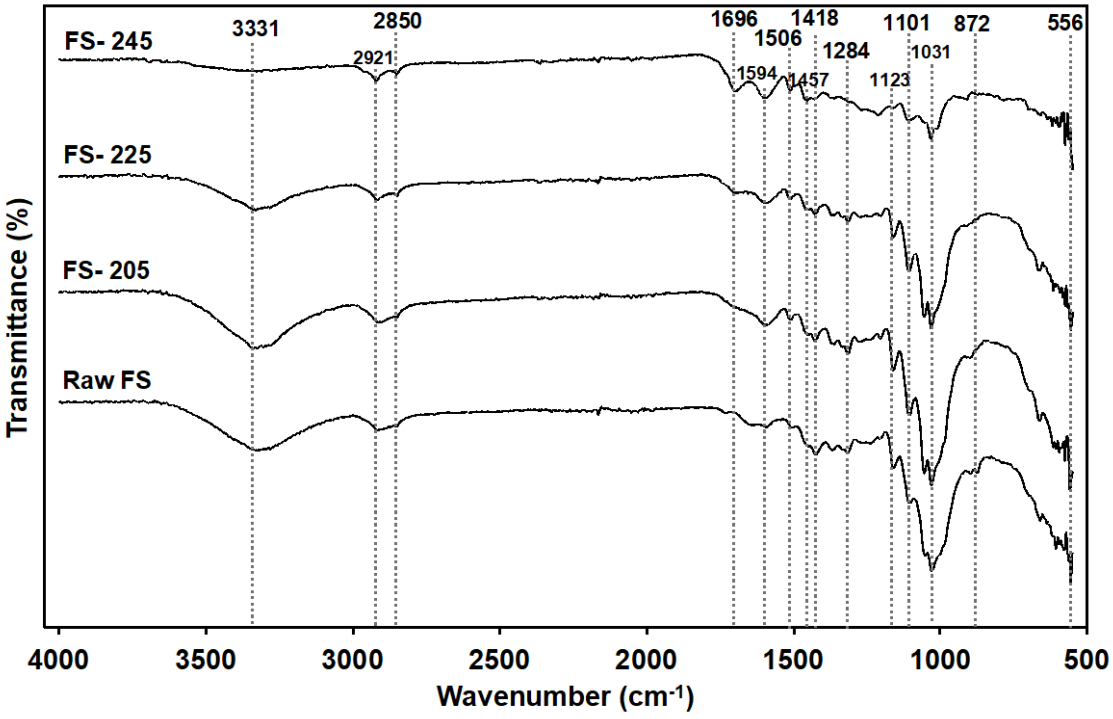

Figure 6.11: FTIR spectra of raw FS and hydrochars.

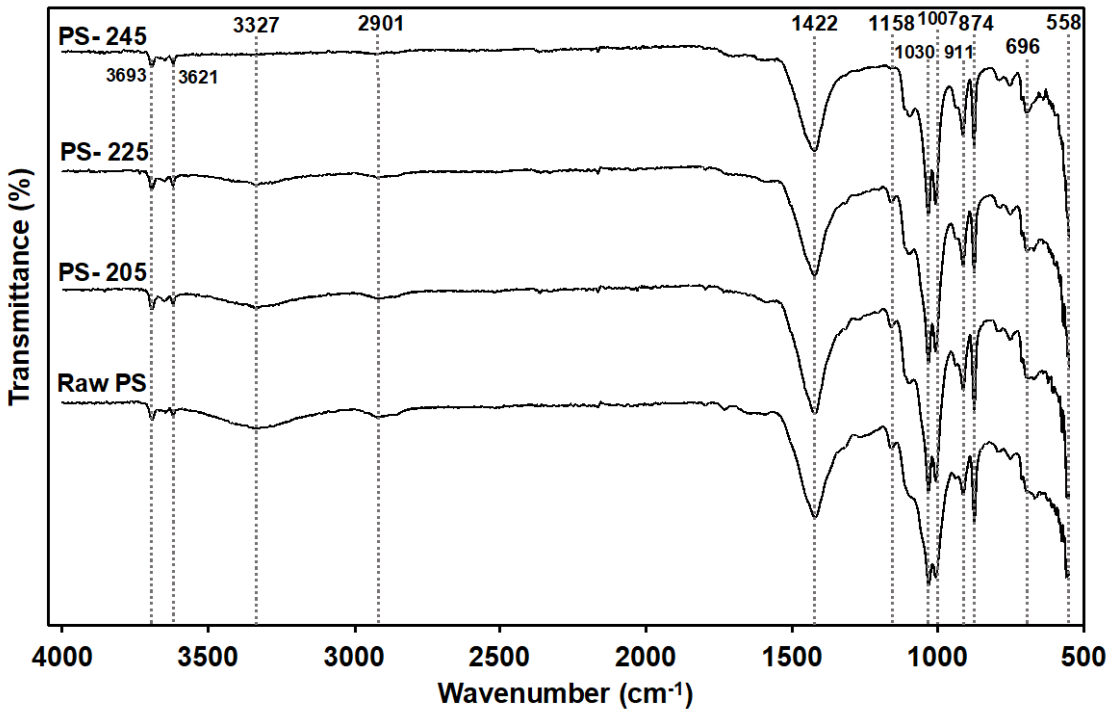

Figure 6.12: FTIR spectra of raw PS and hydrochars.

6.7. Carbon Mass Distribution

The carbon mass balance is presented in Figure 6.13. The carbon content in the solid phase for RF, FS and PS ranged from 53.78-91.26 %, 81.94-83.54 % and 52.44-81.98 %, respectively. The carbon retained in the hydrochar for RF and PS decreased as the temperature increased; however, no significant change was observed for FS. The carbon retained in FS hydrochar increased from 81.98 % to 88.98 % at 225 °C. The overall results showed that most of the carbon fraction is retained in the hydrochar after HTC treatment.

A negligible fraction of carbon was transferred into the liquid phase. It is essential to mention that the total organic carbon (TOC) analysis of the liquid products was not conducted immediately after HTC treatment. Although the liquid samples were stored in centrifuge tubes at a 4 °C environment, after 24 h (see Figure A 1 from APPENDICES), it was observed the formation of black precipitates in the walls of the container and on the surface of the process wastewater. This could be due to the presence of reactive by-products in the liquid phase as a result of hydrolysis during HTC, and these components may have polymerised during the cooling process resulting in the formation of precipitates. The solids were filtered through 0.25-0.45 µm nylon syringe filters before analysis, which could have contributed to the negligible carbon percentage in the liquid phase after analysis.

The carbon fraction in the gas phase was estimated by the difference using the carbon fraction in solid and liquid fractions. From Figure 6.11, higher reaction temperatures resulted in higher carbon fractions transferred to the gas phase. This could be due to increased rate of decarboxylation. The highest carbon fractions in the gas phase calculated were at 245 °C, corresponding to 45.32 %, 17.10 % and 47.17 % for RF, FS and PS, respectively.

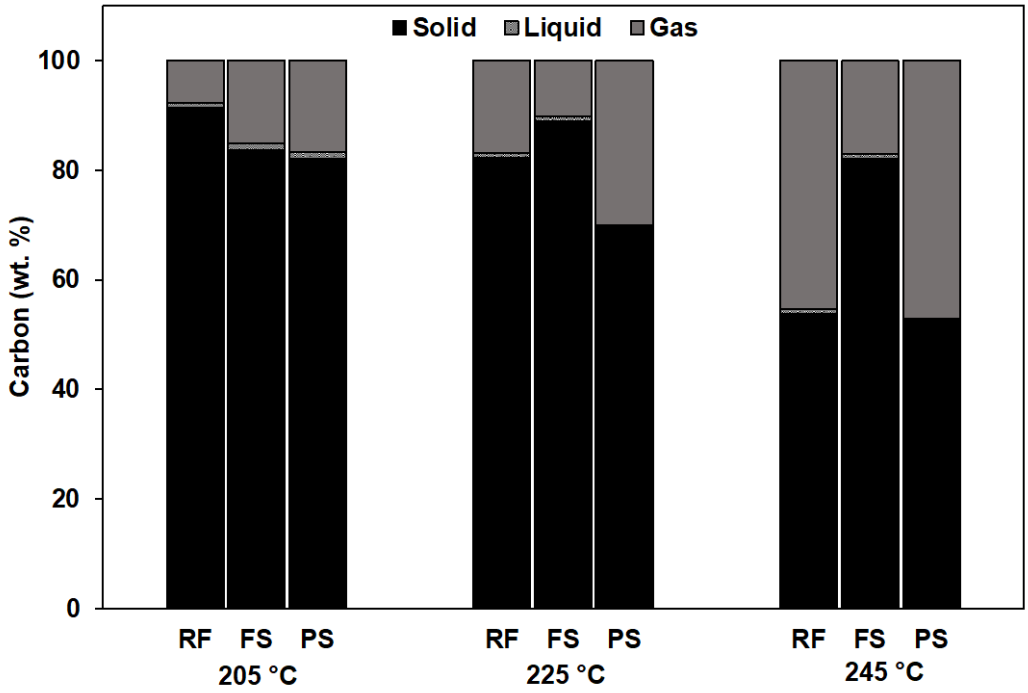

Figure 6.13: Carbon mass distribution between solid, liquid and gas phase.

6.8. Combustion Performance of Hydrochar Fuels

6.8.1. TG-DTG profiles

Thermogravimetric analysis (TGA) is a valuable technique used to assess the combustion properties of fuel materials. The decomposition behaviour, represented by the TGA-DTG curves, is of utmost importance to determine the thermal reactivity and decomposition stages resulting from the increase in temperature. The thermogravimetry (TG) profile of the raw samples and hydrochar at different reaction temperatures and the corresponding derivative thermogravimetry (DTG) are illustrated in Figure 6.14-Figure 6.16. The units are expressed in %/°C. For better evaluation of the combustion behaviour of the samples, the TG-DTG profiles were divided into four stages. The first stage is dehydration, which occurred below 200 °C and corresponded to the removal of

residual moisture. The second stage, which occurred between 200-400 °C, was attributed to the combustion of volatile organic matter such as cellulose and hemicellulose, as well as partial decomposition of lignin. The third stage, which occurred between 400-600 °C, was related to char combustion, which is associated with lignin decomposition. Lastly, the fourth stage occurred at temperatures higher than 600 °C, was associated with the volatile inorganic decomposition, and is considered the burnout stage.

The variation of the HTC reaction temperatures resulted in hydrochar with a TG-DTG pattern distinctive from that of the raw feedstock, especially for hydrochar obtained at 205 °C and 225°C. At this temperature range, the rate of mass loss increased dramatically, and this observation is more pronounced at 205 °C where the $(dm/dt)_{max}$ increased from 1.90-3.78 %/°C, 1.51-4.34 %/°C, and from 1.39-1.88 %/°C for RF, FS and PS respectively. In contrast, the maximum rate of mass loss decreased drastically at 245 °C, reaching values of 0.56 %/°C, 0.51 %/°C and 0.26 %/°C for RF, FS and PS, respectively. Moreover, the corresponding temperature (T_m) was relatively lower than that of the raw samples. This could be because, during the HTC, the substrates decomposed into products with simpler chemical structures and higher reactivity compared to the raw samples (Lin et al., 2015b). Thus, during the combustion process, the chemical bonds of these samples are easily broken, resulting in an increased rate of combustion.

The reduced mass loss rate at 245 °C is attributed to the decreased volatile content in the form of cellulose and hemicellulose, which almost wholly decompose as the temperature approaches 250 °C (Xiao et al., 2012), it is also due to the increased fixed carbon in the form of lignin which has higher thermal stability (Kang et al., 2013). Furthermore, the peaks in the range of 385-512 °C became more pronounced for hydrochar obtained at 245°C, especially for RF. This implies that more fixed carbon was generated with an increase in HTC reaction temperature.

6.8.2. *Ignition temperature*

The combustion parameters are summarised in Table 6.1. The ignition temperature determines how easily a given fuel is ignited, and the values were in the range of 294.96-316.53 °C, 292.30-315.05 °C and 309.00-314.57 °C, for RF, RF and PS, respectively. All hydrochars obtained at HTC treatment of 205 and 225 °C presented higher ignition temperatures compared to the raw substrates. This

translated to a higher ignition index (D_i), which implies better combustion performance.

6.8.3. Burnout temperature

The burnout temperature is a vital fuel parameter. It indicates the maximum temperature at which the fuel is almost completely consumed during combustion (Lu and Chen, 2015). The results on the burnout temperatures are also presented. Generally, fuels with high burnout temperatures require longer residence time and higher temperatures to achieve complete combustion. The increase in reaction temperatures led to reduced burnout temperatures; this is more pronounced for RF and FS at 245 °C, where a reduction of ~ 40 °C was observed. The burnout temperature for PS was the least affected.

6.8.4. Combustibility index

The calculated combustibility index (S) of the raw samples and corresponding hydrochar been are given in Table 6.1. A higher S value suggests a more active combustion ability. Hydrochar produced HTC treatment of 205 and 225 °C presented S values greater than that of the raw samples due to the increased maximum weight loss rate. When comparing the samples, FS-205 °C performed best S value $20.3 \times 10^{-7}\%^2/\mathrm{min}^2$. Those values were followed by $16.94 \times 10^{-7}\%^2/\mathrm{min}^2$, $11.00 \times 10^{-7}\%^2/\mathrm{min}^2$ and $10.47 \times 10^{-7}\%^2/\mathrm{min}^2$ for RF-205 °C, FS-225 °C and PS-225°C, respectively. These results suggest an improved combustion performance. Therefore, HTC is effective in producing hydrochar with enhanced combustion properties under appropriate reaction temperatures. When comparing the three substrates, PS samples presented the lowest combustion performance.

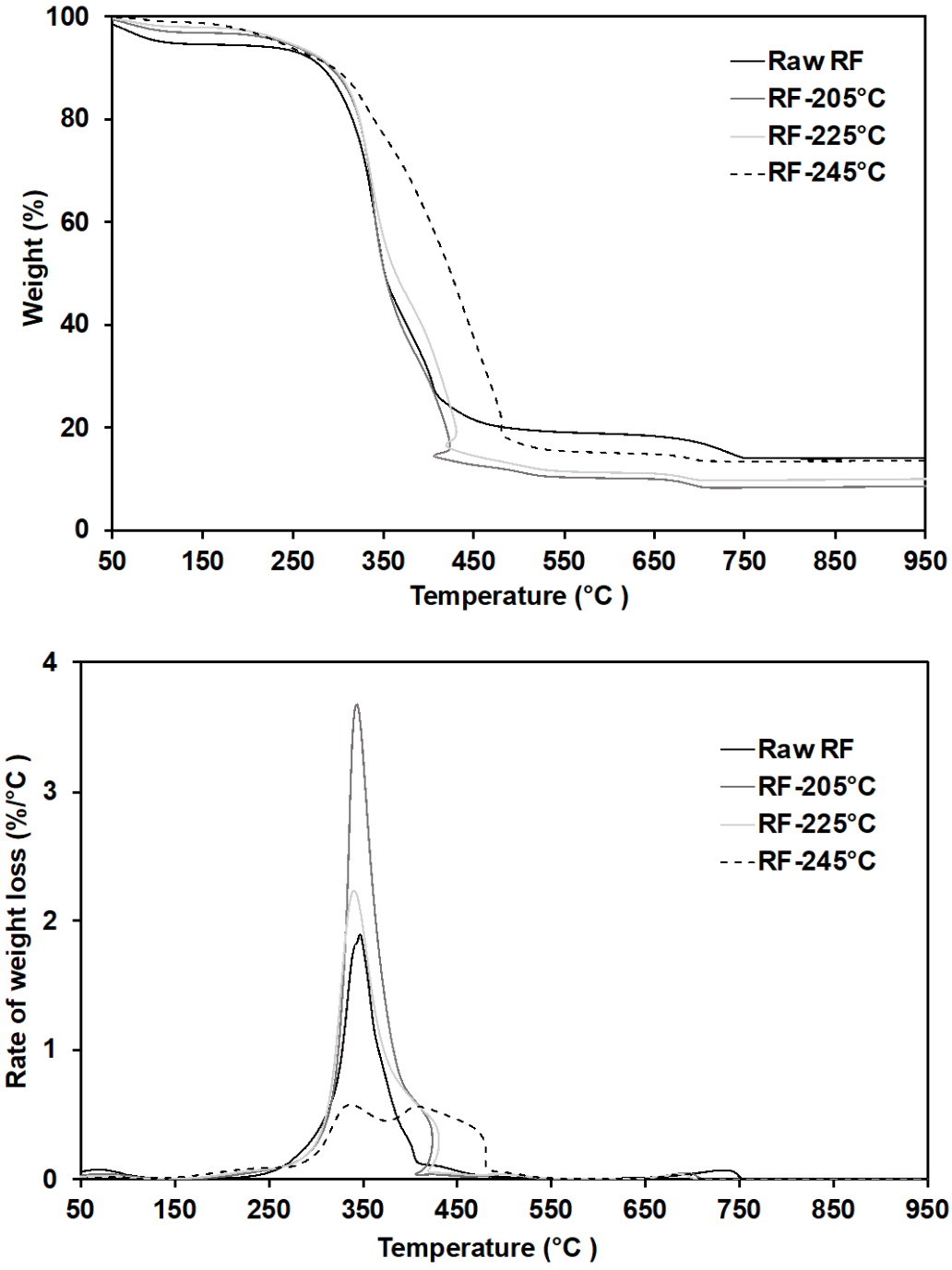

Figure 6.14: TG-DTG profiles of raw RF and hydrochar obtained at different HTC temperatures.

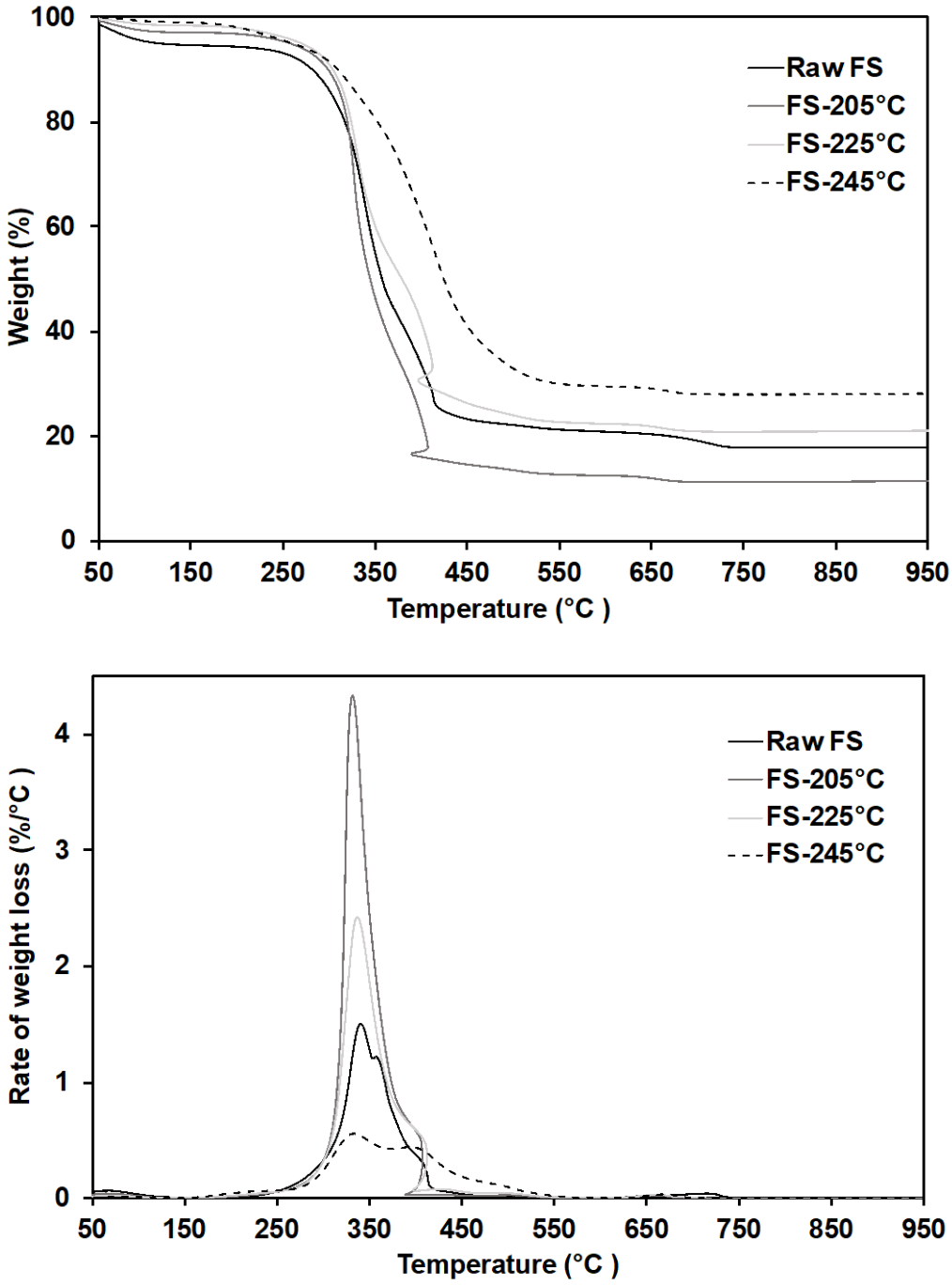

Figure 6.15: TG-DTG profiles of raw FS and hydrochar obtained at different HTC temperatures.

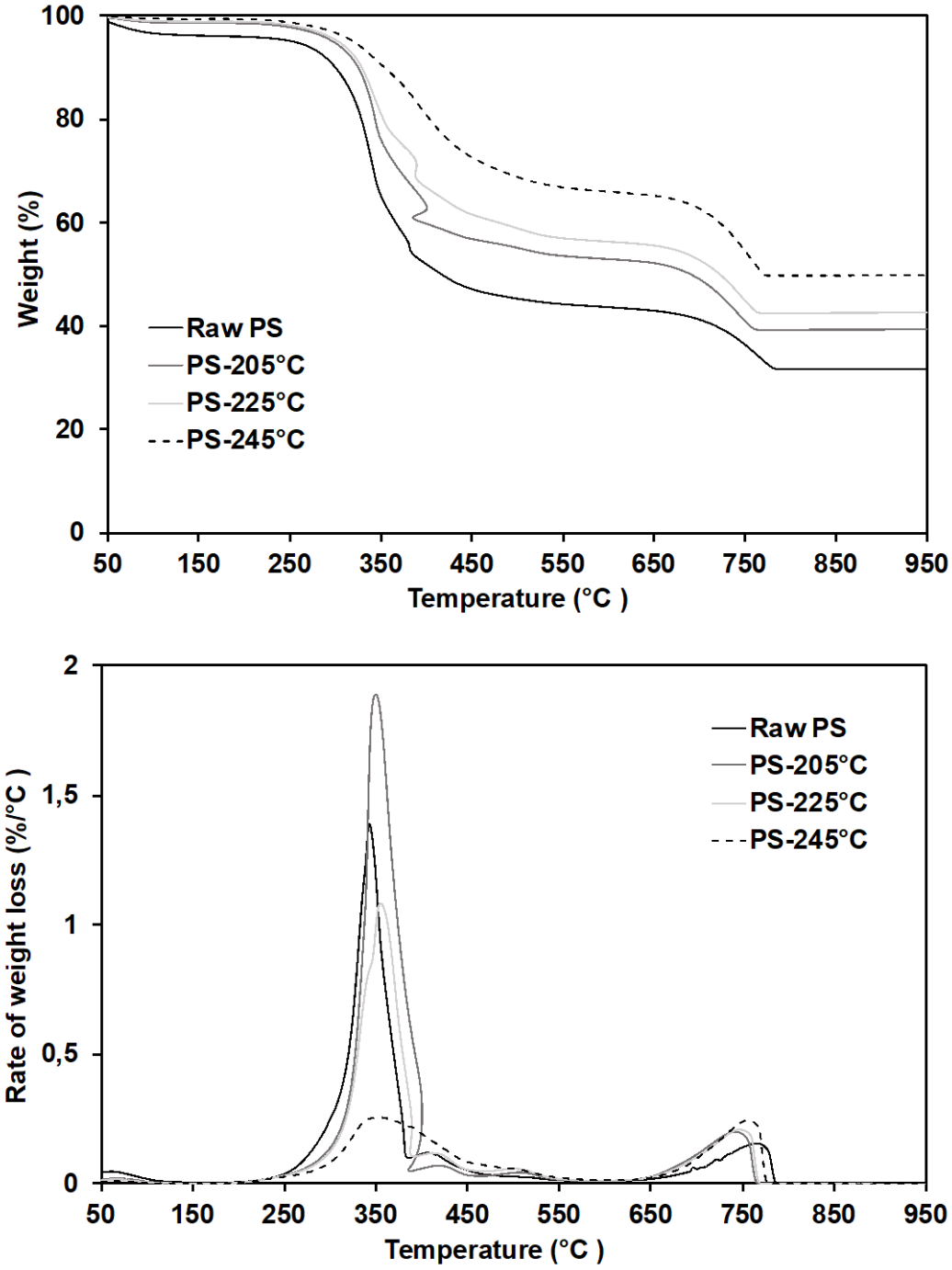

Figure 6.16: TG-DTG profiles of raw PS and hydrochar obtained at different HTC temperatures.

Table 6.1: Combustion parameters of the raw samples and hydrochars.

Sample	T_i (°C)	T_b (°C)	t_i (min)	T_{max} (°C)	$(dm/dt)_{max}$ (%/min)	D_i ($\times 10^{-2}$%/min^3)	S ($\times 10^{-7}$%^{2}/min^2°C^3)
Raw							
RF	305.54	746.32	14.13	345.61	37.95	17.18	8.12
RF-205	316.53	705.60	15.59	343.00	73.91	29.03	16.94
RF-225	307.22	697.36	15.05	340.87	44.98	18.66	11.00
RF-245	294.96	703.32	14.38	337.32	11.23	4.57	2.85
Raw							
FS	306.17	726.80	14.07	342.76	30.09	13.95	6.32
FS-205	315.05	681.04	15.48	331.72	86.75	35.22	20.3
FS-225	307.85	684.29	15.03	336.30	48.17	20.27	10.47
FS-245	292.30	685.99	14.29	332.37	10.15	4.615	2.11
Raw							
PS	309.65	786.96	14.24	344.63	27.80	12.60	4.38
PS-205	320.67	762.19	15.78	349.93	37.61	14.30	5.18
PS-225	314.57	767.44	15.52	356.82	20.04	7.67	2.72
PS-245	309.00	772.13	15.26	352.92	5.13	2.01	0.62

6.8.5. Residual ash

The ash content remained after combustion of the raw samples, and the hydrochar obtained at different HTC treatment temperatures are presented in Figure 6.17. Results showed that residual ash composition changed significantly. The residual ash composition varied from 9.56-14.85 %, 11.89-28.50 % and 33.00-50-26 % for RF, FS and PS, respectively. In General, PS hydrochar presented the highest residual ash composition post-combustion, especially at HTC-245 °C, where 50.52% ash weight was observed. The utilisation of fuel with high ash has negative implications to the environment and the technical design of a processing plant, as this requires further processing and disposal. Thus, based on these results, PS hydrochar is considered unfit for fuel application. RF hydrochar presented ash residues relatively lower than the raw substrates at all HTC temperatures. This could be because, during HTC, the inorganic components present in the RF raw samples is partially dissolved in the process water. For solid fuel applications, low ash is preferred as it prevents problems with is associated with fouling, scaling, slagging and corrosion in combustion chambers.

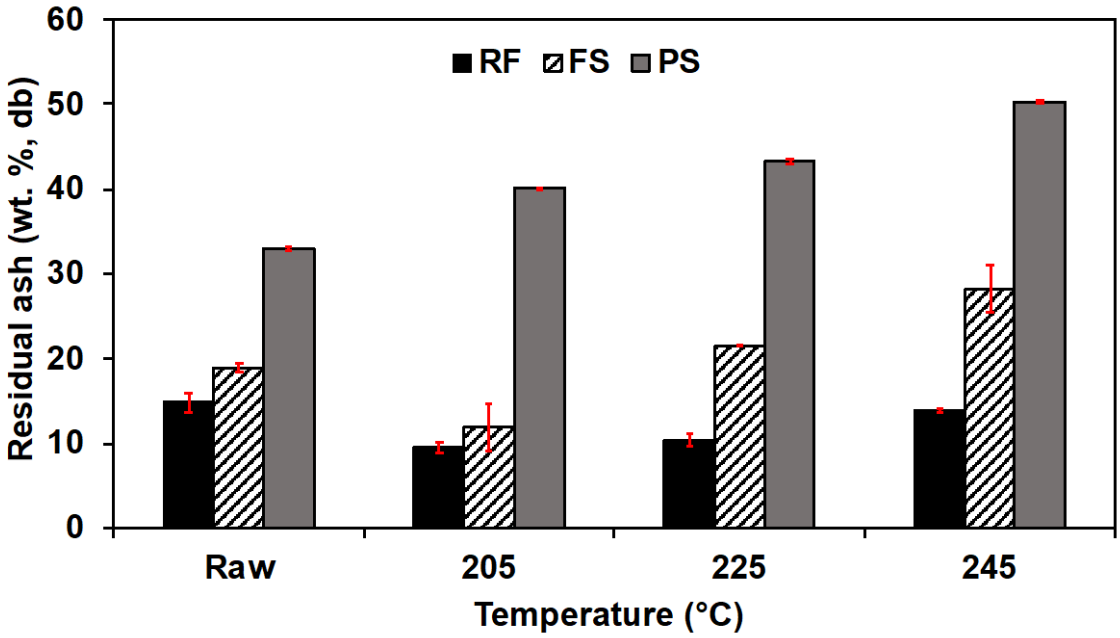

Figure 6.17: Residual ash of the raw samples and hydrochars post-combustion.

Based on the results obtained in this study, PS was concluded to be an unsuitable substrate for HTC treatment to produce hydrochar for solid fuel applications due to the significantly increased ash retained in the char, low combustion performance, elevated residual ash post-combustion and overall low calorific values. In contrast, RF and FS were considered suitable for HTC conversion; however, RF is preferable mainly because the hydrochar produced presented relatively low ash content compared to its raw substrate and all FS samples, which is of utmost importance for solid fuel application. It also presented relatively high fixed carbon and calorific values and more uniform hydrochar particles. Thus, the subsequent chapter covers the modelling and optimisation of hydrochar production via hydrothermal carbonisation of RF.

CHAPTER 7: MODELLING AND OPTIMISATION OF HYDROCHAR PRODUCTION FROM PAPER MILL RAW FIBRE REJECTS

7.1. Fitting of the Models

In this study, DoE-RSM was used to study the influence of HTC reaction temperature, residence time and solid load on the mass yield and calorific value of hydrochar obtained from recycling paper waste. The experimental and the predicted values of the response variables for hydrochar production are listed in Table 7.1. Results show a satisfactory agreement between the experimental and predicted values obtained from DoE-RSM Design. The percentage difference between the experimental and the predicted values for hydrochar yield and calorific values ranged between 0.01-7.55 % and 0-1.74 %, respectively, with an average percentage difference of 2.11 % and 1.64 %, respectively. The experimental data were used to calculate the coefficients of the second-order polynomial equation, and the regression coefficients are summarised in the subsequent subsections.

7.2. Response Surface Analysis of Hydrochar Yield

By applying multiple regression analysis on the experimental data, the hydrochar yield is expressed as a quadratic regression model of HTC reaction temperature (X_1), residence time (X_2) and solid load (X_3), as given by equation 7.1.

$$H_Y(\%) = 78.41 - 12.38X_1 - 16.81X_2 + 1.02X_3 - 10.36X_1X_2 + 0.0862X_1X_3 + 0.4487X_2X_3 - 7.08{X_1}^2 + 2.88{X_2}^2 + 1.86{X_3}^2 \quad (7.1)$$

Coefficients of the model were assessed by regression analysis in order to assess the need to exclude non-significant terms from the model. The ANOVA quadratic regression model for hydrochar yield and (H_Y) is presented in Table 7.2. For any given term in the model, a large regression coefficient and a small p-value indicate a more significant effect on the corresponding response variables. The F-value of 80.17 and p-value less than 0.0001 indicate that the model was highly significant and adequately fits the response data. In terms of Lack of Fit, there is a 16.27 % chance that a lack of fit this large could occur due to noise. Moreover, the value of the determination coefficient (R^2 = 0.9863) indicates that the second-order polynomial adequately represented the data, and the model explains 98.63% of the variation in hydrochar yield. Thus, only 1.37 % of the total variation was not explained by the model.

Table 7.1: Experimental design for hydrochar production with experimental and predicted values for hydrochar yield and HHV.

Run No.	T(°C)	t (h)	Solid load	Hydrochar Yield (%)		HHV (MJ/ kg, db.)	
	X_1	X_2	X_3	Experimental	Predicted	Experimental	Predicted
1	230	1.75	0.12	80.57	81.29	17.51	17.76
2	230	0.5	0.10	94.36	98.10	14.99	14.86
3	210	0.5	0.12	95.37	95.38	14.33	14.33
4	250	0.5	0.08	91.97	90.20	15.98	16.00
5	210	3	0.12	82.27	83.39	17.99	17.99
6	250	3	0.08	35.62	34.96	22.46	22.47
7	230	3	0.10	65.62	64.48	19.85	19.92
8	230	1.75	0.10	76.12	78.41	18.11	17.93
9	250	1.75	0.10	54.66	58.95	19.84	20.06
10	210	0.5	0.08	94.80	94.41	14.24	14.43
11	250	0.5	0.12	93.11	91.52	16.19	16.11
12	230	1.75	0.10	77.58	78.41	18.23	17.93
13	230	1.75	0.10	80.51	78.41	17.71	17.93
14	230	1.75	0.10	81.63	78.41	17.81	17.93
15	230	1.75	0.08	77.38	79.25	18.00	17.69
16	250	3	0.12	38.33	38.07	22.86	22.69
17	230	1.75	0.10	79.59	78.41	17.90	17.93
18	230	1.75	0.10	80.23	78.41	17.69	17.93
19	210	3	0.08	79.68	80.63	17.89	17.98
20	210	1.75	0.10	85.41	83.72	17.20	16.92

Table 7.2: ANOVA results for hydrochar yield response surface.

Source	SS[a]	df[b]	MS[c]	F-value	p-value
Model	5370.55	9	596.73	**80.17**	**< 0.0001**
X_1	1533.63	1	1533.63	206.05	< 0.0001
X_2	2825.42	1	2825.42	379.60	< 0.0001
X_3	10.40	1	10.40	1.40	0.2644
X_1X_2	859.26	1	859.26	115.44	< 0.0001
X_1X_3	0.0595	1	0.0595	0.0080	0.9305
X_2X_3	1.61	1	1.61	0.2164	0.6517
X_1^2	137.81	1	137.81	18.52	0.0016
X_2^2	22.74	1	22.74	3.06	0.1110
X_3^2	9.52	1	9.52	1.28	0.2844
Residual	74.43	10	7.44		
Lack of Fit	53.52	5	10.70	2.56	0.1627
Pure Error	20.91	5	4.18		
Cor. Total	5444.98	19			
Model statistics					
Std. Dev.	2.73		**R^2**	**0.9863**	
Mean	77.24		Adjusted R^2	0.9740	
C.V. %	3.53		Predicted R^2	0.9289	
			Adeq Precision	**32.7291**	

a: sum of squares. b: degree of freedom. c: mean square. p-values < 0.05 indicate model term is significant.

7.3. Response Surface Analysis of Calorific Value

By applying multiple regression analysis on the experimental data, the calorific value (HHV) is expressed as a quadratic regression model of HTC reaction temperature (X_1), residence time (X_2) and solid load (X_3), as given by equation 7.2.

$$\begin{aligned}\text{HHV (MJ/ kg)} = {} & 17.93 + 1.57\,X_1 + 2.53X_2 + 0.031X_3 + 0.73X_1X_2 \\ & + 0.0525X_1X_3 + 0.025X_2X_3 + 0.5623{X_1}^2 - 0.5377{X_2}^2 \\ & - 0.2027{X_3}^2\end{aligned} \qquad (7.2)$$

The ANOVA quadratic regression model for calorific value (HHV) is shown in Table 7.3. The F-value of 168.28 and p-value less than 0.0001 indicate that the

model was highly significant and properly fits the response data. In terms of Lack of Fit, there is a 31.23 % chance that a lack of fit this large could occur due to noise. Moreover, the value of the determination coefficient (R^2 = 0.9934) indicates that the second-order polynomial adequately represented that data, and the model explains 99.34 % of the variation in HHV. Thus, only 0.66 % of the total variation was not explained by the model.

Table 7.3: ANOVA results for HHV response surface.

Source	SS[a]	df[b]	MS[c]	F-value	p-value
Model	94.38	9	10.49	**168.28**	**< 0.0001**
X_1	24.59	1	24.59	394.52	< 0.0001
X_2	64.11	1	64.11	1028.74	< 0.0001
X_3	0.0096	1	0.0096	0.1542	0.7028
X_1X_2	4.26	1	4.26	68.41	< 0.0001
X_1X_3	0.0220	1	0.0220	0.3538	0.5652
X_2X_3	0.0050	1	0.0050	0.0802	0.7828
X_1^2	0.8694	1	0.8694	13.95	0.0039
X_2^2	0.7952	1	0.7952	12.76	0.0051
X_3^2	0.1130	1	0.1130	1.81	0.2078
Residual	0.6232	10	0.0623		
Lack of Fit	0.3823	5	0.0765	1.59	0.3123
Pure Error	0.2409	5	0.0482		
Cor. Total	95.01	19			
Model statistics					
Std. Dev.	0.2496		**R^2**	**0.9934**	
Mean	17.84		Adj. R^2	0.9875	
C.V. %	1.40		Pred. R^2	0.9651	
			Adeq. Precision	**47.3314**	

a: sum of squares. b: degree of freedom. c: mean square. p-values < 0.05 indicate model terms are significant.

7.4. Effect of Process Parameters on Model Responses

7.4.1. Hydrochar yield

For the H_Y model, the p-values values of the independent variables, reaction temperature (X_1), reaction time (X_2) and the interaction term (X_1X_2), were lower than 0.0001, indicating that the terms were the most significant model variables and had the most considerable influence on the hydrochar yield. Moreover, the quadratic term of the temperature (X_1^2) with a p-value of 0.0016 indicates a relatively weaker influence but significance in the model response. Other terms such as the ratio solid load (X_3), the interaction between reaction temperature and solid load (X_1X_3), the quadratic effect of reaction residence time (X_2^2) and solid load (X_3^2) had p-values higher than 0.05, which indicates that these terms had no significant effect on the hydrochar yield.

7.4.1.1. The interactive effect between temperature, residence time and solid load on hydrochar yield.

The response surface plots as a result of the interaction between the HTC reaction temperature (X_1) and residence time (X_2), residence time and solid load (X_3), as well as the interaction between X_3 and X_1 on hydrochar yield are shown in Figure 7.1a-c, to further evaluate their effects on the variation in hydrochar yield at a fixed solid load of 0.10. Figure 7.1a represents the effect of reaction temperature and residence time on the hydrochar yield. The result shows that hydrochar yield is highly influenced by reaction temperature (X_1) and residence time (X_2), and the increase in both factors results in a decrease in hydrochar yield, forming a curve-shaped response surface. Reaction temperature ($F= 206.05$; $p < 0.0001$) and residence time ($F = 379.60$; $p < 0.0001$) had a highly significant negative linear and interactive effect ($F = 115.44$; $p < 0.0001$) on the hydrochar yield, while reaction temperature alone had a weaker but significant negative quadratic effect on the hydrochar yield ($F = 18.52$; $p = 0.0016$). The hydrochar yield first increased with an increase in reaction temperature and residence time up to a specific point, then decreased with a further increase in reaction temperature and residence time. This finding is consistent with reported literature (Kannan et al., 2017). Within this design space, residence time showed a slightly higher significant influence on hydrochar yield compared to reaction temperature. Increasing the residence time from 0.5 h to 3 h at the most severe reaction temperature (250 °C) and fixed solid load of 0.10

resulted in a net 60.64 % hydrochar yield decrease, while the decrease in yield associated with elevating the reaction temperature from 210 °C to 250 °C at the most severe reaction time (3 h) and solid load of 0.10, led to a net 55.96 % hydrochar yield decrease. Thus, the increment of residence time resulted in higher conversion rates. In general, high HTC reaction severity favours the hydrolysis of the polymeric structure of hemicellulose and cellulose into monomers, which consequently undergo a series of reactions, including dehydration, decarboxylation condensation and polymerisation, resulting in low hydrochar yield (Wang et al., 2018). The highest hydrochar decrease was observed when the HTC temperature was increased from 230 °C to 250 °C, where a decrease of 46.26 % was observed, compared to 19.57 % decrease when the reaction temperature was increased from 210 °C to 230 °C. Hemicellulose starts hydrolysing at 180 °C, cellulose starts slow degradation at 220 °C, and lignin starts to slowly break down at 255 °C (Xiao et al., 2012, Saha et al., 2019a), thus, as the temperature approaches 250 °C, both hemicellulose and cellulose almost completely decompose translating in a significant mass loss by the solid phase. These results are consistent with reported works (Lin et al., 2015b, Saha et al., 2019a, Saha et al., 2019b). Similarly, the highest hydrochar yield decrease was observed when residence time was increased from 1.75 h to 3 h (41.21 %) compared to a 33.79 % decrease when residence time was increased from 0.5 to 1.75 h.

As for the interaction between solid load and residence time (Figure 7.1b), and between solid load and temperature (Figure 7.1c). Although the linear term of solid load (X_3), the interaction between the solid load and residence time (X_2X_3) and the quadratic term of the solid load (X_3^2) had a positive effect on hydrochar yield, i.e. the hydrochar yield first decreased and then increased when the variables were increased. These terms did not have a significant effect on the model ($p > 0.05$ for X_3, X_2X_3 and X_3^2); therefore, they do not significantly explain the variation in hydrochar yield. Similarly, for Figure 7.1c, although the interaction between the solid load and temperature (X_1 X_3) have a positive effect on the hydrochar yield, the term did not significantly explain the variation in hydrochar yield ($F = 0.008$; $p > 0.05$). Further information on the effect of each factor on hydrochar yield is available in Figure B 1. The regression coefficients for the intercept, linear, quadratic and interaction terms are presented in Table 7.4.

In summary, the minimum hydrochar yield observed was 35.62 % obtained at 250 °C for 3 h at a solid load of 0.08, while the maximum hydrochar yield recorded

was 95.37 % obtained at 210 °C for 0.5 h at a solid load of 0.12. The quadratic effect of residence time (X_2^2), solid load (X_3), the interaction between the solid load and the residence time (X_2X_3), the interaction between the solid load and reaction temperature (X_1X_3) as well as the quadratic term of the solid load (X_3^2) did not significantly explain the model; therefore they are not significant for optimisation of the hydrochar yield.

7.4.2. Calorific values

For the HHV model, the p-values values for reaction temperature (X_1), reaction time (X_2) and the interaction term (X_1X_2) were lower than 0.0001, indicating that the terms were the most significant variables and had the largest influence on the calorific value. Furthermore, the quadratic term of the reaction temperature (X_1^2) and residence time (X_2^2) with p-values of 0.0039 and 0.0051, respectively, imply a weaker influence but still significant on the model response. Terms such as the solid load (X_3), the interaction between reaction temperature and solid load (X_1X_3), and quadratic effect of solid load (X_3^2) had p-values higher than 0.05, which indicates that these terms had no significant effect on the calorific value.

7.4.2.1. The interactive effect between temperature, residence time and solid load on calorific value.

The calorific value is an important factor, as it provides the quantity of total energy present in the hydrochar. The combined effects of the three process variables on the calorific value at a fixed solid load of 0.10 are shown in Figure 7.1d-f. Similar to hydrochar yield, the calorific value was highly influenced by reaction temperature (X_1) and residence time (X_2); in contrast to the hydrochar yield trend, the increase in reaction temperature and time resulted in hydrochar with a higher calorific value. Figure 7.1d represents the effect of reaction temperature and residence time on HHV. Reaction temperature ($F= 394.52$; $p < 0.0001$) and residence time ($F = 1028.74$; $p < 0.0001$) had a highly significant positive linear and interactive effect ($F = 68.41$; $p < 0.0001$) on the calorific value. Moreover, reaction temperature had a weaker but significant positive quadratic effect on the hydrochar yield ($F = 13.95$; $p = 0.0039$), while the residence time had a weaker but significant negative quadratic effect on HHV ($F = 12.76$; $p = 0.0051$). This implies that the calorific value increased with an increase in reaction temperature and time and then

decreased with a further increase in reaction time. Since the HHV in lignocellulose biomass follows the following trend lignin > cellulose > hemicellulose > extractives > ash (Reza et al., 2013a, Kambo and Dutta, 2015), therefore, higher reaction severity favours increased rate of devolatilization of components with lower thermal stability (cellulose and hemicellulose) and increases the content of fractions with higher thermal stability (lignin), as a consequence, hydrochar with higher calorific value is obtained (Kang et al., 2013, Reza et al., 2013a, Basso et al., 2013).

Concerning the interaction between the solid load and residence time (Figure 7.1e), and between the solid load and temperature (Figure 7.1f). The linear term of solid load ratio (X_3), the interaction between solid load and residence time (X_2X_3) had a positive effect on HHV, while the quadratic term of the solid load (X_3^2) had a negative effect on the calorific value, i.e. HHV first increased and then decreased when the variables increased. However, similar to hydrochar yield, these terms did not have a significant effect on the model ($p > 0.05$ for X_3, X_2X_3 and X_3^2); therefore, they do not significantly explain the variation in calorific value. Likewise, for Figure 8.1f, the interaction between solid load and temperature (X_1 X_3) have a positive effect on the calorific value; however, the term did not significantly explain the variation in calorific values ($F = 0.3538$; $p > 0.05$).

To summarise, the maximal HHV recorded was 22.86 MJ/ kg, which is approximately equivalent to the HHV of coal used for commercial utility in South Africa (Makgato and Chirwa, 2017). The maximal HHV observed corresponds to an increase of 49.80 % of the HHV of the original feedstock and was obtained at 250 °C, reaction time of 3 hours and solid load of 0.12. The minimum hydrochar yield recorded was 14.24 MJ/ kg obtained at 210 °C for 0.5 h at a solid load of 0.08. The solid load (X_3), the interaction between the solid load and the residence time (X_2X_3), the interaction between the solid load and reaction temperature (X_1X_3) as well as the quadratic term of the solid load (X_3^2) did not significantly explain the model; therefore they are not significant for optimisation of the calorific value of the hydrochar.

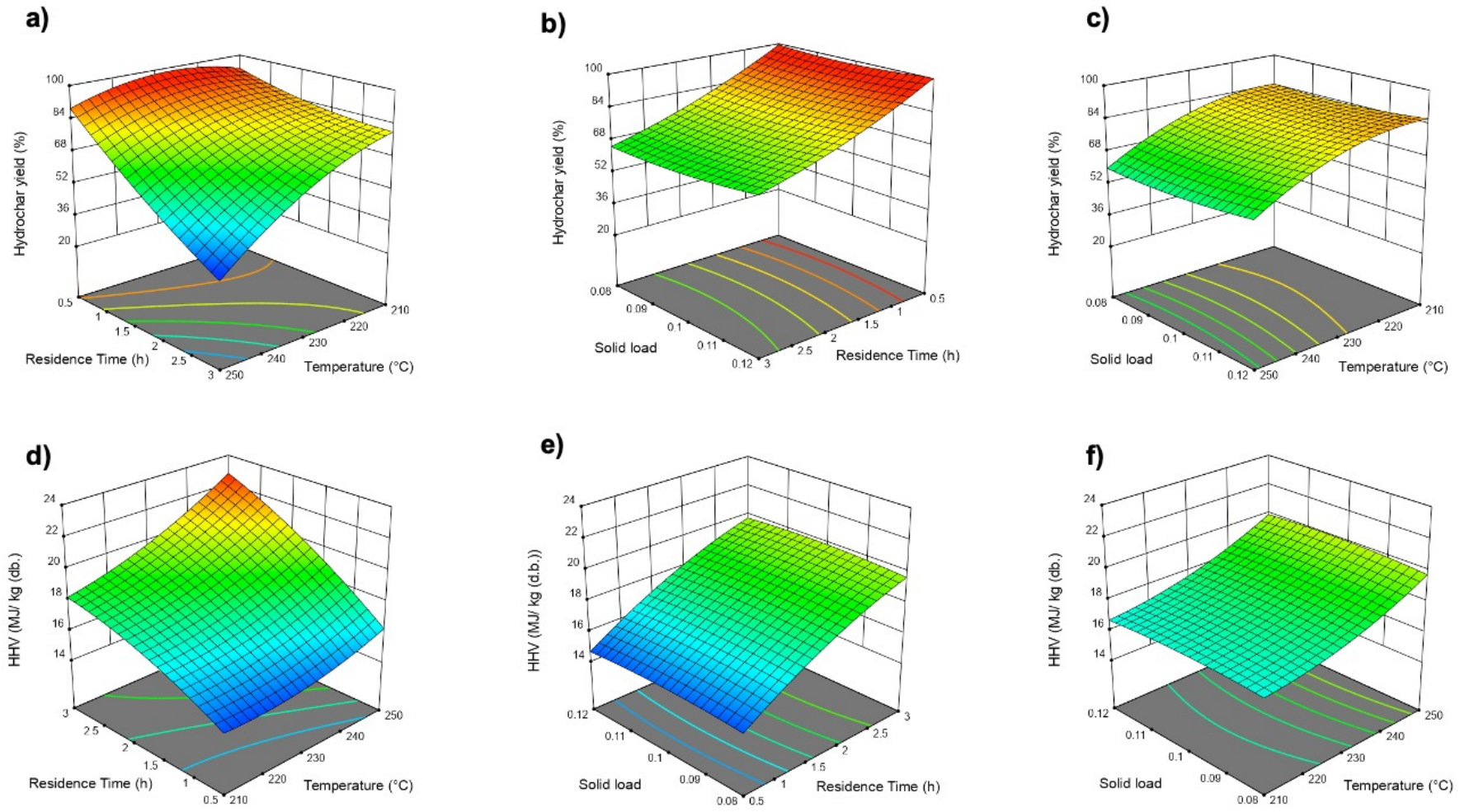

Figure 7.1: Response surface plots showing the effect of a) T and t on hydrochar yield; b) t and solid load on hydrochar yield; c) T and solid load on hydrochar yield; d) T and t on HHV; e) t and solid load on HHV and f) T and solid load on HHV.

Table 7.4: Regression coefficient values for hydrochar yield and HHV.

Model parameters	H_Y	HHV
β_0	78.41[a]	17.93[a]
Linear effects		
β_1	-12.38[a]	1.57[a]
β_2	-16.81[a]	2.53[a]
β_3	1.02[NS]	0.031[NS]
Interaction effects		
β_{12}	-10.36[a]	0.73[a]
β_{13}	0.0862[NS]	0.0525[NS]
β_{23}	0.4487[NS]	0.025[NS]
Quadratic effects		
β_{11}	-7.08[b]	0.5623[b]
β_{22}	2.88[NS]	-0.5377[c]
β_{33}	1.86[NS]	-0.2027[NS]

Statistically significant at [a] $p < 0.0001$, [b] $p < 0.01$, [c] $p < 0.05$ and [NS]: non-significant.

7.5. Final Modified Equations in Terms of Coded Factors

To further improve the reliability of the model, a backward model reduction was performed for p-values coded at α = 0.1 to consider only the significant terms. Therefore, the reduced model for hydrochar yield in terms of the coded equation was given as follows:

$$H_Y(\%) = 78.64 - 12.38X_1 - 16.81X_2 - 10.36X_1X_2 + -6.38{X_1}^2 + 3.57{X_2}^2 \quad (7.3)$$

The new model has as higher F-value compared the full model (F = 155.96; $p < 0.0001$) non-significant Lack of Fit (F = 2; p =0.2311), higher adjusted R^2 value (0.9761) and higher adequate precision (43.7416).

Similarly, the reduced model for HHV was given by equation 7.4.

$$\text{HHV (MJ/ kg)} = 17.90 + 1.57\,X_1 + 2.53X_2 + 0.73X_1X_2 + 0.4862{X_1}^2 - 0.6138{X_2}^2 \quad (7.4)$$

The new model has as higher F-value compared the full model (F = 341.40; $p < 0.0001$) higher Lack of Fit (F-value = 1.23; p-value = 0.4322), higher adjusted R^2 value (0.9890) and higher adequate precision (63.7181).

The reduced ANOVA quadratic regression model for hydrochar yield and calorific value are presented in Table 7.5 and Table 7.6, respectively, and the regression coefficients for the reduced models are summarised in Table 7.7. Results suggest that the data obtained are reliable and the developed models are adequate to make predictions within the design space and optimise HTC process parameters for hydrochar production.

Table 7.5: Reduced model ANOVA results for hydrochar yield response surface.

Source	SS [a]	df [b]	MS [c]	F-value	p-value
Model	5348.95	5	1069.79	**155.96**	**< 0.0001**
X_1	1533.63	1	1533.63	223.59	< 0.0001
X_2	2825.42	1	2825.42	411.92	< 0.0001
X_1X_2	859.26	1	859.26	125.27	< 0.0001
X_1^2	130.31	1	130.31	19.00	0.0007
X_2^2	40.87	1	40.87	5.96	0.0285
Residual	96.03	14	6.86		
Lack of Fit	75.12	9	8.35	2.00	0.2311
Pure Error	20.91	5	4.18		
Cor. Total	5444.98	19			
Model statistics					
Std. Dev.	2.62		R^2	0.9824	
Mean	77.24		**Adjusted R^2**	**0.9761**	
C.V. %	3.39		**Predicted R^2**	**0.9577**	
			Adeq. Precision	**43.7416**	

a: sum of squares. b: degree of freedom. c: mean square. p-values < 0.05 indicate model terms are significant.

Table 7.6: Reduced model ANOVA results for HHV response surface.

Source	SS[a]	df[b]	MS[c]	F-value	p-value
Model	94.23	5	18.85	**341.40**	**< 0.0001**
X_1	24.59	1	24.59	445.36	< 0.0001
X_2	64.11	1	64.11	1161.30	< 0.0001
X_1X_2	4.26	1	4.26	77.22	< 0.0001
X_1^2	0.7566	1	0.7566	13.71	0.0024
X_2^2	1.21	1	1.21	21.83	0.0004
Residual	0.7729	14	0.0552		
Lack of Fit	0.5320	9	0.0591	1.23	0.4322
Pure Error	0.2409	5	0.0482		
Cor. Total	95.01	19			
Model statistics					
Std. Dev.	0.2350				
Mean	17.84		R^2	0.9919	
C.V. %	1.32		**Adj. R^2**	**0.9890**	
			Pred. R^2	**0.9832**	
			Adeq. Precision	**63.7181**	

a: sum of squares. b: degree of freedom. c: mean square. p-values < 0.05 indicate model terms are significant.

Table 7.7: Regression coefficient values for reduced hydrochar yield and HHV values.

Model parameters	H_Y	HHV
β_0	78.64 [a]	17.90 [a]
Linear effects		
β_1	-12.38 [a]	1.57 [a]
β_2	-16.81[a]	2.53 [a]
Interaction effects		
β_{12}	-10.36 [a]	0.73 [a]
Quadratic effects		
β_{11}	-6.38 [c]	0.4862 [c]
β_{22}	3.57 [d]	-0.6138 [b]

Statistically significant at [a] $p < 0.0001$, [b] $p < 0.001$, and [c] $p < 0.01$, and [d] $p < 0.05$.

7.6. Optimum Operating Conditions for Hydrochar Fuel Recovery

The criteria set for optimisation were minimum level for HTC reaction temperature and residence time, and solid load set at maximum (i.e. 12 % wt. dry sludge with 88 % water) with the aim of minimising costs associated with the energy required to heat the water. The goal was to obtain maximal hydrochar yield and calorific value of at least 17 MJ/ kg, which falls in the range of the HHV of meta-lignite/ sub-bituminous coal ash-free basis calorific values (Grammelis et al., 2016). Thus, based on the defined limits under the design space investigated, a maximal solid yield of **74.39 %** with a calorific value of **18.50 MJ/ kg** could be obtained at the reaction temperature of **231.62 °C** and residence time of **1.99 h**, thus considered the optimal HTC operating condition.

7.7. Properties of Produced Hydrochars

7.7.1. Proximate composition

The proximate composition and the elemental analysis of the raw sludge and hydrochars are presented in Table 7.8. From the results, it is evident that, in contrast to reaction temperature and residence time, the solid load had little influence on the volatile matter (VM) and fixed carbon (FC) composition. The initial VM and FC was 60.22 % and 25.90 %, respectively. However, HTC reactions conducted at a residence time of 0.5 h resulted in a gradual increase in the volatile matter and a

decrease in fixed carbon, which consequently translated into a lower fuel ratio compared to the original substrate. In contrast, VM had a negative correlation, and FC had a positive correlation when HTC reaction time was ≥ 1.75 h and with further increase in reaction severity, leading to a substantial decrease in VM with a simultaneous increase in FC. The maximum VM decrease and FC increment were observed at the highest reaction severity (SF = 6.67, see Table A 2 from APPENDICES), where the VM reduced by 48.75 % while the FC increased by approximately 2.14 times compared to the initial substrate. As a result, hydrochars with improved and energy densification and enhanced fuel properties were obtained (Table 7.9). This is due to carbonisation mechanisms observed in reported studies (Saha et al., 2019a, Volpe et al., 2018, Kim et al., 2015, Hoekman et al., 2011). Furthermore, the increased fuel ratio (i.e. ratio of FC to VM) obtained at higher reaction severity suggests improved combustibility of the hydrochar fuel (Afolabi et al., 2020). The fuel ratio of the hydrochar increased from 0.43 to 1.86, with the highest value recorded at HTC temperature of 250 (°C), the residence time of 3 h and solid load of 0.08.

As previously discussed, the energetic application of high ash hydrochar fuel has negative environmental and process development implications. Therefore, fuels with low ash content are of utmost advantage. In general, the ash composition was relatively lower than the initial substrate. This could be attributed to due to the dissolution of inorganics into the liquid phase during HTC reaction mechanisms at SF ≤ 6.44. However, the hydrochar obtained 250 °C and 3 hours showed a gradual increase in content from 13.88 to 14.77% and 16.55 % at solid load of 0.08 and 0.12, respectively, due to the retention of inorganics in the solid phase (McGaughy and Reza, 2018). The ash content values obtained in this work were observed to be lower than those reported in previous studies for hydrochar preparation from paper mill sludge (Oumabady et al., 2020, Saha et al., 2019b, Lin et al., 2015b).

Table 7.8: Proximate and elemental analysis of raw sludge at hydrochars at obtained different HTC reaction conditions

Operating parameters			Proximate composition (db)				Elemental composition (db)				
T (°C)	t (h)	Solid load	VM (%)	FC (%)	Ash (%)	Fuel Ratio	C (%)	H (%)	O[a] (%)	N (%)	S (%)
		Raw sludge	60.22	25.90	13.88	0.43	39.30	5.12	39.44	BD	2.27
210	0.5	0.08	67.81	24.90	7.28	0.37	41.79	5.46	44.56	0.40	0.50
		0.12	69.73	23.92	6.35	0.34	40.88	5.26	46.91	0.21	0.38
	1.75	0.10	64.69	26.08	9.24	0.40	46.10	6.18	37.68	0.32	0.48
	3	0.08	63.82	29.19	6.99	0.46	46.23	5.84	40.63	0.31	BD
		0.12	61.27	30.26	8.47	0.49	47.42	5.93	37.37	0.33	0.49
230	0.5	0.10	70.44	24.41	5.15	0.35	35.62	4.46	54.20	0.21	0.37
	1.75	0.08	60.79	30.36	8.85	0.50	46.40	5.83	38.13	0.32	0.47
		0.10	59.81	31.59	8.60	0.53	46.10	5.76	38.71	0.35	0.49
		0.12	56.85	33.15	10.00	0.58	43.43	5.36	40.86	0.00	0.35
	3	0.10	48.22	43.76	8.01	0.91	47.93	5.38	37.82	0.38	0.48
250	0.5	0.08	73.02	22.70	4,28	0.31	41.67	5.93	47.30	0.34	0.48
		0.12	65.62	25.70	8.68	0.39	42.06	5.47	43.39	0.39	BD
	1.75	0.10	39.32	47.47	13.21	1.21	50.25	5.14	30.98	0.42	BD
	3	0.08	29.83	55.40	14.77	1.86	56.27	4.71	23.22	0.51	0.52
		0.12	30.86	52.59	16.55	1.70	57.13	4.97	20,33	0.50	0.53

db: dry basis. BD: below detection limit. a: estimated by difference.

7.7.2. Elemental composition

In terms of elemental composition, the solid load had little influence on the chemical composition of the hydrochar. The hydrochars obtained at higher reaction severities showed significant changes in elemental CHONS composition compared to the raw sample. These findings are consistent with previous studies (Saha et al., 2019b). all hydrochars obtained had increased carbon content and, in most cases, decreased oxygen content. The carbon increased from 39.30 % to 57.13 % due to carbonisation mechanisms, translating to a higher carbon densification factor higher than 1 in all cases, with the exception of hydrochar obtained at 230 °C, 0.5 h and solid load of 0.10 (see Table 7.9). The range of 1-1.5 in carbon densification factor was in line with reported studies (Lu et al., 2013, Afolabi et al., 2020). Moreover, the values of the carbon retained in the hydrochar ranged from 50.53-99.98 %. This suggests that after HTC, most of the carbon fraction remained in the solid phase. The substantial decrease in carbon content at the highest rection severity could be associated with the increased rate of decarboxylation.

The influence of carbon and oxygen content on the calorific value of the samples have also been investigated. In terms of carbon content, the result suggests a strong linear correlation ($R^2 = 0.8872$; $p < 0.0001$) between the calorific values and the carbon content of the raw sludge and the produced hydrochars, as shown in Figure 7.2. This trend is consistent with reported works (Afolabi et al., 2020, Kannan et al., 2017). This suggests that increased carbon content produces hydrochars with higher calorific values.

There was also a strong linear correlation (R2 = 0.8572; $p < 0.0001$) between the calorific values and the oxygen content of the raw sludge and the produced hydrochars, as shown in Figure 7.3. This implies that, contrary to carbon content, decreased oxygen content results in hydrochar with higher calorific values.

Table 7.9: Carbon and energy properties of hydrochars obtained at different HTC reaction conditions.

Operating parameters			Carbon properties			Energy properties		
T (°C)	t (h)	Solid load	C_{char}(%)	C_D	$C_{increase}$ (%)	E_D	$HHV_{improvement}$ (%)	E_Y (%)
210	0.5	0.08	99,88	1,06	6,36	0,93	-6,64	88,51
		0.12	98,29	1,04	4,05	0,94	-6,07	89,58
	1.75	0.10	99,28	1,17	17,34	1,13	12,71	96,27
	3	0.08	92,87	1,18	17,65	1,17	17,23	93,41
		0.12	98,35	1,21	20,68	1,18	17,94	97,03
230	0.5	0.10	84,74	0,91	-9,35	0,98	-1,74	92,72
	1.75	0.08	90,51	1,18	18,09	1,18	17,97	91,28
		0.10	92,12	1,17	17,32	1,17	17,38	93,03
		0.12	89,07	1,11	10,54	1,15	14,79	92,49
	3	0.10	79,30	1,22	21,99	1,30	30,12	85,39
250	0.5	0.08	96,61	1,06	6,05	1,05	4,73	96,32
		0.12	98,74	1,07	7,05	1,06	6,13	98,82
	1.75	0.10	69,26	1,28	27,90	1,30	30,02	71,07
	3	0.08	50,53	1,43	43,23	1,47	35,62	52,43
		0.12	55,22	1,45	45,41	1,50	49,85	57,45

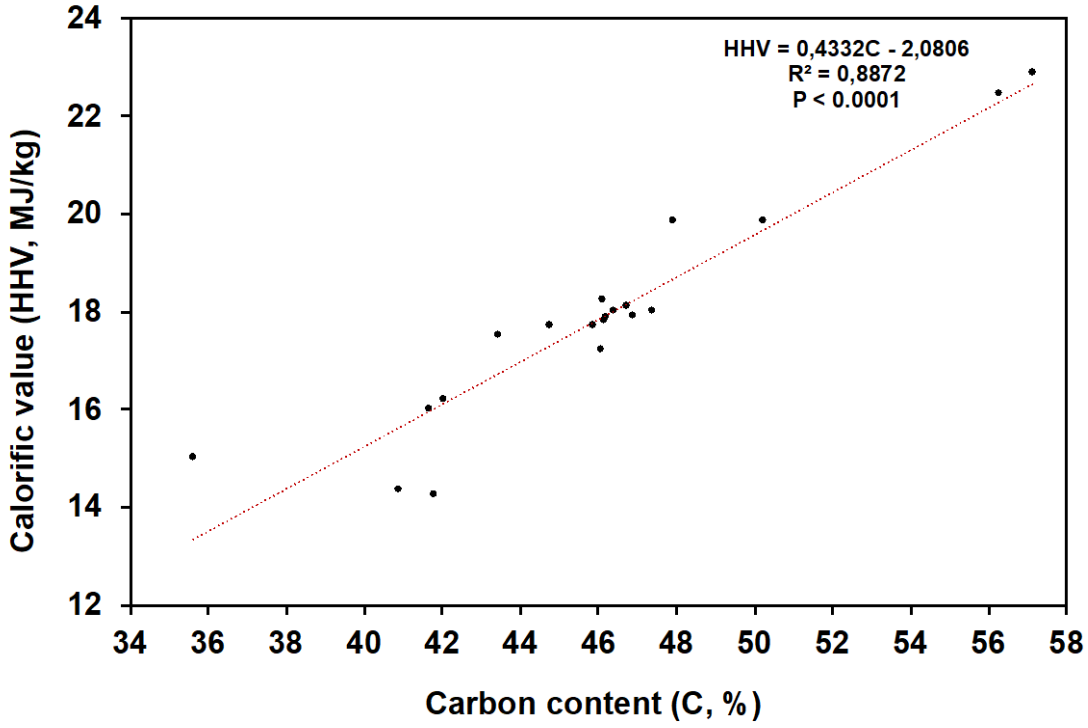

Figure 7.2: Correlation between the raw sample and hydrochars carbon content and calorific values.

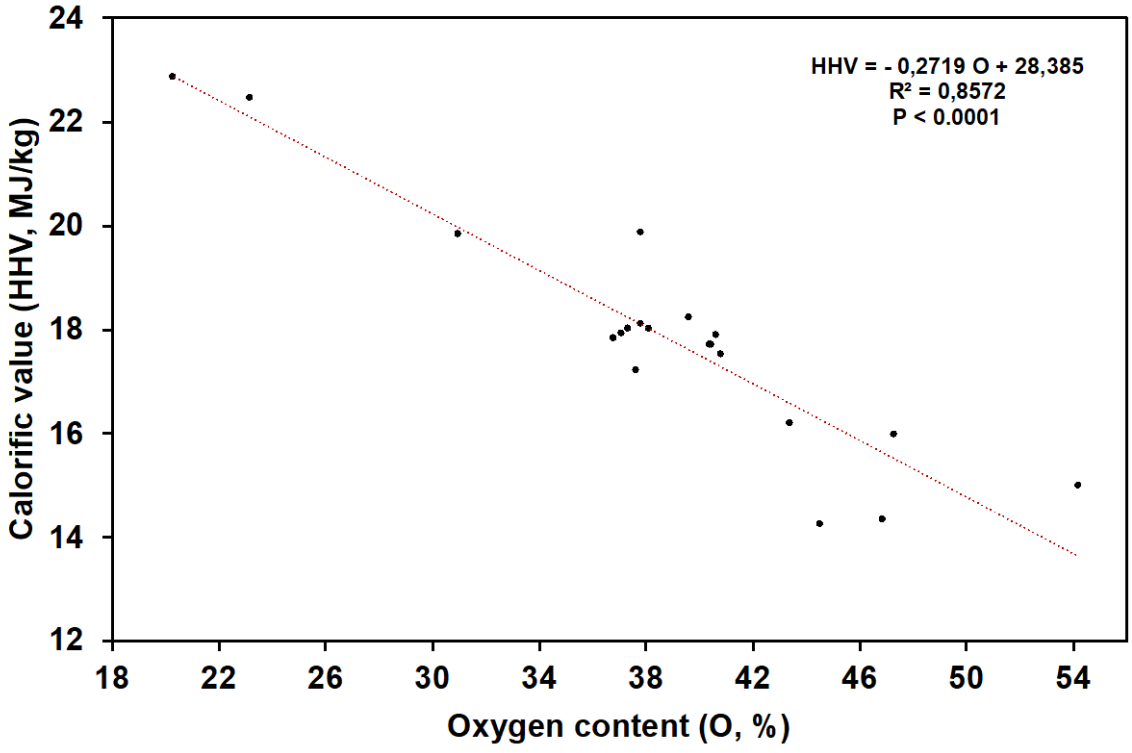

Figure 7.3: Correlation between the raw sample and hydrochars oxygen content and calorific values.

The elemental CHO compositions were used to estimate the molar H/C and O/C ratios and analysed with the Van Krevelen diagram, as illustrated in Figure 7.4,

to further investigate the reaction pathways associated with HTC of recycling paper fibre sludge as well as the coalification degree. For this analysis, the samples have been labelled as reaction temperature- time- solid load. The atomic H/C and O/C ratios of the hydrochars obtained at 0.5 for h, temperatures of 210 and 250, and solid load of 0.12 and 0.08, respectively, were higher than that of the raw substrate. Apart from this case, the H/C and O/C ratios decreased with an increase in reaction severity. The ratios of the hydrochars obtained at 0.5h, temperatures of 210 °C, 230 °C and 250 °C and solid load of 0.08, 0.10 and 0.12, respectively, moved from the upper left to the lower right, suggesting that demethanation occurred. The increase in reaction severity intensified the degree of carbonisation for all other samples, as the ratios of the majority of the hydrochars samples moved from the upper right to the lower left and some even moved as far as towards the upper right, implying that under these operating conditions (T = 210 - 250 °C and t = 1.75 - 3h), the HTC of raw sludge is predominantly governed by dehydration and decarboxylation reactions. During dehydration, the hydroxyl groups are eliminated, while in decarboxylation, the long-chain organic components containing carbonyl and carboxyl groups undergo thermal cracking (Funke and Ziegler, 2010), resulting in hydrochar with higher carbon aromatic structure with enhanced hydrophobicity and thermal stability (He et al., 2013a). This is evident by the substantial decrease in ratios, especially at 250 °C, where the H/C and O/C decreased by approximately 35.50 % and 64 %, respectively. This trend is consistent with reported studies (Zhao et al., 2014, Berge et al., 2011). For fuel applications, low H/C and O/C atomic ratios are desired due to decreased smoke, water vapour and energy losses during combustion (Kambo and Dutta, 2014). The quality of the hydrochar produced at more severe carbonisation treatments resembles that of peat/ lignite and even sub-bituminous coal (Basu, 2018, Agraniotis et al., 2017). These results further suggest the improvement of hydrochar fuel properties as a result of hydrothermal carbonisation.

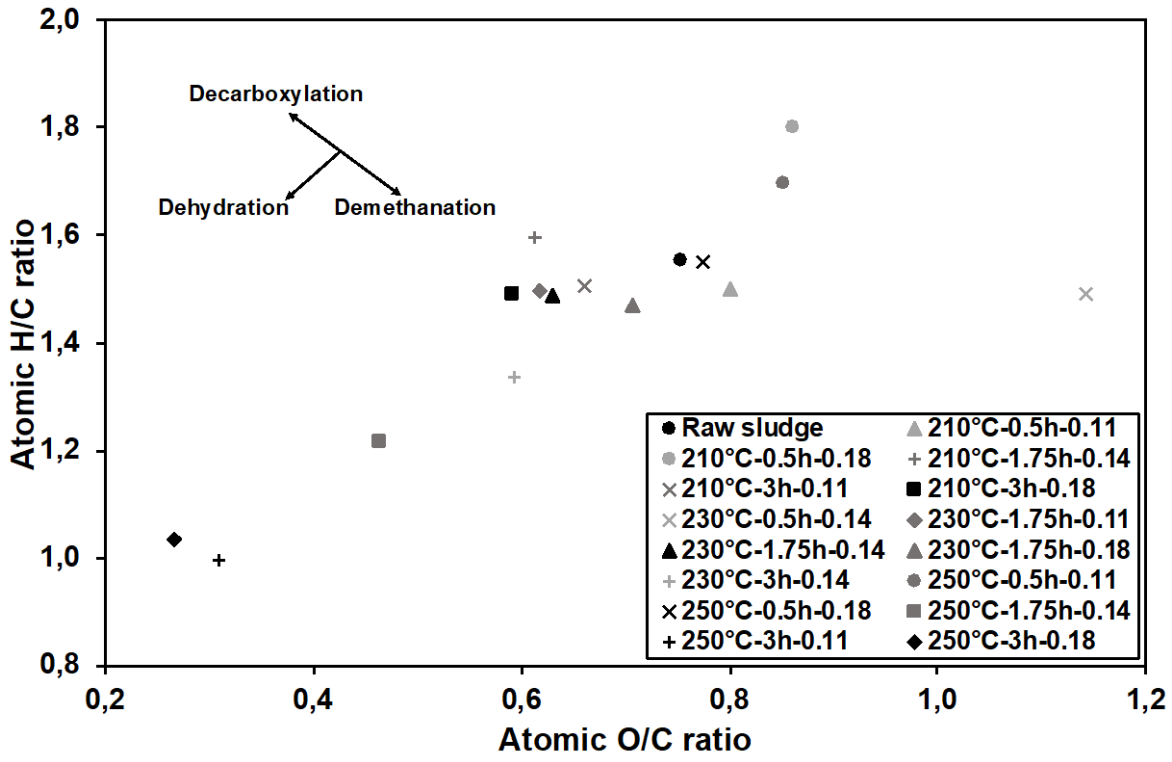

Figure 7.4: Van Krevelen diagram of raw sludge and hydrochars obtained at varying HTC operating conditions.

7.7.3. Surface morphology of the RF and hydrochars

The microstructural changes of the hydrochars produced at varying reaction conditions in comparison to the raw substrate are shown in Figure 7.5. The SEM images reveal that HTC treatment resulted in hydrochar with distinctive surface morphology in comparison to the raw substrate. The morphology of the raw sample consisted of long flat fibril structures with smooth surfaces, which varied with the increase in reaction severity. The hydrochars obtained at 0.5 h for all reaction temperatures retained the fibrous structure. However, when the reaction time was 1.75 h, there was the formation of micro-fissures in the hydrochar, the fibres became shorter with rougher and more irregular surfaces with an increase in reaction temperature. At the maximum reaction time (3h), the hydrochar presented microstructural fragmentations, formation of agglomerated particles and porous features. The agglomerated particles increased significantly when the HTC temperature was 250 °C, where the fibrous structure completely disappeared. These observations confirm that the degradation of organic components, mainly cellulose and hemicellulose, occurred as a result of hydrothermal decomposition during HTC (Xiao et al., 2012, Gai et al., 2016). Furthermore, the characteristics such as micro-fissures, fragmentations and enhanced porous have a positive impact

on the thermal reactivity of the hydrochar fuel during incineration, as these will facilitate both air access and distribution.

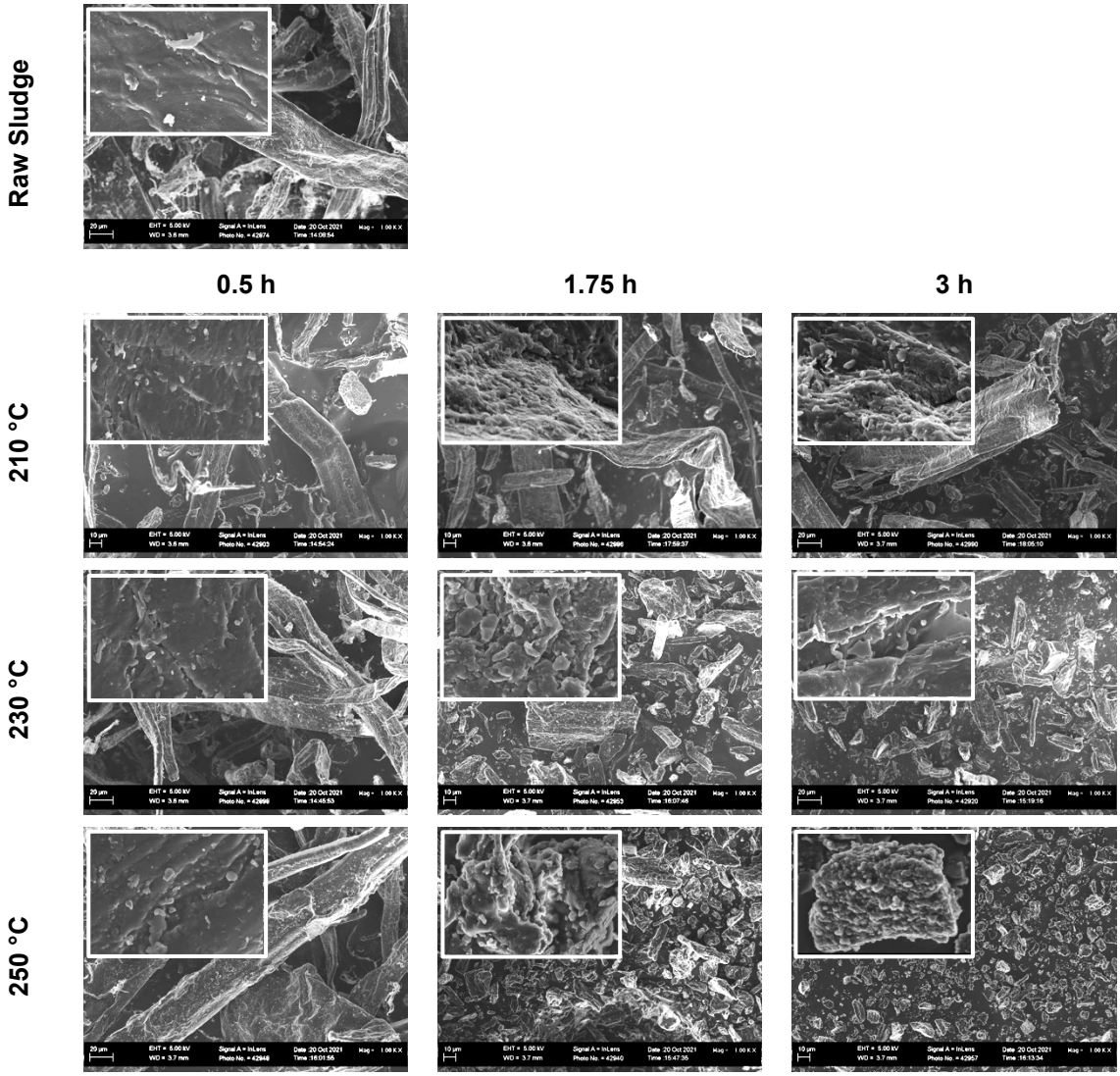

Figure 7.5: SEM micrographs of raw sludge and hydrochars obtained at different HTC reaction conditions with magnifications of 1000 and 18000 times.

7.7.4. Thermal combustion behaviour

The TG and DTG profiles of the raw sample and derived hydrochars obtained at different HTC treatment conditions are presented in Figure 7.6 and Figure 7.7. The complete combustion of the samples occurred in four major stages. The peaks at the first stage, which occurred between 50-150 °C for all samples, are attributed to residual moisture loss present in the samples as a result of the dehydration reaction. At this stage, the maximum peak was about 0.076 °C / min. for the raw substrate and varied from 0.014-0.054°C/ min for the hydrochars. From Figure 8.6, it is possible to observe that the residual moisture decreased after HTC treatment, thus, suggesting the improvement in hydrochar hydrophobic properties. Following

dehydration, the samples exhibited two combustion stages. The first stage occurred between 200 and 400 °C, is mostly associated with volatile matter release in the form of cellulose ad hemicellulose (Poomsawat and Poomsawat, 2021, Xiao et al., 2012), leading to char combustion, as discussed in section 6.8. The second combustion stage occurred between 400-600 °C, is associated with oxidation of carbonaceous material (char) in the form of lignin, as well as residual volatile matter present in the samples. The last stage considered the burnout stage, occurred at temperatures higher than 600 °C, and the peaks are attributed to the oxidation of inorganic volatiles, leading to complete combustion.

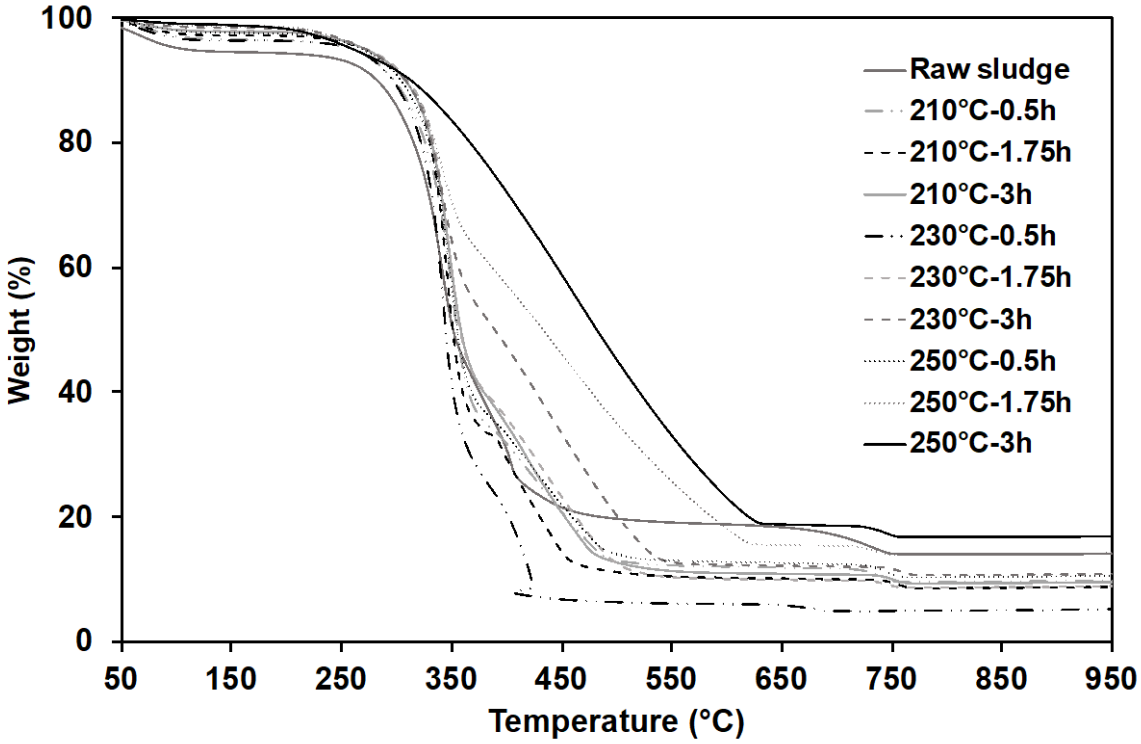

Figure 7.6: TG profiles of raw sludge and hydrochars obtained at varying HTC reaction conditions.

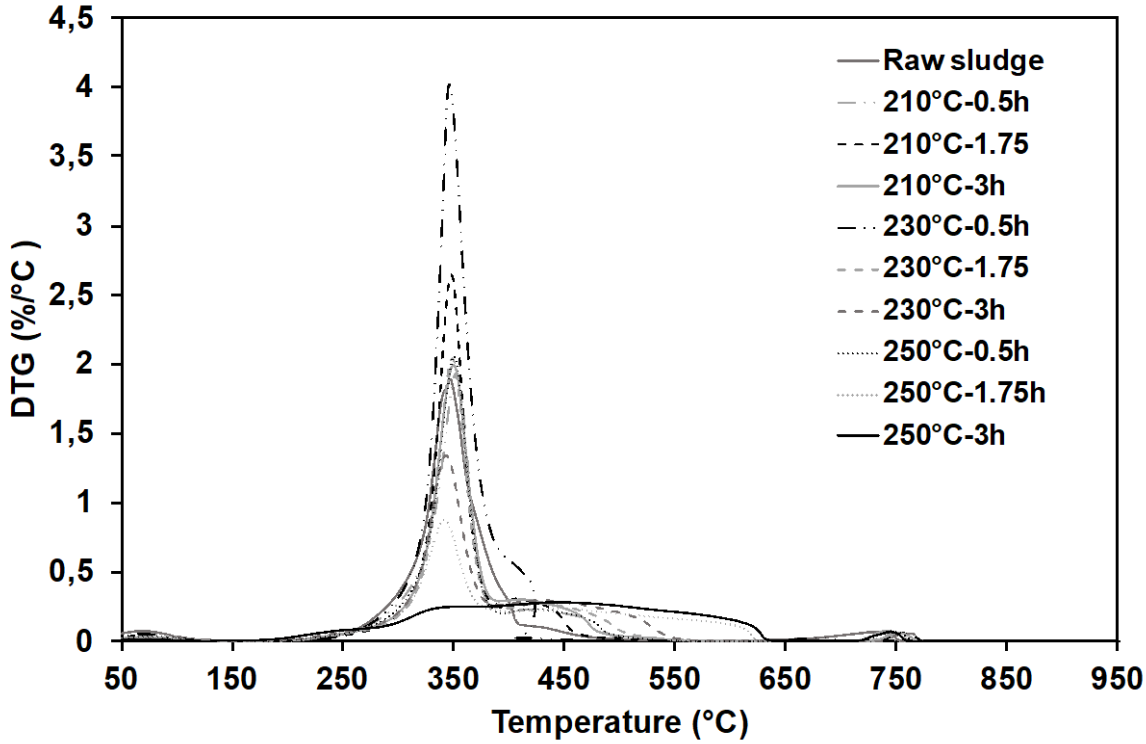

Figure 7.7: TG profiles of raw sludge and hydrochars obtained at varying HTC reaction conditions.

7.8. Energy Assessment

Table 7.10 represents the energy balance of the present study. The evaluation was done based on the assumption that the reactor was preheated prior to HTC. Results show that water consumption had a significant influence on the amount of energy (Q_{in}) required for the HTC process, which increased with a decrease in solid load. This is especially true for the carbonisation of sludge with a solid load of 0.08 at 250 °C, which required additional 1.05 % energy from an external source to heat the system. The energy output (Q_{out}) depends on the hydrochar yield and HHV of the produced fuel. Hence, the values were not significantly affected by the solid load fractions but by the variation of reaction temperatures. Therefore, due to the reaction mechanisms discussed in section 7.4, the Q_{out} decreased with increased reaction temperatures. Moreover, although higher reaction temperatures led to overall lower energy recovery, the resulting hydrochar offered better quality due to increased energy per unit weight of hydrochar. To summarise, up to 58.34 % of the energy generated from the hydrochar fuel combustion could be recovered in the form of heat or power, whilst the remaining 41.66 % of the combustion energy could be used to process HTC of the recycling paper sludge to produce hydrochar fuel. Lastly, for more efficient energy recovery, the solid load should be kept to a maximum while still ensuring

complete dispersion of the solids in the reaction medium. Additional benefits of lower water consumption include lower residence time, earlier polymerisation and higher hydrochar yield (Heidari et al., 2019, Funke and Ziegler, 2010).

Table 7.10: Evaluation of energy balance of hydrochar fuel production from RF by HTC, averaged for all residence times.

Solid Load	T (°C)	Q_{water} (kJ)	Q_{sludge} ($x10^{-3}$ kJ)	Total Q_{in} (kJ)	Q_{out} (kJ)	$Q_{recovery}$ (%)
0.08	210	71.53	1.51	71.53	107.69	33.57
	230	79.18	1.67	79.19	108.08	26.74
	250	88.82	1.83	88.82	87.87	- 1.08
0.10	210	70.22	1.89	70.23	142.64	50.77
	230	77.61	2.14	77.62	132.79	41.55
	250	86.22	2.28	86.22	104.43	17.44
0.12	210	68.58	2.25	68.59	164.61	58.34
	230	75.45	2.56	75.45	167.60	54.98
	250	83.88	2.73	83.88	137.12	38.83

7.8.1. *Electricity generation potential*

To further assess the energetic potential of hydrochar fuel, hydrochar electricity generation potential the optimised HTC reaction conditions was estimated for one of the coal-fired power stations in South Africa, and presented in Table 7.11. The Arnot Power Station is located 50 km east of Middleburg and has an efficiency of 35.60 (Eskom, 2021). Over the past three years, the plant produced proximately 9 675 GWh (Eskom, 2021), which averages to about 3225 GWh per year. From the optimised results, and considering the substantial amount of the underutilised paper sludge generated on dry weight, the hydrochar fuel recovery could generate over 2 million gigajoules per year, which is equivalent to about 21 % of the energy currently generated from coal at Arnot power plant, and equivalent to ~0.4% of the electricity produced from coal in South Africa in 2020 (CSIR, 2021). This underlines the potential of paper sludge for an additional renewable energy source, coal replacement or co-combustion.

Table 7.11: PMS hydrochar electricity generation potential for Arnot Coal Power Plant (APP).

Parameters	Symbol	Value	Reference
SA amount of paper sludge generated per year (tonnes, db)	M_{PMS}	500,000	Boshoff et al. (2016)
Optimised hydrochar yield (%)	H_Y	74.3	Current study
Optimised hydrochar calorific value (GJ/ tonnes)	HHV	18.50	Current study
Average efficiency of coal-fired power plants (%)	η	35.20	Eskom (2021)
Proximate electricity production from coal at APP in 2020 (GWh)	E	3,225	Eskom (2021)
Electricity production from coal at APP	E_C	11,610,000	
Electricity production from hydrochar (GWh)		672.82	
Electricity production from hydrochar (GJ)	E_{HC}	2,422,152	
Fraction of coal replaceable by hydrochar at APP (%)		20.86	

CHAPTER 8: CONCLUSIONS AND RECOMMENDATIONS

In this study, the hydrothermal carbonisation (HTC) process under subcritical water conditions was investigated as an alternative technology to address the underutilised pulp and paper mill sludge generated in South Africa and reduce the environmental and economic implications associated with current disposal practices. The HTC treatment of wastes from different mill streams converted the wastes into clean high-value hydrochar fuel with improved physicochemical characteristics, including lower sulphur and nitrogen content (less than 1 %), higher calorific values and overall enhanced fuel properties compared to the raw substrates, which contributes positively for fuel application. Lower H/C and O/C ratios were achieved due to dehydration and decarboxylation reaction mechanisms. Combustion performance was significantly enhanced by HTC treatment, leading to increased ignition temperature and decreased burnout temperatures at 205°C and 225°C. Additionally, for the first time, the HTC process parameters were optimised to maximise the hydrochar yield and calorific value of pulp and paper mill sludge by means of response surface methodology (RSM). The variation in solid load did not have any significant influence on mass yield, calorific value and overall hydrochar properties, but the water consumption affected the energy input for the HTC process. The energy assessment showed that up to 58.3 % of the energy generated from the hydrochar fuel combustion could be recovered in the form of heat or power, which is of great economic viability. The evaluation on the electricity potential showed that hydrochar obtained at the optimised process conditions could generate over 2 million gigajoules per year from the sludge generated annually in South Africa, which is equivalent to 20.9 % of the electricity currently generated from coal at one of South Africa's coal-fired power plant. Thus, adopting HTC technology to address pulp and paper mill sludge to produce hydrochar to play a role in the energy field as an alternative for coal or in co-combustion could contribute to the diversification of fuel supplies and energy security while reducing wastes and costs associated with sludge disposal and environmental implications, including emissions from landfills.

Future work should consist of extensive tests at the predicted optimised process conditions in order to ensure consistent hydrochar product from pulp and paper sludge processing. Variables such as heating rate and feedstock particle size effect on hydrochar characteristics need further analysis to provide an additional reference for process enhancement. Additionally, an assessment of the possible

environmental risks of utilising the pulp and paper sludge hydrochars as a solid fuel to determine their potential as a viable fuel should be conducted.

The substantial demand for process water could represent a burden in terms of production costs. Therefore, the recirculation of HTC process wastewater should be extensively investigated in order to determine the potential to increase the process efficiency while reducing the wastewater generated and wastewater treatment costs, in addition to recovering heat, thereby reducing external heat consumption.

The pH of process wastewater generally drops post-HTC reactions due to the formation of organic acids. Thus, further investigation is needed on the potential of organic acids in process water to catalyse the HTC reactions during recirculation, thereby reducing the energy demand. Moreover, studies on the anaerobic digestion of HTC wastewater should be conducted for potential methane production.

An evaluation of the effect of HTC process conditions on the filterability of the pulp and paper mill hydrochars should be conducted to further optimise the reaction severity for adequate filterability.

Higher reaction severity favoured the formation of gaseous products due to increased decarboxylation rate; therefore, a compressive analysis of the compounds in the gaseous products by mass spectrometer should be conducted especially at temperatures $\geq$ 250 °C and moderate to longer residence times, to assess gas fuel (such as methane) potential.

This research was limited to single batch operation with low capacity. Thus, a larger-scale operation should be explored to evaluate the efficiency and maintenance of semi-continuous production. This includes designing, building and operating a semi-continuous HTC pilot plant based on the combination of the optimised results in order to process pulp and paper mill sludge in an environmentally friendly manner that will accommodate safe disposal, recycling and application of the products.

A comprehensive techno-economic assessment should be conducted for pulp and paper waste solid fuel recovery with the aim of providing an economic basis for industrial-scale design and production.

Apart from solid fuel, hydrochar has a variety of other applications, including adsorbent. Thus, it would be interesting to explore the adsorption capacity of hydrochar derived activated carbon in contaminant removal from wastewater.

REFERENCES

Abidi, N., Cabrales, L. & Haigler, C. H. 2014. Changes in the cell wall and cellulose content of developing cotton fibers investigated by FTIR spectroscopy. *Carbohydrate Polymers,* 100**,** 9-16. https://doi.org/10.1016/j.carbpol.2013.01.074

Afolabi, O. O. D., Sohail, M. & Cheng, Y.-L. 2020. Optimisation and characterisation of hydrochar production from spent coffee grounds by hydrothermal carbonisation. *Renewable Energy,* 147**,** 1380-1391. 10.1016/j.renene.2019.09.098

Agar, D. & Wihersaari, M. 2012. Bio-coal, torrefied lignocellulosic resources–Key properties for its use in co-firing with fossil coal–Their status. *Biomass and Bioenergy,* 44**,** 107-111.

Agraniotis, M., Bergins, C., Stein-Cichoszewska, M. & Kakaras, E. 2017. 5 - High-efficiency pulverized coal power generation using low-rank coals. *In:* Luo, Z. & Agraniotis, M. (eds.) *Low-Rank Coals for Power Generation, Fuel and Chemical Production.* Woodhead Publishing.

Alive2green. 2019. *South Africa is drowning in its own waste – are our regulators taking this crisis seriously?* [Online]. Available: https://alive2green.com/south-africa-is-drowning-in-its-own-waste-are-our-regulators-taking-this-crisis-seriously/ [Accessed 18-08 2020].

Antero, R. V. P., Alves, A. C. F., de Oliveira, S. B., Ojala, S. A. & Brum, S. S. 2020. Challenges and alternatives for the adequacy of hydrothermal carbonization of lignocellulosic biomass in cleaner production systems: A review. *Journal of Cleaner Production,* 252**,** 119899. https://doi.org/10.1016/j.jclepro.2019.119899

Areeprasert, C., Coppola, A., Urciuolo, M., Chirone, R., Yoshikawa, K. & Scala, F. 2015. The effect of hydrothermal treatment on attrition during the fluidized bed combustion of paper sludge. *Fuel Processing Technology,* 140**,** 57-66. https://doi.org/10.1016/j.fuproc.2015.08.013

AVA-CO2 Schweiz AG 2012. Energy of the future. *AVA-CO2 The minus is the plus.*

Baccile, N., Weber, J. & Falco, C. 2013. Sustainable carbon materials from hydrothermal processes. *In:* Titirici, M. (ed.). UK: John Wiley & Sons, Ltd.

Bahar, K., Zeynep, C. & Orhan, I. 2011. Pollution Prevention in the Pulp and Paper Industries. InTech.

Bajpai, P. 2015. *Management of Pulp and Paper Mill Waste*, Springer International Publishing.

Barbier, J., Charon, N., Dupassieux, N., Loppinet-Serani, A., Mahé, L., Ponthus, J., Courtiade, M., Ducrozet, A., Quoineaud, A.-A. & Cansell, F. 2012. Hydrothermal conversion of lignin compounds. A detailed study of fragmentation and condensation reaction pathways. *Biomass and Bioenergy,* 46**,** 479-491. https://doi.org/10.1016/j.biombioe.2012.07.011

Bargmann, I., Matthias, C., Rillig, M. C., Kruse, A., Greef, J.-M. & Kücke, M. 2014. Effects of hydrochar application on the dynamics of soluble nitrogen in soils and on plant availability. *Plant Nutrition and Soil Science,* 177. https://doi.org/10.1002/jpln.201300069

Basso, D., Castello, D., Baratieri, M. & Fiori, L. 2013. Hydrothermal Carbonization of Waste Biomass: Progress Report and Prospects. *21st European Biomass Conference and Exhibition.* Copenhagen, Denmark: University of Trento, Department of Civil, Environmental and Mechanical Engineering.

Basu, P. 2010. Biomass Pyrolysis and Gasification: Practical Design and Theory. *Elsevier Inc, Oxford*.

Basu, P. 2018. Chapter 11 - Biomass Combustion and Cofiring. *In:* Basu, P. (ed.) *Biomass Gasification, Pyrolysis and Torrefaction (Third Edition).* Academic Press.

Behrendt, F., Neubauer, Y., Oevermann, M., Wilmes, B. & Zobel, N. 2008. Direct liquefaction of biomass. *Chemical Engineering and Technology,* 31**,** 667–677.

Berge, N. D., Ro, K. S., Mao, J., Flora, J. R., Chappell, M. A. & Bae, S. 2011. Hydrothermal carbonization of municipal waste streams. *Environmental Science & Technology,* 45**,** 5696-5703.

Bergius, F. 1913. Die Anwendung hoher Drucke bei chemischen Vorgangen und eine Nachbildung des Entstehungsprozesses der Steinkhole. Wilhelm Knapp, Halle a. d. Saale.

Berl, E. & Schimdt, A. 1932. Die Inkohlung von cellulose und lignin in neutralem medium. *Liebigs Annalen der Chemie,* 493**,** 160–177.

Bernardo, M., Lapa, N., Gonçalves, M., Mendes, B., Pinto, F., Fonseca, I. & Lopes, H. 2012. Physico-chemicalpropertiesofcharsobtainedintheco-pyrolysisofwastemixtures. *Journal of Hazardous Materials*. 10.1016/j.jhazmat.2012.03.077

Besse, X., Schuurman, Y. & Guilhaume, N. 2015. Hydrothermal conversion of lignin model compound eugenol. *Catalysis Today,* 258**,** 270-275. https://doi.org/10.1016/j.cattod.2014.12.010

Black, J. T. & Kohser, R. A. 2017. *DeGarmo's Materials and Processes in Manufacturing*, Wiley.

Boshoff, S., Gottumukkala, L. D., van Rensburg, E. & Görgens, J. 2016. Paper sludge (PS) to bioethanol: Evaluation of virgin and recycle mill sludge for low enzyme, high-solids fermentation. *Bioresource Technology***,** 103-111. https://doi.org/10.1016/j.biortech.2015.12.028

Buswell, A. M. & Mueller, H. F. 1952. Mechanism of Methane Fermentation. *Industrial & Engineering Chemistry,* 44**,** 550-552. 10.1021/ie50507a033

Buttmann, M. 2011. Klimafreundliche Kohle durch Hydrothermale Karbonisierung von Biomasse. *s.l. : Chemie Ingenieur Technik,* 83**,** 1890-1896.

Cabrera, M. N. 2017. Pulp Mill Wastewater: Characteristics and Treatment,. *Biological Wastewater Treatment and Resource Recovery.*

Calitz, J. & Wright, J. 2021. Statistics of utility-scale power generation in South Africa in 2020. Council for Scientific and Industrial Research - Energy Centre.

Canales, A., Pareilleux, R. J. L., Goma, G. & Huyard, A. 1994. Decreased sludge production strategy for domestic wastewater treatment. *Water Sci. Technol.,* 30**,** 97-106.

Chen, C., Liu, G., An, Q., Lin, L., Shang, Y. & Wan, C. 2020. From wasted sludge to valuable biochar by low temperature hydrothermal carbonization treatment: Insight into the surface characteristics. *Journal of Cleaner Production,* 263**,** 121600. https://doi.org/10.1016/j.jclepro.2020.121600

Coates, J. 2006. Interpretation of Infrared Spectra, A Practical Approach. *Encyclopedia of Analytical Chemistry.*

Danso-Boateng, E., Shama, G., Wheatley, A. D., Martin, S. J. & Holdich, R. G. 2015. Hydrothermal carbonisation of sewage sludge: Effect of process conditions on product characteristics and methane production. *Bioresource Technology,* 177**,** 318-327. https://doi.org/10.1016/j.biortech.2014.11.096

Demirbas, A. & Arin, G. 2002. An overview of biomass pyrolysis. *Energy Sources,* 24**,** 471-482.

Department of Energy. *Directorate: Energy data collection, management and analysis* [Online]. Available:

http://www.energy.gov.za/files/media/explained/South-African-Coal-Sector-Report.pdf [Accessed 12-11-2021].

Department of Environmental Affairs. 1996. *The Constitution of the Republic of South Africa, (Act No. 108 of 1996)* [Online]. Available: https://www.environment.gov.za/constitution_republic_south_africa_act_no_108_1996 [Accessed 04-04-2020].

Department of Environmental Affairs. 1998. *National Environmental Management Act, (Act No. 107 of 1998)* [Online]. Available: https://www.environment.gov.za/sites/default/files/gazetted_notices/nema107of1998_draftregulationsonadoptionofenvironmentalmanagemen%20instruments_gn987_gg41114_0.pdf [Accessed 04-04-2020].

Dillen, J. R., Dillén, S. & Hamza, M. 2016. Pulp and Paper: Wood Sources. 10.1016/B978-0-12-803581-8.09802-7.

Elliott, R. 1988. *Cast Iron Technology*, Butterworth-Heinemann.

Escala, M., Zumbühl, T., Koller, C., Junge, R. & Krebs, R. 2013. Hydrothermal Carbonization as an Energy-Efficient Alternative toEstablished Drying Technologies for Sewage Sludge: A FeasibilityStudy on a Laboratory Scale. *Energy Fuels*. 10.1021/ef3015266

Eskom. 2021. *Coal fired power station* [Online]. https://www.eskom.co.za/eskom-divisions/gx/coal-fired-power-stations/. [Accessed 05-12-2021].

Fakkaew, K., Koottatep, T. & Polprasert, C. 2018. Faecal sludge treatment and utilization by hydrothermal carbonization. *Journal of Environmental Management,* 216**,** 421- 426.

Fang, J., Zhan, L., O, k. Y. S. & Gao, B. 2018a. Minireview of potential applications of hydrochar derived from hydrothermal carbonization of biomass. *Journal of Industrial and Engineering Chemistry.* 10.1016/j.jiec.2017.08.026.

Fang, J., Zhan, L., Ok, Y. S. & Gao, B. 2018b. Minireview of potential applications of hydrochar derived from hydrothermal carbonization of biomass. *Journal of Industrial and Engineering Chemistry,* 57**,** 15-21. 10.1016/j.jiec.2017.08.026

FpmSeta 2014. Fibre Processing & Manufacturing Sector Education and Training Authority.

Fryer, D. M. & Harvey, J. F. 1998. *High Pressure Vessels*, Springer, Boston, MA. https://doi.org/10.1007/978-1-4615-5989-4

Fuertes, A. B., Arbestain, M. C., Sevilla, M., Maciá-Agulló, J. A., Fiol, S., López, R., Smernik, R. J., Aitkenhead, W. P., Arce, F. & Macías, F. 2010. Chemical and

structural properties of carbonaceous products obtained by pyrolysis and hydrothermal carbonisation of corn stover. *Soil Research,* 48. 10.1071/sr10010

Funke, A. & Ziegler, F. 2010. Hydrothermal carbonization of biomass: A summary and discussion of chemical mechanisms for process engineering. *Biofuels, Bioproducts and Biorefining,* 4**,** 160-177. 10.1002/bbb.198

Gai, C., Guo, Y., Liu, T., Peng, N. & Liu, Z. 2016. Hydrogen-rich gas production by steam gasification of hydrochar derived from sewage sludge. *International Journal of Hydrogen Energy,* 41**,** 3363-3372. https://doi.org/10.1016/j.ijhydene.2015.12.188

Gajić, A. & Koch, H.-J. 2012. Sugar Beet (Beta vulgaris L.) Growth Reduction Caused by Hydrochar Is Related to Nitrogen Supply. *Environmental Quality,* 41.

Gao, W., Wang, X.-H., Yang, H.-P. & Chen, H.-P. 2012. Characterization of products from hydrothermal treatments of cellulose. *Energy* 42**,** 457–65.

Gibril, M. E., Lekha, P., Andrew, J., Sithole, B., Tesfaye, T. & Ramjugernath, D. 2018. *Beneficiation of pulp and paper mill sludge: production and characterisation of functionalised crystalline nanocellulose* [Online]. Available: https://doi.org/10.1007/s10098-018-1578-3 [Accessed 8 20].

Glaser, B., Haumaier, L., Guggenberger, G. & Zech, W. 2001. The 'Terra Preta' phenomenon: a model for sustainable agriculture in the humid tropics. *The Science of Nature*. 10.1007/s001140000193

Gómez, J., Corsi, G., Pino-Cortés, E., Díaz-Robles, L. A., Campos, V. & Cubillos, F. 2020. Modeling and simulation of a continuous biomass hydrothermal carbonization process, Chemical Engineering Communications. Chemical Engineering Communications. *Chemical Engineering Communications*. DOI:10.1080/00986445.2019.1621858

Government Gazette. 2005. *No. 39 of 2004: National Environment Management: Air Quality Act, 2004.* [Online]. Available: https://www.environment.gov.za/sites/default/files/legislations/nema_amendment_act39.pdf [Accessed 05-04-2020].

Government Gazette. 2009. *No. 59 of 2008: National Environmental Management: Waste Act, 2008.* [Online]. Cape Town, Republic of South Africa. Available: https://www.environment.gov.za/sites/default/files/legislations/nema_amendment_act59.pdf [Accessed 05-04-2020].

Government, S. A. 2019. *Carbon Tax Act* [Online]. Available: https://www.gov.za/sites/default/files/gcis_document/201905/4248323-5act15of2019carbontaxact.pdf [Accessed 11-06-2020].

Grammelis, P., Margaritis, N. & Karampinis, E. 2016. 2 - Solid fuel types for energy generation: Coal and fossil carbon-derivative solid fuels. *In:* Oakey, J. (ed.) *Fuel Flexible Energy Generation.* Boston: Woodhead Publishing.

Güleç, F., Riesco, L. M. G., Williams, O., Kostas, E. T., Samson, A. & Lester, E. 2021. Hydrothermal conversion of different lignocellulosic biomass feedstocks – Effect of the process conditions on hydrochar structures. *Fuel,* 302**,** 121166. https://doi.org/10.1016/j.fuel.2021.121166

Guo, S., Dong, X., Liu, K., Yu, H. & Zhu, C. 2015. Chemical, energetic, and structural characteristics of hydrothermal carbonization solid products for lawn grass. *BioResources,* 10**,** 4613-4625.

He, C., Giannis, A. & Wang, J. 2013a. Conversion of sewage sludge to clean solid fuel using hydrothermal carbonization: Hydrochar fuel characteristics and combustion behavior. *Applied Energy,* 111**,** 257-266.

He, C., Giannis, A. & Wang, J.-Y. 2013b. Conversion of sewage sludge to clean solid fuel using hydrothermal carbonization: Hydrochar fuel characteristics and combustion behavior. *Applied Energy,* 111**,** 257-266. 10.1016/j.apenergy.2013.04.084

Heidari, M., Dutta, A., Acharya, B. & Mahmud, S. 2019. A review of the current knowledge and challenges of hydrothermal carbonization for biomass conversion. *Journal of the Energy Institute,* 92**,** 1779-1799.

Heilmann, S. M., Jader, L. R., Sadowsky, M. J., Schendel, F. J., Von Keitz, M. G. & Valentas, K. J. 2011. Hydrothermal carbonization of distiller's grains. *Biomass and Bioenergy*. 10.1016/j.biombioe.2011.02.022

Hoekman, S. K., Broch, A. & Robbins, C. 2011. Hydrothermal Carbonization (HTC) of Lignocellulosic Biomass. *Energy & Fuels,* 25**,** 1802-1810. 10.1021/ef101745n

Hoekman, S. K., Broch, A., Robbins, C., Zielinska, B. & Felix, L. 2013. Hydrothermal carbonization (HTC) of selected woody and herbaceous biomass feedstocks. *Biomass Convers Bioref* 3**,** 113–26.

Hubbe, M. A., Metts, J. R., Hermosilla, D., Blanco, M. A., Yerushalmi, L., Haghighat, F., Lindholm-Lehto, P., Khodaparast, Z., Kamali, M. & Elliott, A. 2016.

Wastewater treatment and reclamation: A review of pulp and paper industry practices and opportunities. *Bioresour Technol,* 11**,** 7953-8091.

International, A. 2015. ASTM D7582 - 15. *Standard Test Methods for Proximate Analysis of Coal and Coke by Macro Thermogravimetric Analysis.* West Conshohocken: PA: ASTM International.

IOL. 2018. *Shortage of landfill sites a stink for SA's recycling plans* [Online]. Available: https://www.iol.co.za/news/south-africa/shortage-of-landfill-sites-a-stink-for-sas-recycling-plans-17234012 [Accessed 21-08-2020].

Kambo, H. S. & Dutta, A. 2014. Strength, storage, and combustion characteristics of densified lignocellulosic biomass produced via torrefaction and hydrothermal carbonization. *Applied Energy,* 135**,** 182-191. https://doi.org/10.1016/j.apenergy.2014.08.094

Kambo, H. S. & Dutta, A. 2015. A comparative review of biochar and hydrochar in terms of production, physico-chemical properties and applications. *Renewable and Sustainable Energy Reviews,* 45**,** 359-378. 10.1016/j.rser.2015.01.050

Kang, S., Li, X., Fan, J. & Chang, J. 2012. Characterization of Hydrochars Produced by Hydrothermal Carbonization of Lignin, Cellulose, d-Xylose, and Wood Meal. *Industrial & Engineering Chemistry Research,* 51**,** 9023-9031. 10.1021/ie300565d

Kang, S., Li, X., Fan, J. & Chang, J. 2013. Hydrothermal conversion of lignin: A review. *Renewable and Sustainable Energy Reviews,* 27**,** 546-558. https://doi.org/10.1016/j.rser.2013.07.013

Kannan, S., Gariepy, Y. & Raghavan, G. S. V. 2017. Optimization and characterization of hydrochar produced from microwave hydrothermal carbonization of fish waste. *Waste Management,* 65**,** 159-168. https://doi.org/10.1016/j.wasman.2017.04.016

Kaur, R., Tyagi, R. D. & Zhang, X. 2020. Review on pulp and paper activated sludge pretreatment, inhibitory effects and detoxification strategies for biovalorization. *Environmental Research,* 182**,** 109094. 10.1016/j.envres.2019.109094

Kim, D., Yoshikawa, K. & Park, K. Y. 2015. Characteristics of Biochar Obtained by Hydrothermal Carbonization of Cellulose for Renewable Energy. *Energies,* 8**,** 14040-14048.

Kirmse, W. 2012. *Organic elemental analysis: ultramicro, micro, and trace methods*, Elsevier Science.

Kläusli, T. 2012. *Ava-CO2 presentation* [Online]. Available: http://greentecheurope.com/AVA-CO2-Interview-cleancoal_v1083 [Accessed 02-06-2020].

Kleiner, K. 2009. The bright prospect of biochar. *Nature Reports,* 3**,** 72–74.

Kruse, A., Funke, A. & Titirici, M. 2013. Hydrothermal conversion of biomass to fuels and energetic materials. *Current Opinion in Chemical Biology,* 17**,** 515-521. https://doi.org/10.1016/j.cbpa.2013.05.004

Kumar, S., Loganathan, V. A., Gupta, R. B. & Barnett, M. O. 2011. An assessment of U (VI) removal from groundwater using biochar produced from hydrothermal carbonization. *Journal of environmental management,* 92.

Lekha, P., Andrew, J. E., Gibril, M. & Sithole, B. 2017. Pulp and Paper mill sludge: a potential resource for producing high-value products. . *TAPPSA*, p.1.

Lenntech Water treatment & purification. n.d. *Sludge Treatment* [Online]. [Accessed].

Li, X., Wei, Y., Xu, J., Xu, N. & He, Y. 2018. Quantitative visualization of lignocellulose components in transverse sections of moso bamboo based on FTIR macro- and micro-spectroscopy coupled with chemometrics. *Biotechnology for Biofuels,* 11. 10.1186/s13068-018-1251-4

Li, X.-G., Ma, B.-G., Xu, L., Hu, Z.-W. & Wang, X.-G. 2006. Thermogravimetric analysis of the co-combustion of the blends with high ash coal and waste tyres. *Thermochimica Acta,* 441**,** 79-83. https://doi.org/10.1016/j.tca.2005.11.044

Liang, X. & Yang, J. 2009. Synthesis of a novel carbon based strong acid catalyst through hydrothermal carbonization. *Catalysis Letters,* 132**,** 460-463.

Libra, J. A., Ro, K. S., Kammann, C., Funke, A., Berge, N. D., Neubauer, Y., Titirici, M.-M., Fühner, C., Bens, O., Kern, J. & Emmerich, K.-H. 2011. Hydrothermal carbonization of biomass residuals: a comparative review of the chemistry, processes and applications of wet and dry pyrolysis. *Biofuels,* 2**,** 71-106. 10.4155/bfs.10.81

Likon, M. & Trebe, P. 2012. Recent Advances in Paper Mill Sludge Management. *In:* Show, K., Guo, X. (ed.) *Industrial Waste.* Croatia: InTech.

Lin, Y., Ma, X., Ning, X. & Yu, Z. 2015a. TGA–FTIR analysis of co-combustion characteristics of paper sludge and oil-palm solid wastes. *Energy Conversion and Management,* 89**,** 727-734.

Lin, Y., Ma, X., Peng, X., Hu, S., Yu, Z. & Fang, S. 2015b. Effect of hydrothermal carbonization temperature on combustion behavior of hydrochar fuel from paper sludge. *Applied Thermal Engineering,* 91**,** 574-582. https://doi.org/10.1016/j.applthermaleng.2015.08.064

Liu, Z., Quek, A. & Balasubramanian, R. 2014. Preparation and characterization of fuel pellets from woody biomass, agro-residues and their corresponding hydrochars. *Applied Energy,* 113**,** 1315-1322.

Lu, J.-J. & Chen, W.-H. 2015. Investigation on the ignition and burnout temperatures of bamboo and sugarcane bagasse by thermogravimetric analysis. *Applied Energy,* 160**,** 49-57.

Lu, X. & Berge, N. D. 2014. Influence of feedstock chemical composition on product formation and characteristics derived from the hydrothermal carbonization of mixed feedstocks. *Bioresour Technol,* 166**,** 120–31. http://dx.doi.org/10.1016/j.biortech.2014.05.015.

Lu, X., Flora, J. R. V. & Berge, N. D. 2014. Influence of process water quality on hydrothermal. 154**,** 229–39.

Lu, X., Jordan, B. & Berge, N. D. 2012. Thermal conversion of municipal solid waste via hydrothermal carbonization: Comparison of carbonization products to products from current waste management techniques. *Waste Management,* 32**,** 1353-1365.

Lu, X., Pellechia, P. J., Flora, J. R. V. & Berge, N. D. 2013. Influence of reaction time and temperature on product formation and characteristics associated with the hydrothermal carbonization of cellulose. *Bioresource Technology,* 138**,** 180-190. https://doi.org/10.1016/j.biortech.2013.03.163

Majewski, W., A. & Jääskeläinen, H. 2004. Environmental Effects of Emissions. *DieselNet Technology Guide*.

Mäkelä, M., Benavente, V. & Fullana, A. 2015. Hydrothermal carbonization of lignocellulosic biomass: Effect of process conditions on hydrochar properties. 155**,** 576-584. 10.1016/j.apenergy.2015.06.022

Mäkelä, M., Benavente, V. & Fullana, A. 2016. Hydrothermal carbonization of industrial mixed sludge from a pulp and paper mill. *Bioresource Technology,* 200**,** 444-450. https://doi.org/10.1016/j.biortech.2015.10.062

Makgato, S. S. & Chirwa, E. M. 2017. Waterberg coal characteristics and SO2 minimum emissions standards in South African power plants. *Journal of Environmental Management,* 201**,** 294-302.

Mau, V., Quance, J., Posmanik, R. & Gross, A. 2016. Phases' characteristics of poultry litter hydrothermal carbonization under a range of process parameters. *Bioresource Technology,* 219**,** 632-642. https://doi.org/10.1016/j.biortech.2016.08.027

McGaughy, K. & Reza, M. T. 2018. Recovery of Macro and Micro-Nutrients by Hydrothermal Carbonization of Septage. *Journal of Agricultural and Food Chemistry,* 66**,** 1854-1862. 10.1021/acs.jafc.7b05667

McKeen, L. W. 2012. 11 - Fluoropolymers. *In:* Mckeen, L. W. (ed.) *Film Properties of Plastics and Elastomers.* 3 ed. Boston: William Andrew Publishing.

Méndez, A., Fidalgo, J. M., Guerrero, F. & Gascó, G. 2009. Characterization and pyrolysis behaviour of different paper mill waste materials. *Journal of Analytical and Applied Pyrolysis,* 86**,** 66-73. 10.1016/j.jaap.2009.04.004

Merzari, F., Lucian, M., Volpe, M., Andreottola, G. & Fiori, L. 2018. Hydrothermal Carbonization of Biomass: Design of a Bench-Scale Reactor for Evaluating the Heat of Reaction. *Chemical Engineering Transactions,* 65**,** 43-48. 10.3303/cet1865008

Mott, R. L. 2008. *Applied Strength of Materials*.

Müller, J. B. & Vogel, F. 2012. Tar and coke formation during hydrothermal processing of glycerol and glucose. Influence of temperature, residence time and feed concentration. *The Journal of Supercritical Fluids*. DOI:10.1016/j.supflu.2012.06.016.

Mumme, J., Eckervogt, L., Pielert, J., Diakité, M., Rupp, F. & Kern, J. 2011. Hydrothermal carbonisation of anaerobically digested maize silage. *Bioresource Technology,* 102**,** 9255–9260.

Nizamuddin, S., Baloch, H. A., Griffin, G. J., Mubarak, N. M., Bhutto, A. W., Abro, R., Mazari, S. A. & Ali, B. S. 2017. An overview of effect of process parameters on hydrothermal carbonization of biomass. *Renewable and Sustainable Energy Reviews,* 73**,** 1289-1299. 10.1016/j.rser.2016.12.122.

Oliveira, I., Blöhse, D. & Ramke, H.-G. 2013. Hydrothermal carbonization of agricultural residues. *Bioresour Technol,* 142**,** 138–46.

Oumabady, S., S, P. S., Kamaludeen, S. P. B., Ramasamy, M., Kalaiselvi, P. & Parameswari, E. 2020. Preparation and Characterization of Optimized

Hydrochar from Paper Board Mill Sludge. *Scientific Reports,* 10**,** 773. https://doi.org/10.1038/s41598-019-57163-7

Paper Manufactory Association of South Africa. 2012. *Summary findings from 2012 production, import and export statistics* [Online]. Available: https://www.thepaperstory.co.za/wp-content/uploads/2017/06/PAMSA-2012-report_final1.pdf. [Accessed 25-05-2020].

Paper Manufactory Association of South Africa. 2013. *South African Pulp and Paper Industry | Summary findings from 2013 production, import and export statistics* [Online]. Available: https://www.thepaperstory.co.za/wp-content/uploads/2017/06/PAMSA-2013-report-final.pdf [Accessed 25-05-2020].

Paper Manufactory Association of South Africa. 2014. *Summary findings on 2014 production, import and export statistics* [Online]. Available: https://www.thepaperstory.co.za/wp-content/uploads/2017/06/PAMSA-2014-stats-report-final_Aug2015.pdf [Accessed 25-05-2020].

Paper Manufactory Association of South Africa. 2015. *Summary findings on 2015 production, import and export statistics* [Online]. Available: https://www.thepaperstory.co.za/wp-content/uploads/2017/05/PAMSA-2015-stats-report-FINAL.pdf [Accessed 25-05-2020].

Paper Manufactory Association of South Africa. 2018. *Production summary 2018* [Online]. Available: https://www.thepaperstory.co.za/the-economic-story/production-statistics/pamsa-2018-industry-statistics-summary-edited/ [Accessed 25-05-2020].

Penninger, J. M. L., Kersten, R. J. A. & Baur, H. C. L. 1999. Reactions of diphenylether in supercritical water — mechanism and kinetics. *The Journal of Supercritical Fluids,* 16**,** 119-132. https://doi.org/10.1016/S0896-8446(99)00024-8

Peterson, A. A., Vogel, F., Lachance, R. P. & Fröling, M. 2008. Thermochemical biofuel production in hydrothermal media: A review of sub- and supercritical water technologies. *Energy and Environmental Science 1, 32-65.,* 1**,** 32-65.

Pokhrel, D. & Viraraghavan, T. 2004. Treatment of pulp and paper mill wastewater—a review. *Science of The Total Environmen,* 333**,** 37-58. 10.1016/j.scitotenv.2004.05.017

Poomsawat, S. & Poomsawat, W. 2021. Analysis of hydrochar fuel characterization and combustion behavior derived from aquatic biomass via hydrothermal

carbonization process. *Case Studies in Thermal Engineering,* 27**,** 101255. https://doi.org/10.1016/j.csite.2021.101255

Prawisudha, P., Namioka, T. & Yoshikawa, K. 2012. Coal alternative fuel production from municipal solid wastes employing hydrothermal treatment. *Appl Energy*.

Ramke, H., Blöhse, D., Lehmann, H. & Fettig, J. 2009. Hydrothermal carbonization of organic waste. *In:* Cossu, R., Diaz, L. F. & Stegmann, R. (eds.) *Twelfth International Waste Management and Landfill Symposium.* Sardinia, Italy.

Reza, M. T., Andert, J., Wirth, B., Busch, D., Pielert, J., Lynam, J. G. & Mumme, J. 2014a. Hydrothermal Carbonization of Biomass for Energy and Crop Production. *Appl. Bioenergy,* 1**,** 11-29. 10.2478/apbi-2014-0001

Reza, M. T., Lynam, J. G., Uddin, M. H. & Coronella, C. J. 2013a. Hydrothermal carbonization: Fate of inorganics. *Biomass and Bioenergy,* 49**,** 86-94. 10.1016/j.biombioe.2012.12.004

Reza, M. T., Lynam, J. G., Vasquez, V. R. & Coronella, C. J. 2012. Pelletization of biochar from hydrothermally carbonized wood. *Environmental Progress & Sustainable Energy,* 21**,** 225-234.

Reza, M. T., Uddin, M. H., Lynam, J. G., Hoekman S.K. & Coronella, C. J. 2014b. Hydrothermal carbonization of loblolly pine: reaction chemistry and water balance. *Biomass Convers Bioref,* 4**,** 311–21.

Reza, M. T., Yan, W., Uddin, M. H., Lynam, J. G., Hoekman, S. K. & Coronella, C. J. 2013b. Reaction kinetics of hydrothermal carbonization loblolly pine. *bioresour,* 139**,** 161-9.

Rillig, M. C., Wagner, M., Salem, M., Antunes, P. M., George, C. & Ramke, H.-G. 2010. Material derived from hydrothermal carbonization: Effects on plant growth and arbuscular mycorrhiza. *Applied Soil Ecology,* 45**,** 238–242.

Ro, K. S., Novak, J., Bae, S., Flora, J. R. V. & Berge, N. D. 2010. Greenhouse gas emission from soil amended with biochar made from hydrothermally carbonizing swine solids. *American Chemical Society National Meeting.* San Francisco, CA.

Röthlein, B. 2006. Magic Coal from the Steam Cooker. *s.l. : Max Planck Research*.

Saha, N., Saba, A. & Reza, M. T. 2019a. Effect of hydrothermal carbonization temperature on pH, dissociation constants, and acidic functional groups on hydrochar from cellulose and wood. *Journal of Analytical and Applied Pyrolysis,* 137**,** 138-145. 10.1016/j.jaap.2018.11.018

Saha, N., Saba, A., Saha, P., McGaughy, K., Franqui-Villanueva, D., Orts, W., Hart-Cooper, W. & Reza, M. 2019b. Hydrothermal Carbonization of Various Paper Mill Sludges: An Observation of Solid Fuel Properties. *Energies,* 12**,** 858. 10.3390/en12050858

Santos, J., V.,, Fregolente, L. G., Laranja, M. J., Moreira, A. B., Ferreira, O. P. & Bisinoti, M. C. 2021. Hydrothermal carbonization of sugarcane industry by-products and process water reuse: structural, morphological, and fuel properties of hydrochars. *Biomass Conversion and Biorefinery*. 10.1007/s13399-021-01476-z

Scott, G. M. 1995. Sludge Characteristics and Disposal Alternatives for the Pulp and Paper Industry *International Environmental Conference Proceedings.* Atlanta, GA: TAPPI Press.

Sevilla, M. & Fuertes, A. 2009. The production of carbon materials by hydrothermal carbonization of cellulose. *Carbon,* 47**,** 2281-2289.

Sharma, R., Jasrotia, K., Singh, N., Ghosh, P., Srivastava, S., Sharma, N. R., Singh, J., Kanwar, R. & Kumar, A. 2020. A Comprehensive Review on Hydrothermal Carbonization of Biomass and its Applications. *Chemistry Africa*. 10.1007/s42250-019-00098-3

Sher, E. 1998. Chapter 2 - Environmental Aspects of Air Pollution. *In:* Sher, E. (ed.) *Handbook of Air Pollution From Internal Combustion Engines.* San Diego: Academic Press.

Sinnott, R. K. 1993. Chapter 13 - Mechanical Design of Process Equipment. *In:* Sinnott, R. K. (ed.) *Coulson and Richardson's Chemical Engineering (Second Edition).* 2 ed. Amsterdam: Pergamon.

Smith, A. M., Singh, S. & Ross, A. B. 2016. Fate of inorganic material during hydrothermal carbonisation of biomass: Influence of feedstock on combustion behaviour of hydrochar. *Fuel,* 169**,** 135-145. https://doi.org/10.1016/j.fuel.2015.12.006

South African Government. 2019. *President Cyril Ramaphosa signs 2019 Carbon Tax Act into law* [Online]. Available: https://www.gov.za/speeches/publication-2019-carbon-tax-act-26-may-2019-0000 [Accessed 08-07 2020].

South African Revenue Service. 2019. *Carbon Tax* [Online]. Available: https://www.sars.gov.za/ClientSegments/Customs-Excise/Excise/Environmental-Levy-Products/Pages/Carbon-

Tax.aspx#:~:text=The%20first%20phase%20has%20a,and%20annually%20by%20inflation%20thereafter. [Accessed 08-07 2020].

Spitzer, R. Y., Mau, V. & Gross, A. 2018. Using hydrothermal carbonization for sustainable treatment and reuse of human excreta. *Journal of Cleaner Production,* 205**,** 955-963. https://doi.org/10.1016/j.jclepro.2018.09.126

Stirling, R. J., Snape, C. E. & Meredith, W. 2018. The impact of hydrothermal carbonisation on the char reactivity of biomass. *Fuel Processing Technology,* 177**,** 152-158. 10.1016/j.fuproc.2018.04.023

Stoica, A., Sandberg, M. & Holby, O. 2009. Energy use and recovery strategies within wastewater treatment and sludge handling at pulp and paper mills. *Bioresource Technology,* 100**,** 3497-3505. https://doi.org/10.1016/j.biortech.2009.02.041

TerraNova. 2017. *TerraNova® Ultra process* [Online]. Available: https://terranova-energy.com [Accessed 05-07 2020].

Thriveni, T., Whan Ahn, J. & Ramakrisna, C. 2017. Arsenic Oxyanions Removal from Waste Water by Accelerated Carbonation. *Journal of MMIJ,* 133**,** 1-3. 10.2473/journalofmmij.133.1

Titirici, M.-M. & Antonietti, M. 2010. Chemistry and materials options of sustainable carbon materials made by hydrothermal carbonization. *Chemical Society Reviews,* 39**,** 103-116.

Titirici, M.-M., Thomas, A. & Antonietti, M. 2007. Back in the black: hydrothermal carbonization of plant material as an efficient chemical process to treat the CO2 problem? *New Journal of Chemistry,* 31. 10.1039/b616045j

Tyagi, V. K. & Lo, S.-L. 2013. Sludge: A waste or renewable source for energy and resources recovery? *Renewable and Sustainable Energy Reviews,* 25**,** 708-728. 10.1016/j.rser.2013.05.029

Unur, E. 2013. Functional nanoporous carbons from hydrothermally treated biomass for environmental purification. *Microporous and Mesoporous Materials,* 168**,** 92-101. 10.1016/j.micromeso.2012.09.027.

Van der Stelt, M., Gerhauser, H., Kiel, J. & Ptasinski, K. 2011. Biomass upgrading by torrefaction for the production of biofuels: A review. *Biomass and Bioenergy,* 35**,** 3748-3762.

Venderbosch, R. H. & Sander, C. 2008. Hydroconversion of wet biomass: A review. *Report GAVE-9919.*

Volpe, M., Wüst, D., Merzari, F., Lucian, M., Andreottola, G., Kruse, A. & Fiori, L. 2018. One stage olive mill waste streams valorisation via hydrothermal carbonisation. *Waste Management,* 80**,** 224-234. 10.1016/j.wasman.2018.09.021

Wahyudiono, Kanetake, T., Sasaki, M. & Goto, M. 2007. Decomposition of a lignin model compound under hydrothermal conditions. *Chemical Engineering Technology.,* 30**,** 1113-1122. https://doi.org/10.1002/ceat.200700066

Wahyudiono, Sasaki, M. & Goto, M. 2009. Conversion of biomass model compound under hydrothermal conditions using batch reactor. *Fuel,* 88**,** 1656-1664. https://doi.org/10.1016/j.fuel.2009.02.028

Wang, Q., Li, H., Chen, L. & Huang, X. 2001. Monodispersed hard carbon spherules with uniform nanopores. *Carbon,* 39**,** 2211–2214.

Wang, T., Zhai, Y., Zhu, Y., Li, C. & Zeng, G. 2018. A review of the hydrothermal carbonization of biomass waste for hydrochar formation: Process conditions, fundamentals, and physicochemical properties. *Renewable and Sustainable Energy Reviews,* 90**,** 223-247.

Wang, Y., Sun, Y., Jiang, L., Liu, L. & Li, Y. 2020a. Characteristics of Corrosion Related to Ash Deposition on Boiler Heating Surface during Cofiring of Coal and Biomass. *Journal of Chemistry,* 2020.

Wang, Z., Zhai, Y., Wang, T., Peng, C., Li, S., Wang, B., Liu, X. & Li, C. 2020b. Effect of temperature on the sulfur fate during hydrothermal carbonization of sewage sludge. *Environmental Pollution,* 260**,** 114067. 10.1016/j.envpol.2020.114067

Wei, L., Sevilla, M., Fuertes, A. B., Mokaya R. & G., Y. 2011. Hydrothermal carbonization of abundant renewable natural organic chemicals for high-performance supercapacitor electrodes. *Adv. Energy Mater.,* 1**,** 356-361.

World Bank. 2019. *Pricing Carbon* [Online]. Available: https://www.worldbank.org/en/programs/pricing-carbon [Accessed 30-06 2020].

Xiao, L.-P., Shi, Z.-J., Xu, F. & Sun, R.-C. 2012. Hydrothermal carbonization of lignocellulosic biomass. *Bioresource Technology,* 118**,** 619-623. https://doi.org/10.1016/j.biortech.2012.05.060

Xu, C., Cheng, L., Shen, P. & Liu, Y. 2007. Methanol and ethanol electrooxidation on pt and pd supported on carbon microspheres in alkaline media. *Electrochemistry Communications,* 9**,** 997-1001.

Yan, W., Hoekman, S. K., Broch, A. & Coronella, C. J. 2014. Effect of hydrothermal carbonization reaction parameters on the properties of hydrochar and pellets. *Environmental Progress & Sustainable Energy*. 10.1002/ep.11974.

Yang, W., Wang, H., Zhang, M., Zhu, J., Zhou, J. & Wu, S. 2016. Fuel properties and combustion kinetics of hydrochar prepared by hydrothermal carbonization of bamboo. *Bioresource Technology,* 205**,** 199-204. https://doi.org/10.1016/j.biortech.2016.01.068

Yay, A. S. E., Birinci, B., Açıkalın, S. & Yay, K. 2021. Hydrothermal carbonization of olive pomace and determining the environmental impacts of post-process products. *Journal of Cleaner Production,* 315**,** 128087. https://doi.org/10.1016/j.jclepro.2021.128087

Yokoyama, S. 2008. *The Asian Biomass Handbook: A Guide for Biomass Production and Utilisation,* The Japan Institute of Energy.

Zhao L, Fan, L. Z., Zhou, M. Q., Guan, H., Qiao, S., Antonietti, M. & Titirici, M.-M. 2010. Nitrogen-containing hydrothermal carbons with superior performance in supercapacitors. *Adv. Mater.,* 22**,** 5202-5206. 10.1002/adma.201002647

Zhao, P., Shen, Y., Ge, S. & Yoshikawa, K. 2014. Energy recycling from sewage sludge by producing solid biofuel with hydrothermal carbonization. *Energy Conversion and Management,* 78**,** 815–821.

APPENDICES

Appendix A: Process Severity, proximate analysis data and RSM variables condition and responses data.

To evaluate the impact of the mutual effect of HTC temperature and residence time in the conversion of feedstock, the reaction severity factor (SF)was given by equation A 1 and A 2, based on Arrhenius equation (Heidari et al., 2019, Wang et al., 2018).

$$R_O = t \times e^{[(T-100)/14.75]} \quad (A.1)$$

$$SF = \log R_O \quad (A.2)$$

Where R_O represents the reaction ordinate (min), t is the residence time (min), T is the HTC reaction temperature (°C) and SF is the severity factor or the logarithm of the reaction ordinate. The evaluation of the severity factors determined at different reaction conditions for the pre-liminary and optimisation experiments are presented on table A 1 and A 2, respectively.

Table A 1: Severity factors for preliminary experiments conducted at varying reaction HTC temperatures for 180 min.

Temperature (°C)	SF
205	5.35
225	5.94
245	6.52

Table A 2: Severity factors for optimisation experiments conducted at varying reaction temperatures and residence times.

Temperature (°C)	Time (min)	SF
210	30	4.72
	105	5.26
	180	5.49
230	30	5.30
	105	5.85
	180	6.08
250	30	5.89

	105	6.44
	180	6.67

Table A 3: Proximate composition estimation by thermogravimetry adopting ASTM D7582-15.

Sample	MC_{Av} (%)	SD_{MC}	VM_{av} (%)	SD_{VM}	A_{av} (%)	SD_A
RF raw	5.21	0.13	55.09	2.44	13.15	1.55
RF 205	2.82	0.29	61.31	1.69	9.68	0.47
RF 225	2.17	0.01	50.43	0.16	10.56	0.18
RF 245	1.58	0.00	25.40	1.71	13.99	0.37
FS raw	6.01	0.01	57.27	0.86	11.54	0.71
FS 205	2.58	0.18	54.01	0.82	15.82	0.58
FS 225	1.83	0.20	41.40	0.71	20.83	0.64
FS 245	1.35	0.10	20.41	1.52	25.88	0.75
PS raw	3.85	0.17	36.48	0.52	30.30	0.25
PS 205	1.40	0.24	27.10	1.08	40.50	0.09
PS 225	1.18	0.18	23.60	0.25	42.15	0.82
PS 245	0.65	0.10	13.28	0.83	49.90	0.08

MC: moisture content

VM: volatile matter

A: ash content

SD: standard deviation

Av: average

Table A 4: Response and variables condition for the optimisation of hydrochar yield (HY).

Run	T (°C)	t (h)	SL	HY av (%)	HY av (%, db)	SD
1	230	2.79	2.79	2.79	2.79	2.79
2	230	1.14	1.14	1.14	1.14	1.14
3	210	0.85	0.85	0.85	0.85	0.85
4	250	0.50	0.50	0.50	0.50	0.50
5	210	0.29	0.29	0.29	0.29	0.29
6	250	0.33	0.33	0.33	0.33	0.33
7	230	2.46	2.46	2.46	2.46	2.46
8	230	2.96	2.96	2.96	2.96	2.96
9	250	2.43	2.43	2.43	2.43	2.43

10	210	1.07	1.07	1.07	1.07	1.07
11	250	1.67	1.67	1.67	1.67	1.67
12	230	1.82	1.82	1.82	1.82	1.82
13	230	2.70	2.70	2.70	2.70	2.70
14	230	2.47	2.47	2.47	2.47	2.47
15	230	1.29	1.29	1.29	1.29	1.29
16	250	1.07	1.07	1.07	1.07	1.07
17	230	0.88	0.88	0.88	0.88	0.88
18	230	1.92	1.92	1.92	1.92	1.92
19	210	0.68	0.68	0.68	0.68	0.68
20	210	1.11	1.11	1.11	1.11	1.11

T: temperature

t: reaction time

SL: solid load

HY: Hydrochar yield

Av: average

SD: standard deviation

Table A 5: Response and variables condition for the optimisation of higher heating value (HHV).

Run	T (°C)	t (h)	SL	HHV av (MJ/ kg)	HHV av (MJ/kg, db)	SD
1	230	1.75	0.12	17.18	17.51	0.83
2	230	0.5	0.10	14.47	14.99	0.44
3	210	0,5	0.12	13.81	14.33	0.19
4	250	0.5	0.08	15.42	15.98	0.40
5	210	3	0.12	17.63	17.99	0.58
6	250	3	0.08	22.20	22.46	0.59
7	230	3	0.10	19.57	19.85	0.38
8	230	1.75	0.10	17.70	18.11	0.74
9	250	1.75	0.10	19.49	19.84	0.99
10	210	0.5	0.08	13.65	14.24	0.96
11	250	0.5	0.12	15.71	16.19	0.14
12	230	1.75	0.10	17.78	18.23	0.27
13	230	1.75	0.10	17.29	17.71	0.51
14	230	1.75	0.10	17.40	17.81	0.48
15	230	1.75	0.08	17.57	18.00	0.27

16	250	3	0.12	22.58	22.86	0.12
17	230	1.75	0.10	17.49	17.90	0.14
18	230	1.75	0.10	17.26	17.69	0.39
19	210	3	0.08	17.43	17.89	0.36
20	210	1.75	0.10	16.75	17.20	0.54

T: temperature

t: reaction time

SL: solid load

HY: Hydrochar yield

Av: average

SD: standard deviation

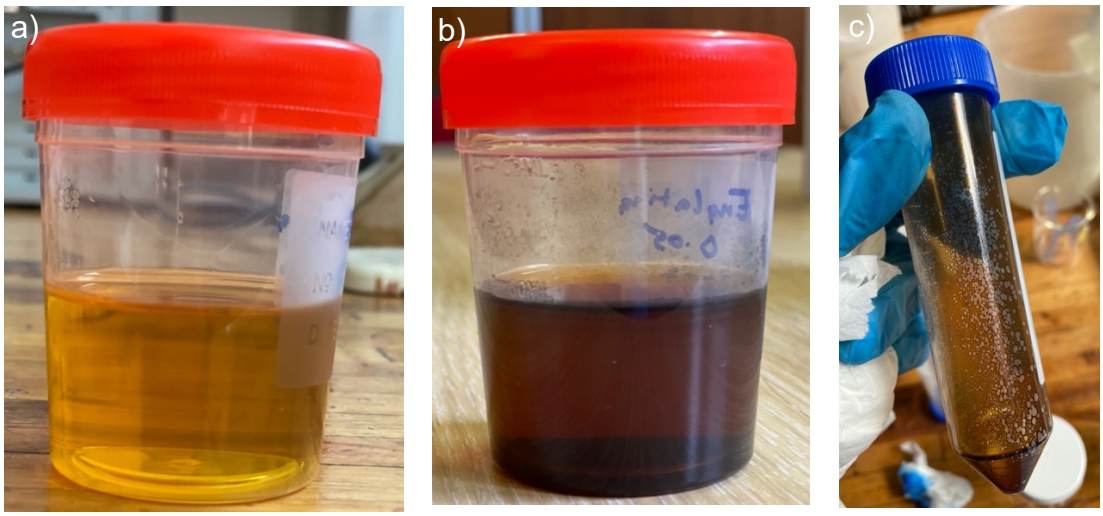

Figure A 1: Process wastewater from RF hydrochar produced at 245 for 3 hours. a) wastewater recovered right after hydrochar filtration; b) same sample after 24h of storage; c) centrifuge tube with product formation on the walls.

Appendix B: Effect of Individual Factors on Hydrochar Yield and Calorific Values.

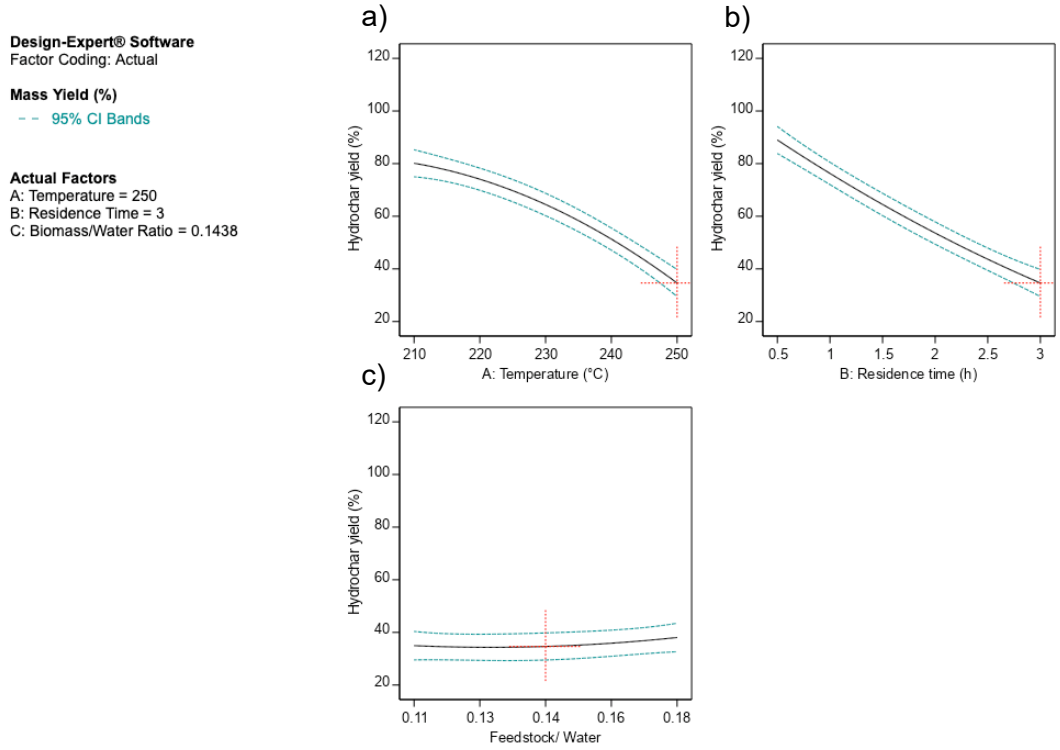

Figure B 1: Effect of a) temperature, b) residence time and c) solid load on hydrochar yield at maximum reaction severity.

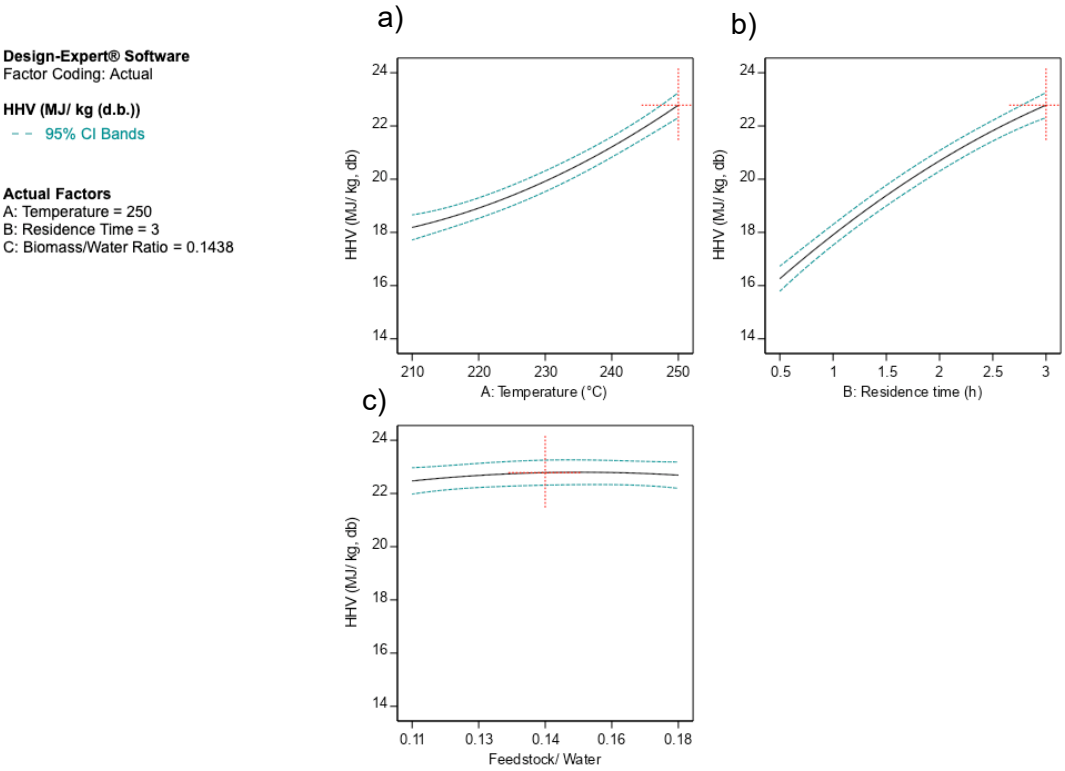

Figure B 2: Effect of a) temperature, b) residence time and c) solid load on calorific value at maximum reaction severity.

Appendix C: Effect of Process Conditions on Hydrochar Yield and HHV.

Table C 1: Effect of HTC reaction temperature and residence time on hydrochar yield and calorific values.

Temperature (h)	Time (min)	SF	HY * (%)	HHV (MJ/ kg)	Process wastewater pH
220	60	5.31	93.60	15.83	6.22
	120	5.79	74.44	17.90	4.00
	300	6.01	65.43	19.22	4.19
240	60	5.90	84.54	16.63	4.77
	120	6.38	50.25	21.27	3.83
	300	6.60	39.93	22.18	3.46
260	60	6.49	73.86	17.75	4.49
	120	6.97	34.93	21.59	3.40
	300	7.19	32.86	21.95	3.51

*HY: hydrochar yield.

Appendix D: Visual Aspects of the Hydrochars Obtained from the Optimisation Studies.

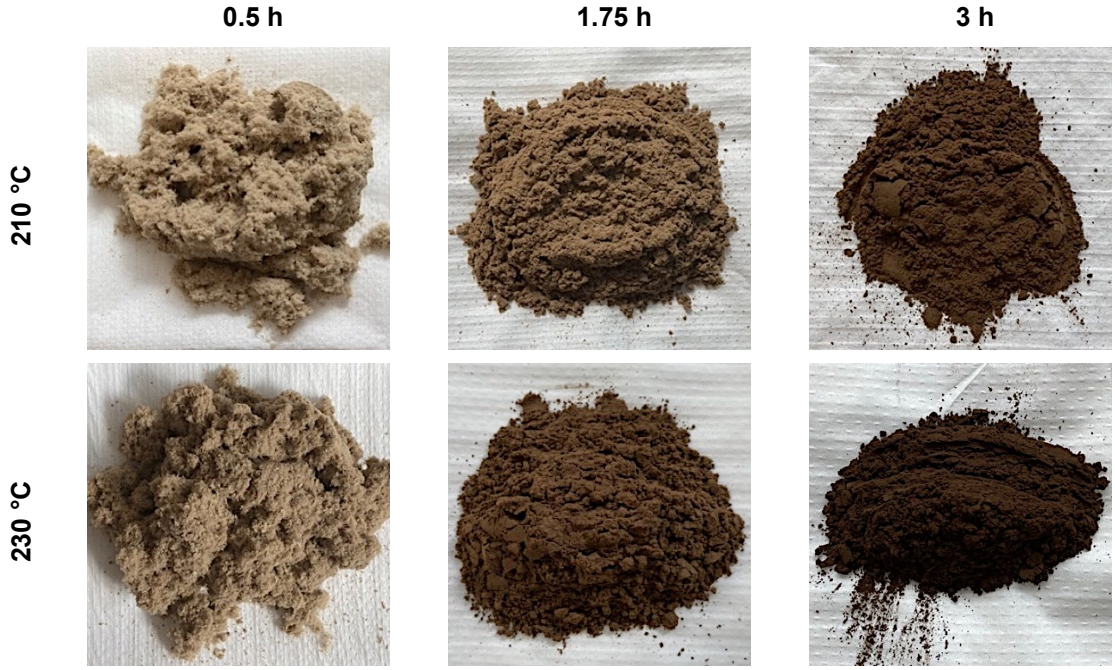

250 °C

Figure D 1: Visual assessment of ground hydrochars obtained at different reaction severities for process optimisation.